MARK-SPACE DIFFERENTIAL ELECTROLYTIC POTENTIOMETRY USING SOLID ELECTRODES COATED WITH CARBON NANOTUBES IN TITRIMETRY AND AS A DETECTOR IN FLOW INJECTION ANALYSIS

BY

ABDALGHAFFAR MOHAMMAD ABDALGHAFFAR OSMAN

A Dissertation Presented to the

DEANSHIP OF GRADUATE STUDIES

KING FAHD UNIVERSITY OF PETROLEUM & MINERALS

DHAHRAN, SAUDI ARABIA

In Partial Fulfillment of the
Requirements for the Degree of

DOCTOR OF PHILOSOPHY

In

CHEMISTRY

MAY 2016

KING FAHD UNIVERSITY OF PETROLEUM & MINERALS

DHAHRAN- 31261, SAUDI ARABIA

DEANSHIP OF GRADUATE STUDIES

This thesis, written by **ABDALGHAFFAR MOHAMMAD ABDALGHAFFAR OSMAN** under the direction of his thesis advisor and approved by his thesis committee, has been presented and accepted by the Dean of Graduate Studies, in partial fulfillment of the requirements for the degree of **DOCTOR OF PHILOSOPHY IN CHEMISTRY**.

Dr. Abduallah Abulkibash
(Advisor)

24/5/2016

Dr. Abdulaziz Alsaadi
Department Chairman

Dr. Mazen Mohammad Khaled
(Co-Advisor)

Dr. Salam A. Zummo
Dean of Graduate Studies

Dr. Reyad Shawabkeh
(Member)

2/6/16

Date

Dr. Ghassan A. Oweimreen
(Member)

for

Dr. Muataz Ali Atieh
(Member)

DEDICATION

I dedicate this work to my

Mother

Father

Wife and Children

ACKNOWLEDGMENT

Firstly, I would like to express my sincere gratitude to my advisor Prof. Abdullah Abulkibash for his cooperation and patience. His guidance helped me in my PhD research and writing of this dissertation.

Besides my advisor, I would like to thank the rest of my dissertation committee: Dr. Muataz Ali Atieh who gave access to the laboratory and research facilities during the first part of my research, Dr. Mazen Mohammad Khaled, the co-advisor, Prof. Ghassan A. Oweimreen and Prof. Reyad Shawabkeh for their insightful comments and encouragement.

My sincere thanks also goes to Mr. Rashid Muhammad, lecturer and engineer in Physics department who helped me a lot in the designing and fixing electric circuits that I used during the second part of my work.

I thank KFUPM for providing me a golden opportunity and rewarding scholarship to pursue my PhD. My gratitude of thanks also extends to all Faculty I took courses with them at the Department of Chemistry for the valuable knowledge I obtained from through my exciting study, in particular, I am grateful to Dr. Abdunnasir Kawde.

Last but not the least, I would like to thank my family: my parents for supporting me spiritually throughout my life in general and for sending prayers at all time, my wife, who was patient during my long absence from home due to my busy time in the pursuit of the degree and to my beloved kids, from whom I was mentally away.

TABLE OF CONTENTS

LIST OF TABLES

LIST OF FIGURES

LIST OF ABBREVIATIONS

CFX	:	Ciprofloxacin
DEP	:	Differential electrolytic potentiometry
d.c	:	Direct current
m.s.b	:	Mark space bias
CVD	:	Chemical vapors deposition
FIA	:	Flow injection analysis
SIA	:	Sequential injection analysis
CNTs	:	Carbon nanotubes
Ag/CNTs	:	Silver modified with carbon nanotubes
SEM	:	Scanning electron microscopy
TEM	:	Transmission electron microscopy

ABSTRACT

Full Name : Abdalghaffar Mohammad Abdalghaffar Osman

Thesis Title : Mark-Space Differential Electrolytic Potentiometry Using Silver Electrodes Coated with Carbon Nanotubes in Titrimetry and Flow Injection Analysis

Major Field : Chemistry

Date of Degree : May, 2016

In this work, silver metal wires have been successfully coated by carbon nanotubes (CNTs) using the chemical vapor deposition technique. The growth process of the CNTs was achieved by the thermal decomposition of acetylene gas in the presence of hydrogen gas and ferrocene as a catalyst. The process was optimized to obtain the optimum temperature, the acetylene and hydrogen flow rates and the time to produce both good quality of the CNTs and surface coverage of the silver wires. The produced electrodes were characterized by the scanning electron microscopy, transmission electron microscopy and Raman spectrometry. The CNTs grown were found to be of good quality and aligned to some extent. The Ag/CNTs have been used as an indicating system in the differential electrolytic potentiometry (DEP) techniques. DEP with polarization by a time bias square wave has been applied to different types of titrimetric reaction including acid–base, complexation, precipitation and oxidation – reduction reactions in aqueous solutions. The Ag/CNTs electrodes were found to be stable, sensitive and fast in response. They have been applied to determine ascorbic acid, cyanide and chloride and lead. Some titration methods have been validated and compared to the standard methods. The electrodes have also been used as a detector in the flow injection analysis system with polarization with both direct current

and mark–space biased square wave. They have shown good linearity and limit of detection. The flow injection method was optimized to find the optimum conditions of the current density/percentage bias, the flow rate and the concentration of the reagent. The polarization of the electrodes with the biased square wave were found to be more effective than the direct current polarization.

ملخص الرسالة

الاسم الكامل : عبد الغفار محمد عبد الغفار عثمان

عنوان الرسالة : استخدام الأقطاب الصلبة المغلفة بأنابيب الكربون النانوية كأنظمة كشف في المعايرات وفي التحليل الحقني الإنسيابي باستخدام فرق الجهد التفاضلي منحاز الموجة المربعة

التخصص : كيمياء

تاريخ الدرجة العلمية : مايو 2016

تناولت هذه الدراسة تغليف قضبان الفضّة بطبقة من أنابيب الكربون النانوية باستخدام طريقة الترسيب الكيميائي للأبخرة. تمّت عملية تحضير أنابيب الكربون النانوية هذه عن طريق التكسير الحراري لغاز الأستيلين داخل مفاعل أفقي في وجود غاز الهيدروجين وباستخدام الفرّوسين كمصدر للعامل المحفِّز للتفاعل. تمت دراسة أثر كل من درجة حرارة المفاعل، معدل تدفق كل من غازي الأستيلين والهيدروجين والفترة الزمنية للتفاعل، وذلك بغرض تكوين أنابيب كربونية نانوية بدرجة عالية من الجودة ونسبة تغطية عالية على سطح قضبان الفضة. تم استخدام المجهر الإلكتروني الماسح ومطيافية رامان، إضافة إلى المجهر الإلكتروني النافذ وذلك لتشخيص الكربون المتكوِّن على سطح قضبان الفضة، حيث أظهرت نتائج التشخيص بأنّها متعددة الطبقات وأنَّها على درجة عالية من الجودة.

إستُخدمت قضبان الفضة المغلَّفة بأنابيب الكربون النانوية كأقطاب استشعار في مختلف المعايرات الحجمية باستخدام تقنية فرق الجهد التفاضلي التي تعتمد على استقطاب هذه الأقطاب بواسطة التيار المتردد باستخدام الموجة المربعة ذات الحيود الزمني، حيث تمت دراسة أثر النسبة المئوية لانحياز الموجة المربعة على زيادة الحساسية وسرعة استجابة الأقطاب. إشتملت هذه المعايرات على الأكسدة والاختزال، تكوين المعقدات، تفاعلات الحمض والقاعدة وتفاعلات الترسيب، حيث تم تحديد نقطة النهاية للمعايرات المختلفة.

أوضحت الدراسة حساسية وسرعة استجابة عاليتين لأقطاب الفضة المغلفة بأنابيب الكربون النانويّة، إضافة إلى ثباتيتها لفترات طويلة.

تناولت الدراسة أيضاً استخدام هذه الأقطاب كأنظمة كشف في جهاز الحقن الإنسيابي باستخدام تقنية فرق الجهد التفاضلي التي تعتمد على استقطاب هذه الأقطاب بواسطة كل من التيار المباشر والتيار المتردد باستخدام الموجة المربعة ذات الحيود الزمني، حيث تمت دراسة أثر كل منهما، إضافة إلى تركيز الكاشف ومعدل التدفق. وأوضحت النتائج فعالية هذه الأقطاب كأنظمة كشف في هذا النوع من التحليل. كما تبيَّن أن استخدام الموجة المربعة ذات الحيود الزمني أعطى حساسية أكبر منها في حال استخدام التيار المباشر كوسيلة للاستقطاب.

CHAPTER 1

INTRODUCTION

1.1 Differential Electrolytic Potentiometry

Differential electrolytic potentiometry (DEP) is a technique employed to indicate the end point in titraions. In this technique, a small constant current is applied to two identical indicator electrodes while the potential, ΔE, across them is measured during the titration [1].

In DEP system, no reference electrode is involved. The salt bridge in the reference electrode that causes some difficulties especially in non aqueous systems is eleminated [2]. Moreover, polarizing the indicator electrodes usually remains them active during the course of the titration and therefore enhances the response and also reach the equilibrium in a short period of time. These advantages of the DEP made it a suitable detection system for most of the titrations [3] and the flowing systems [4].

1.2 Carbon Nanotubes

Carbon nanotubes (CNTs) possess remarkable structural, electronic and chemical properties, such as large specific surface and excellent current carrying capability [5], [6]. They have been the subject of many studies in physical, chemical and material areas due to these unique properties. CNTs behave electrically as a semiconductor or as a metal based on their atomic structure. Electrodes made of multiwalled carbon nanotubes have been shown fast electron-transfer kinetics for electrochemical reactions [7]. CNTs have widely

incorporated in different types of electrochemical sensors [8] and biosensors [9] for a wide range of applications.

1.3 Flow injection analysis

Flow injection analysis (FIA) presents an important concept of total automation of solution handling, offering the advantages of fast analysis and low consuption of reagents. It has been employed to automate a wide variety of chemical and biochemical analyses since its invention in the 1970s [10]. Owing to its feasibility in coupling with various types of detectors, the applications are very numerous [11]. FIA based on differential electrolytic potentiometry as a detection system has been applied to pharmaceutical [12] and environmental analyses [13].

1.4 Research Objectives

The objectives of this research are outlined as follows:

1. To prepare silver electrodes coated with carbon nano tubes using chemical vapor deposition method (CVD).
2. To apply these electrodes as a detection system in ion–combination and electron transfer titrations using mark-space bias DEP in aqueous systems.
3. To investigate the applicability of the solid electrodes coated with CNTs as a detection system using dc-DEP in flow injection.
4. To modify the electronic circuit that supplies a time biased square wave to use it as a polarization source in flowing systems.

CHAPTER 2

LITERATURE REVIEW

2.1 Differential Electrolytic Potentiometry

Differential Electrolytic Potentiometry (DEP) is a technique used to indicate the end point in titrimetric reactions. It is based on measuring the potential difference (ΔE) across a pair of identical metallic electrodes polarized by a small constant current and placed in a stirred solution. DEP titration gives a curve, similar to the first differential of the sigmoidal normal potentiometric one [14]. A bimetallic system using two similar electrodes was early applied in electrometric oxidation–reduction titrations to indicate the end point [15]. The two electrodes behave independently of each other, but their behavior is dependent on the magnitude of the current applied and the nature of the ions in the solution [1]. It has been found that a constant potential is reached at a high stirring rate of the titration solution [16].

DEP usually gives better results than those obtained from normal potentiometry, with the advantage that the polarization during titrations produces an electrode response faster than the zero current electrodes. In DEP technique, there is no reference half-cell is included. Therefore, the difficulties caused by the salt bridges are eliminated [1], especially in non–aqueous solutions [2].

Polarization of the electrode may be achieved by different ways. So, the method is named on the basis of the way that electrodes are polarized. Accordingly, the method is called direct current differential electrolytic potentiometry (dc - DEP) if a direct current is applied to polarize the electrodes. Alternating current (a.c. DEP) or periodic current (p.c. DEP)

refers to the technique where the electrodes are polarized by applying pure, symmetrical, bias–free square, sine and triangular wave [17], [18]. The DEP technique takes the name a mark–space bias (m.s.b. DEP) when a time biased square wave, difference in the duration of the negative and positive half cycles of a square wave, is applied to the electrodes [19]. Here, the electrodes are polarized by a direct current component produced from the biased square wave [18].

Optimum titration curves are obtained when a symmetrical, bias–free, wave periodic polarization is applied. Any bias produces a deterioration of the titration curve. This technique gives a sharp peaks and better results than dc–DEP in precipitation and redox titrations in aqueous solutions. This is due to the continuous reversing of the signal that prevents buildup of films on the electrode surface which keeps the electrodes fully active for very long periods. Also, warning is given of the approach of the end-point [17]. The use of a time bias on a periodic wave affect the differential curve, ΔE, but the dc component produced may polarize the electrodes [18].

Bishop, E. studied the precision and accuracy of differential electrolytic potentiometry. He applied it to a random assortment of redox titrations [20]. The results showed an improvement reaches up to a 10 fold in the location of end point compare to the classical potentiometry. He also studied titrations of strong and weak acids and bases using antimony electrodes. The results obtained were favorably compared with classical procedures in accuracy [21]. The high accuracy and precision is attributed to the fast equilibrium attained in the electrode potential, because of the polarization, and also due to the sharpness of the differential peaks.

The different techniques of DEP have been applied to all types of titrations in aqueous solutions with diverse solid electrodes. Silver electrodes and silver-silver halide electrodes have been used in precipitation titrations [22]–[24]. Antimony oxide electrodes have been found to be suitable for acid-base titrations [21], [25], [26]. Platinum have been found to be the best electrode for oxidation-reduction titrations [20]. For complexation titrations, gold amalgam is appropriate as indicating electrodes [27]. DEP techniques have been also applied to different titrations in non–aqueous media [3], [18].

2.2 The Theories of the DEP

The mass and charge transfer processes become pertinent since the titration curves are affected by many titrimetric and electrical parameters.

Kolthoff (12) defines the polarization of an electrode in the means of a passing current through it. The potential of the electrode will change and it will be different from that of the zero-current potential. Depending on the type of polarization the anodic polarization will make the potential of the electrode more positive than that of the zero current. In the case of cathodic polarization, the electrode will attain more negative potential than the zero current electrode. The differences in potentials are due to overpotential.

2.2.1 The Overpotential

An electrode through which a finite current is passing has a potential difference from its zero current or equilibrium value. This difference is called overvoltage or overpotential and is giving the symbol η

In the absence of net current flowing in the external circuit, the sum of cathodic and anodic current is equal to zero i.e. $i_c + i_a = 0 \; and \; i_c = -i_a = i_0$

i_0 represents the exchange current that flows continuously in the compact layer. When $I = 0$, the electrode potential will have the equilibrium zero-current value, E_{eq} with respect to saturated hydrogen electrode.

When a net current is passing through the electrode, its potential will have a new value, E_{we} which is the potential of the working electrode. The difference between E_{we} and E_{eq} is called the overpotential η i.e. $\eta = E_{we} - E_{eq}$

The overpotential η consists of three components; charge transfer or activation overpotential (η_a), the mass transfer or concentration overpotential (η_c) and the resistance overpotential (η_r). η_a occurs due to the slowness of the electrode process, depending upon the nature of electrode surface, its surface conditions and the concentration of electroactive species present in the medium. η_c arises when the passage of current causes a net reaction at the electrode surface and independent of the nature of electrode. This results in a difference in concentrations of reactants and products at the electrode surface from those in the bulk of solution forming concentration gradients. Hence reactants migrate towards and products migrate away from the electrode. η_r could be defined as η_{cs} which represents the overpotential that results from the passage of current as $\eta_{cB} + \eta_{cs}$, where η_{cB} is independent of current and constant for a given bulk concentration.

$$\eta_{cs} = \frac{RT}{nF}\log_e \frac{[Ox]_s}{[\mathrm{Re}d]_s} - \log_e \frac{RT}{nF}\frac{[Ox]_B}{[\mathrm{Re}d]_B} \qquad \text{..... (1)}$$

and the potential of an electrode

$$E = E_0' + \eta_{cB} + \eta_{cs} + \eta_a \qquad \text{..... (2)}$$

and $E = E_0' + \eta_c + \eta_a$ ..... (3)

The resistance overpotential η_r [28], defined by Bowdon and Agar, depends upon the conductivity of the electrolyte solution and the amount of current flowing but not on the electrochemical processes. Adding supporting electrolyte in a proper concentration is sufficient to lower η_r to an insignificant value.

2.2.2 Parameters Involved in the Theoretical Treatment

A list of the parameters involved the theoretical treatment and their definitions is provided here:

A: Projected area of the electrode

x: Thickness of the diffusion layer

r: Roughness factor of the electrode surface

D: Diffusion coefficient

I: Current

k: The conditional overall rates constant

a : The charge transfer coefficient

n: Number of electrons involved in the reaction

E_{we} : Working electrode potential

E_0' : Conditional potential

$[Ox]_B$: Concentration of the oxidized form in the bulk solution

$[Ox]_s$: Concentration of the oxidized form at the surface of the electrode

$[\mathrm{Re}d]_B$: Concentration of the reduced form in the bulk solution

$[\mathrm{Re}d]_s$: Concentration of the reduced form at the surface of the electrode

f and b: Forward or backward electrode reaction

k_f: Specific rate constant for forward reaction

k_b: Specific rate constant for backward reaction

a_{Ox}: Activity of oxidized species

$a_{\mathrm{Re}d}$: Activity of reduced species

The kinetics of an electrode reaction depends on the rates of mass and charge transfer reactions at the electrode surface.

Mass transfer exits in three different forms: diffusion, convection and electro migration. Diffusion occurs due to the change in concentration of electrolyzed species near the electrode forming a concentration gradient between the electrode surface and the bulk of a solution.

Density and concentration gradients form convection. Rapid stirring of solution results in a uniform concentration in the bulk.

Since ions carry the current, electromigration of reacting species will occur. The addition of a background electrolyte minimizes such migration.

In order to calculate $[Ox]_s$ and $[\mathrm{Re}d]_s$ under conditions where η_a is negligible, it is assumed that the electromigration is negligible [29].

Consider the oxidation-reduction reaction.

$$\mathrm{Ox} + \mathrm{ne} \rightleftharpoons \mathrm{Red} \qquad \text{..... (4)}$$

For which the electrode potential is given by

$$E_{we} = E_0' + \frac{RT}{nF} \ln \frac{[Ox]_s}{[\mathrm{Re}d]_s} \qquad \text{..... (5)}$$

At equilibrium for a given current:

rate of electrolysis = rate of diffusion

Therefore, $\frac{I}{nF} = D_{Ox}.A.r\frac{[Ox]_B - [Ox]_s}{\delta x}$ ..... (6)

and $\frac{I}{nF} = D_{\mathrm{Re}d}.A.r\frac{[\mathrm{Re}d]_s - [\mathrm{Re}d]_B}{\delta x}$ ……..…… (7)

Solution of equation (6) and (7) gives the ionic concentrations of the oxidized and reduced species at the electrode surface:

$$[Ox]_s = [Ox]_B - \frac{I\delta x}{nFArD_{Ox}} \quad \text{…….. (8)}$$

$$[\mathrm{Re}d]_s = [\mathrm{Re}d]_B + \frac{I\delta x}{nFArD_{\mathrm{Re}d}} \quad \text{…….. (9)}$$

Substitution of (8) and (9) in (5) gives E_{we} corresponding to a given value of the current

$$E_{we} = E_0' + \frac{RT}{nF}\ln\frac{[Ox]_B - \frac{I\delta x}{nFArD_{Ox}}}{[\mathrm{Re}d]_B + \frac{I\delta x}{nFArD_{\mathrm{Re}d}}} \quad \text{…….. (10)}$$

When the process becomes limited by the diffusion of oxidant to the electrode surface, $[Ox]_{s\to 0}$, so that from (6) the limiting current for cathodic reactions is given by

$$I_{\substack{L_{[\mathrm{Re}d]_{s\to 0}} \\ E\to\infty}} = \frac{nFArD_{\mathrm{Re}d}[\mathrm{Re}d]_B}{\delta x} \quad \text{……..…… (11)}$$

Similarly from (4) the limiting current for anodic reaction is

$$I_{\substack{L_{[Ox]_{s\to 0}} \\ E\to-\infty}} = \frac{nFArD_{Ox}[Ox]_B}{\delta x} \quad \text{…….. (12)}$$

This current is approached asymptotically and would only be obtained for cathodic reactions at $E_{we} = -\infty$ at higher potentials, the current corresponding to a given potential is obtained by solving (10) for I, hence

$$I = \frac{nFAD_{Ox}D_{\mathrm{Red}}}{\delta x}\frac{[Ox]_B - B[\mathrm{Red}]}{BD_{Ox} + D_{\mathrm{Red}}} \qquad \text{..... (13)}$$

Where $B = e^{\frac{nF(E_{we}-E_0')}{RT}}$ ..... (14)

By applying equations (10) and (13) the potential at a specified current and the current at a specified potential both can be calculated. Furthermore, using the convention that a net cathodic current is positive and a net anodic current is negative, the above equations can be applied to both anodic and cathodic reactions.

Considering equations (11) and (12), the parameters that are unknown or difficult to be measured, but which are constant for a given set of conditions may be grouped together in an overall conditional mass transfer rate constant $K_{mass.}$

$$K_{mass,[Ox]} = \frac{D_{Ox}.r}{\delta x} = -\frac{IL_{Ox}}{nFA[Ox]} \qquad \text{..... (15)}$$

Similarly,

$$K_{mass,[\mathrm{Red}]} = \frac{D_{\mathrm{Red}}.r}{\delta x} = -\frac{IL_{\mathrm{Red}}}{nFA[\mathrm{Red}]} \qquad \text{..... (16)}$$

2.2.3 The Charge Transfer Problem

In order to obtain $[Ox]_s$ and $[\mathrm{Re}d]_s$ for substitution in the charge transfer equations, the mass transfer equations have to be applied. There is a connection between mass transfer and charge transfer. Considering again the general reaction

$$\mathrm{Ox} + \mathrm{ne} \underset{\text{ia}}{\overset{\text{ic}}{\rightleftharpoons}} \mathrm{Red} \qquad \ldots\ldots\ldots\ldots\ldots\ldots\ldots\ldots\ldots\ldots (17)$$

and on the passage of a net current I through the electrode, the rate equation is

$$-\frac{da_{Ox}}{dt} = \frac{da_{\mathrm{Re}d}}{dt} = k_f a_{Ox} - k_b a_{\mathrm{Re}d} = \frac{I}{nFA} \qquad \ldots\ldots\ldots\ldots\ldots\ldots\ldots\ldots\ldots\ldots (18)$$

where a_{Ox} and $a_{\mathrm{Re}d}$ are the activities of the oxidized and reduces species, k_f and k_b are the forward and backward reaction rate constants and I is the net current flowing

The specific rates, k_f and k_b can be written in terms of the theory of absolute reaction rates as [30]

$$k_f = \frac{k^B T}{h} e^{-\frac{\Delta G_f^*}{RT}} \qquad \ldots\ldots\ldots\ldots\ldots\ldots\ldots\ldots\ldots\ldots (19)$$

$$k_b = \frac{k^B T}{h} e^{-\frac{\Delta G_b^*}{RT}} \qquad \ldots\ldots\ldots\ldots\ldots\ldots\ldots\ldots\ldots\ldots (20)$$

where ΔG_f^* and ΔG_b^* are the corresponding free energies of the activated state k^B is Boltzmann's constant, h is Plank's constant.

If the potential of the electrode with respect to some reference point such as N.H.E. is. E_{volt} , k_f' and k_b' are the rate constants at $E = 0$ and a is defined as the fraction of the potential favoring the forward reaction, i.e. cathodic reaction, then there will be a free energy change of a nFE per mole and hence the specific rate of the forward reaction become

$$k_f = k_f' e^{-\frac{\alpha nFE}{RT}} \qquad \ldots\ldots\ldots\ldots\ldots\ldots\ldots\ldots\ldots\ldots (21)$$

and similarly a fraction $(1-\alpha)$ of the potential E will favor the backward, i.e. anodic, reaction and thus the specific rate of the backward reaction becomes

$$k_b = k_b' e^{\frac{(1-\alpha)nFE}{RT}} \qquad \ldots\ldots\ldots\ldots\ldots\ldots\ldots\ldots\ldots\ldots (22)$$

Substituting these values in the overall rate equation (19) gives

$$I = nFAa_{Ox}k_f' e^{-\alpha nFE/RT} - a_{\mathrm{Re}d}k_b' e^{(1-\alpha)nFE/RT} \qquad \ldots\ldots\ldots\ldots\ldots\ldots\ldots (23)$$

When no net current is flowing through the external circuit, $I = 0$, and $i_c = -i_a = i_0$, where i_0 is the exchange current; the electrode potential E_{we} will then have the equilibrium value, E_{eq} while $[Ox]$ and $[\mathrm{Re}d]$ will be the bulk concentrations. Thus,

$$i_c = nFAa_{Ox}k_f' e^{-\alpha nFE_{eq}/RT} \qquad \ldots\ldots\ldots\ldots\ldots\ldots\ldots\ldots\ldots\ldots (24)$$

and

$$i_a = -nFAa_{\mathrm{Re}d}k_b' e^{(1-\alpha)nFE_{eq}/RT} \qquad \ldots\ldots\ldots\ldots\ldots\ldots\ldots\ldots\ldots\ldots (25)$$

Substituting in the equation $i_c + i_a = 0$ gives, after simplification

$$E_{eq} = \frac{RT}{nF}\ln\frac{k'_f}{k'_b} + \frac{RT}{nF}\ln\frac{a_{Ox}}{a_{\mathrm{Re}d}} \qquad \ldots\ldots\ldots\ldots\ldots\ldots\ldots\ldots\ldots\ldots (26)$$

Which is the Nernst equation at zero current and from which the definition of E_0 can be seen:

$$E_o = \frac{RT}{nF}\ln\frac{k'_f}{k'_b} = \frac{\Delta G - \Delta G_f}{nF} \qquad \ldots\ldots\ldots\ldots\ldots\ldots\ldots\ldots\ldots\ldots (27)$$

Similarly insertion of f_{Ox} and $f_{\mathrm{Re}d}$, the activity coefficients of Ox and $\mathrm{Re}d$ into equation (26) gives the definition of E'_0

$$E'_0 = E_0 + \frac{RT}{nF}\ln\frac{f_{Ox}}{f_{\mathrm{Re}d}} \qquad \ldots\ldots\ldots\ldots\ldots\ldots\ldots\ldots\ldots\ldots (28)$$

By using an overall rate constant, k, which is defined as

$$k = k'_f f_{Ox} e^{-\alpha nFE_0/RT} = k'_b f_{\mathrm{Re}d} e^{(1-\alpha)nFE_0/RT} \qquad \ldots\ldots\ldots\ldots\ldots\ldots\ldots\ldots\ldots\ldots (29)$$

or

$$k = k^0_f e^{-\alpha nFE'_0/RT} = k^0_b e^{(1-\alpha)nFE'_0/RT} \qquad \ldots\ldots\ldots\ldots\ldots\ldots\ldots\ldots\ldots\ldots (30)$$

and substituting these values in equation (1.23) using the fact that $E = E_{eq} at I = 0$ and the relation $E_{eq} = E'_0 = \frac{RT}{nF}\ln\frac{[Ox]_B}{[\mathrm{Re}d]_B}$ gives

$$I = nFAk\{[Ox]^{(1-\alpha)}[\mathrm{Re}d]^{\alpha} - [Ox]^{(1-\alpha)}[\mathrm{Re}d]^{\alpha}\} = 0 \qquad \ldots\ldots\ldots\ldots\ldots\ldots\ldots\ldots\ldots\ldots (31)$$

But $i_0 = i_c = -i_a$

So,

$$I = nFAk[Ox]^{(1-\alpha)}[\mathrm{Red}]^{\alpha} \quad \ldots\ldots\ldots\ldots\ldots\ldots\ldots\ldots\ldots\ldots (32)$$

When $I \neq 0$, then $i_c \neq -i_a$. In order to calculate I from equation (23), E is not equal to E_{eq}, but equal to the working electrode potential, E_{we}. Using the definitions of the overall rate constant, k, in (29) and (30) and substituting into (23) gives

$$I = nFAk[Ox]e^{-\frac{\alpha nF}{RT}(E_{we}-E_0')} - [\mathrm{Red}]e^{\frac{(1-\alpha)nF}{RT}(E_{we}-E_0')} \quad \ldots\ldots\ldots\ldots\ldots\ldots (33)$$

When $I = 0, [Ox]\&[\mathrm{Red}]$ are the bulk concentrations and $E_{we} = E_{eq}$ but when $I \neq 0$ the concentrations are $[Ox]_s \& [\mathrm{Red}]_s$. From equation (3), $E_{we} - E_0' = \eta_c + \eta_a$ and therefore (33) becomes

$$I = nFA[Ox]_s e^{-\frac{\alpha nF}{RT}(\eta_c+\eta_a)} - [\mathrm{Red}]e^{\frac{(1-\alpha)nF}{RT}(\eta_c+\eta_a)} \quad \ldots\ldots\ldots\ldots\ldots\ldots\ldots (34)$$

Equation (34) can be solved for η_a by substituting from (7)

$$\eta_c = \frac{RT}{nF}\ln\frac{[Ox]_s}{[\mathrm{Red}]_s} \quad \ldots\ldots\ldots\ldots\ldots\ldots\ldots\ldots\ldots\ldots (35)$$

which gives after simplification

$$I = nFAk[Ox]_s^{(1-\alpha)}[\mathrm{Red}]_s^{\alpha}\{e^{-\frac{\alpha nF}{RT}\eta_a} - e^{\frac{(1-\alpha)nF}{RT}\eta_a}\} \quad \ldots\ldots\ldots\ldots\ldots\ldots (36)$$

Which is the charge-transfer and mass-transfer overpotential equation. Calculation of the potential at a given current may be achieved by direct solution of equations (33), (34) and

(36), but in each case the mass transfer problem must be solved in order to determine $[Ox]_s \& [\mathrm{Re}d]_s$ for substitution into (36). Equation (36) is straightforward to solve for supplied values of $\eta_a, k \text{ and } \alpha$. It is also possible by numeral methods [31] to resolve this equation for η_a in terms of supplied values of the current. Finally substitution of the calculated values for $\eta_c \& \eta_a$ in

$$E_{we} = E_0' + \eta_a + \eta_c \qquad \ldots\ldots\ldots\ldots\ldots\ldots\ldots\ldots\ldots\ldots (37)$$

gives E_{we} at the chosen current, the sign of the current will give the correct solution for either anodic or cathodic process.

2.3 Carbon Nanotubes

2.3.1 Definition and Properties

Carbon nanotube (CNT), discovered in 1991[32], is a graphite sheet rolled into cylinders[33]. Since that time, they have attracted much attention due to their excellent physical and chemical properties. CNTs have very low electrical resistivity [34], [35], Individual nanotube was found to carry current with a density exceeding 10^9 A/cm^2 [36]. Depending on their atomic structure, CNTs behave electrically as a metal or as a semiconductor [37], [38]. The subtle electronic properties suggest that CNTs have the ability to promote charge-transfer reactions when used as an electrode [7], [39].

2.3.2 Growth of Carbon Nanotubes

Three methods are mainly used for CNTs growth: laser ablation, arc discharge, and chemical vapor deposition (CVD). The latter one was regarded as the most promising compared with the first two methods although it usually introduces more defects in CNTs during the growth process. The growth process is catalyzed by the most common catalysts: Fe, Co and Ni [40] in their different forms [41]–[43]. These metals have few d-vacancies in their orbitals and consequently both decompose carbon sources and dissolve carbon atoms up to a certain limit [44]. It has been demonstrated that CNT materials contain residual metal impurities from catalysts even after purification[45]. Two different interfaces between CNTs and a metal crystal exist as depicted in Figure 1. CNTs either form an *end-contact* to the metal, involving covalent bonds at the interface, or a *side-contact* forming a weakly bonded interface. Although the end-contact is favorable, side contact with excellent electrical properties has already been reported [46]. CNTs are known to grow predominantly on nonconducting substrates,

that limits applications where conductive substrates/contacts, for instance to form electrodes, are required. However, CNTs have been directly grown on bulk metals [47].

2.3.3 Growth Mechanism of Carbon Nanotubes

Since its discovery, the growth mechanism of CNT is still debatable. Based on the reaction conditions and post-deposition product analyses, several groups have proposed different possibilities. Therefore, no single mechanism has been established so far [48]. The growth of carbon nanotubes from hydrocarbons by CVD method consists of four sequential processes. These include the mass transport of the hydrocarbon and its reaction in the gas phase, the dissociative absorption of the hydrocarbon molecule on the catalyst metal surface, the diffusion of the resulting carbon atoms through the catalyst or on its surface, and finally the precipitation of carbon atoms from the catalyst to form the growing nanotube. The catalytic chemical vapor deposition of the carbon nanotubes on the transition metal catalysts was considered as heterogeneous catalysis [49].

The widely-accepted two general cases for growth mechanisms of CNTs are: (a) tip-growth model, (b) base-growth mode as shown in Figure 2 [49]. The first one is assumed to take place when the catalyst–substrate interaction is weak. Carbon atoms resulting from decomposition of hydrocarbon, on the metal surface, diffuse down through the metal, and the CNTs form across the metal bottom, pushing the whole metal particles off the substrate. In the second mechanism, the CNTs are compelled to emerge out from the metal's apex. This happens when the catalyst–substrate interaction is strong [48], [50].

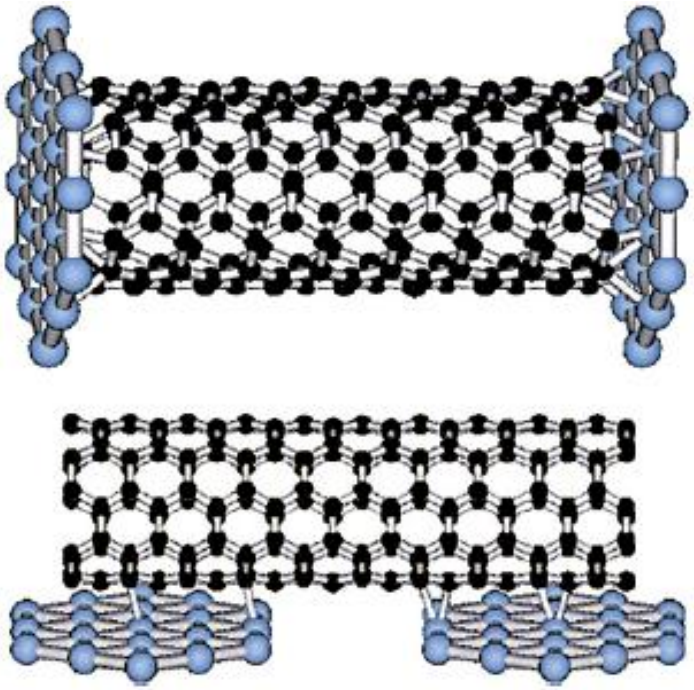

Figure 1: The two types of interface between a metal crystal and a carbon nanotube: end-contact (top) and side-contact (bottom) [46]

(a)

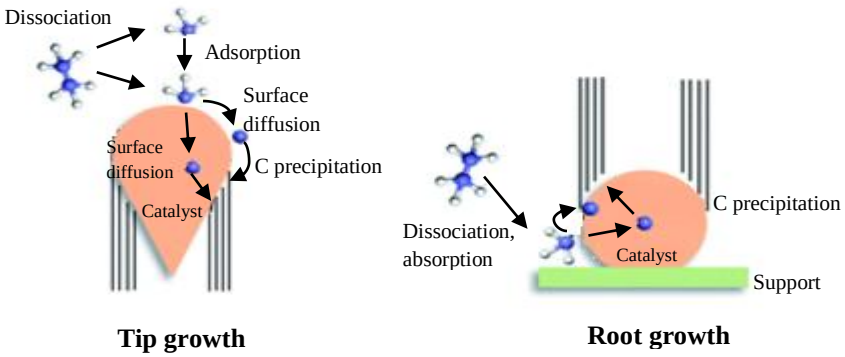

(b)

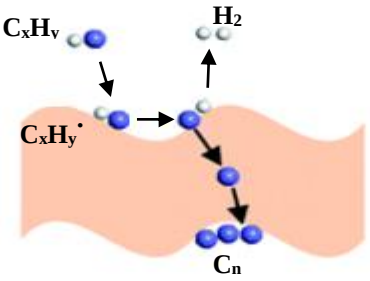

Figure 2: (a) widely accepted mechanisms and processes in carbon nanotube growth, for tip growth and root growth. (b) Simplified model [49].

2.4 Optimization of Carbon Nanotubes Growth by Chemical Vapor Deposition

Carbon nanotubes have been grown through chemical vapor deposition method using different carbon sources, carrier gases, catalysts and different temperatures. Many researches have reported the growth of CNTs in CVD reactors by using acetylene as carbon source, hydrogen as carrier and ferrocene as catalyst.

2.4.1 Effect of Hydrogen Concentration

Hydrogen plays an important role in the growth of carbon nanotubes by thermal CVD. Increasing hydrogen promotes the growth of CNTs while preventing the formation of spherical amorphous carbon particles[51], [52]. Hydrogen prevents the passivation of the catalyst surface caused by excessive carbon deposition [53] and keeps it active which in turn enhances the graphitization degree of the grown CNTs[54]. However, the length of the aligned carbon multiwall nanotubes grown using toluene and ferrocene decreased as the hydrogen gas was increased in the mixture[55]. On other hand, quantum chemical molecular dynamics simulation of early stages in the nucleation process of carbon nanotubes from acetylene feedstock on Fe catalyst highlights the inhibiting effect of hydrogen for the condensation of carbon ring networks [56].

2.4.2 Effect of Temperature

As the growth temperature of CNTs, using C_2H_2 and iron based catalyst, increases from 600 to 1100°C, the growth rate enhances, the amount of crystalline graphitic sheets increases and higher degree of crystalline perfection is obtained [42]–[46]. On the other hand, carbon impurities decrease [62]. Higher temperatures were found to enhance growth of aligned CNTs [63], [64] and affect the tubes length [65].

2.5 Characterization Techniques for Carbon Nanotubes

2.5.1 Scanning and Transition Electron Microscopy

Scanning electron microscopy (SEM) and Transition electron microscopy (TEM) have been used for the characterization of carbon nanotubes[66]. SEM with high resolution is powerful instrument for imaging of fine structures of CNTs and other carbon species by imaging the morphology of the surface. TEM is used to observe the internal structure of carbon nanotubes [67] such as the presence of residual metal catalyst nanoparticles [45], single or multiple CNTs and distances between the concentric tubes [68] and if they are bundles or individual tubes[69].

2.5.2 Raman Spectroscopy

Raman spectroscopy is one of the most powerful tools employed for the characterization of carbon nanotubes without sample preparation. All allotropic forms of carbon are active in Raman spectroscopy [70].

The information provided about vibrational properties can be correlated with the structure and electronic properties of the nanotubes. It gives an indication of the purity of CNTs based on the ratio of G-band (~1580cm^{-1}) to D-band (~1350cm^{-1}). G-band assigns to the in-plane vibration of the C–C bond and D-band is due to distorted sp^2 and it reflects the amount of impurity particles [71]–[73]. Raman spectrum shows a band at about 2700 cm^{-1} called G′-band which may represent more accurate measurement of MWCNTs quality and purity since its intensity is enhanced by the carbon nanotubes [73]. Purification of CNTs with acid increases the structural defect [74].

2.6 Carbon Nanotubes as Electrode Material in Electroanalytical Methods

Due to their unique electronic features and high surface area, CNTs have been widely applied in electrochemical studies and electroanalytical applications as sensors and biosensors. They have been applied in different techniques and achieved significant enhancement in sensitivity for the measurement of diverse analytes ranging from metal ions through gases and organic pollutants to biological markers. CNTs have been incorporated in enzyme-based biosensors, DNA sensors and immunosensors [9]. Electrodes modified with CNTs have been employed in amperometric [75]–[77] and voltammetric measurements [75]–[82]. Very recent potentiometric sensors and biosensors including CNTs or modified CNTs have been applied for biological[83], [84], environmental organic[85] and inorganic [86]–[89] and other analyses [90], [91].

2.7 Flow Injection Analysis

2.7.1 Introduction

Continuous flow chemistry has been widely used in chemical analysis. Recently, this production methodology has been gaining interest in pharmaceutical industry due to inherent increased safety, improved product quality, space savings and overall production capacity increase.

Flow Injection Analysis (FIA) is a simple, versatile and flexible automated technique that has found widespread applications in quantitative analysis. The name "Flow Injection Analysis" was introduced for the first time by Ruzicka and Hansen who have invented this system [10].

In FIA, as depicted in Figure 3 [92], carrier and reagent solutions are propelled by a peristaltic pump while sample solution is introduced through an injection valve into the carrier stream to meet later and react with the reagent in a mixing coil before they pass through a detection system.

For working FIA system, a constant residence time (reproducible timing) of the sample is essential. This assumes absence of compressible air segments in both carrier and reagent streams and the delivery system yields constant flows. Another vital factor for a successful measurement is the control of the sample zone dispersion. Dispersion of sample zone influences the peak height which is frequently used in the evaluation of the results [93], [94].

The second generation of flow injection analysis is called sequential injection analysis (SIA), Figure 4. Same principles of FIA apply in SIA but the flow is programmable rather than continuous [92]. Beside the holding coil and detector, SIA system comprises

an automated high-precision syringe pump and valves controlled by a personal computer.

SIA has advantages over FIA. These include: consumption of smaller reagent volumes and consequently generation of less waste. Moreover, it can be used for constant monitoring of environmental or industrial processes.

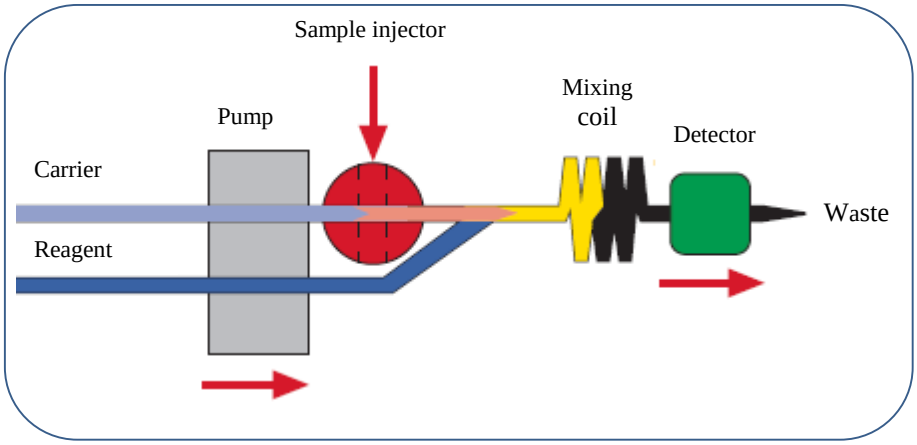

Figure 3: Schematic diagram of the flow injection analysis system with two flowing streams.

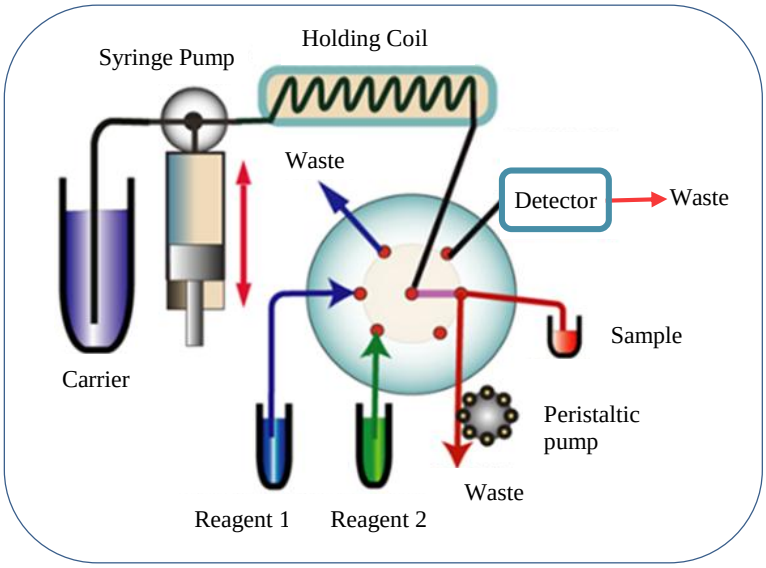

Figure 4: schematic diagram of the sequential injection analysis manifold [189].

2.7.2 Electrochemical Detection in Flow Injection Analysis

In the early stages after the invention of flow injection analysis, electrochemical methods have been established as detection systems. At that time, ion selective electrodes with potentiometric sensing were employed to determine the concentration of certain ions in soil extracts and blood sera [95]. Since that time different electrodes have been incorporated for this purpose. Flow injection analysis coupled to amperometric detection has been applied to different types of analyses including environmental [96], [97], pharmaceutical [98] and food [99] with a variety of working electrodes.

Electrodes modified with CNTs as detectors in flow injection analysis have found wide range of applications in food [100], biological [101], pharmaceutical [101], [102] and environmental [102]–[105] analyses. These electrodes have shown good sensitivity.

2.7.3 Flow Injection/Sequential Injection Coupled to DEP Detectors

Differential electrolytic potentiometry (DEP) has been employed as a detection system in SIA/FIA for the determination of different analytes with various types of electrodes. Ag/AgCl [106] and Ag/AgCl-Pt pair [107] indicating systems were used for chloride detection through precipitation reactions. Cyanide ions were determined by Ni^{2+} [108] and Hg^{2+} [109] using Au/Hg electrodes and by Ag^{+} [13] with Ag/Hg indicator electrodes. SIA/FIA coupled to DEP have been employed in oxidation-reduction reactions using Pt indicator electrodes to determine ascorbic acid with different oxidizing reagents [12], [110]. This technique has been also used to analyze ciprofloxacin [4] and for determination of lysine employing lysine biosensor as DEP indicator electrodes [111]. Among all of the above mentioned analyses, only few reported the employment of mark-space bias polarization as an indicating system.

2.8 Analytes of Concern in This Work

2.8.1 Ciprofloxacin

Ciprofloxacin (CFX) is an important class of antibacterial drugs that is comprehensively used for the treatment of infections of the urinary, respiratory, and gastrointestinal tracts. It is active against Gram-positive and Gram-negative bacterial species. CFX has been used in the treatment of severe typhoid fever [112], malignant external otitis [113] and tumor-like lesions of the rare disease malakoplakia [114]. The structure of this drug is shown in Figure 5,

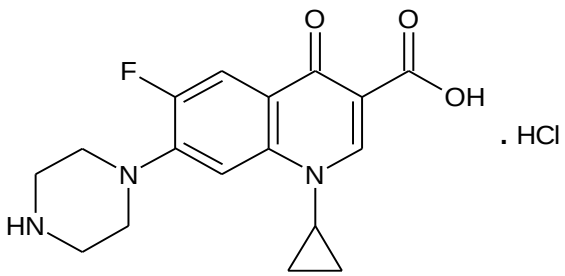

Figure 5: Chemical structure of ciprofloxacin

Different methods have been applied for the determination of ciprofloxacin in its pure form or in matrices. These include spectrophotometric, chromatographic and electrochemical methods [115]. High performance liquid chromatography, a method described in the US Pharmacopeia, has been used for the determination of CFX in human serum [116]–[118]. Spectrophotometry has been applied for CFX determination by measuring the absorbance of its complex with iron (III) [119], [120]. Electrochemical techniques have been widely applied for the determination of CFX in pure form and in various formulations using different types of electrodes [121]–[123].

Electrodes modified with carbon nanotubes (CNTs) have shown excellent response when used in voltammetric determinations [124]–[127].

CFX has been determined in drug formulations using differential electrolytic potentiometric titration method [128]. In this method, the analysis was based on the fast complexation reaction between iron (III) and CFX in sulfuric acid media using silver amalgam electrodes as a suitable indicating system.

FIA methods have been also employed in CFX determinations in pharmaceutical formulations spectrophotometrically by the complexation with iron (III) [129] and with amperometric sensing through screen printed electrodes modified with MWCNTs [102]. DC–DEP technique has been also used as an indicating system for the analysis of CFX [4].

Due to the variety of functional groups found in ciprofloxacin molecule, it can bind with metal ions to form complexes. Ciprofloxacin molecules is zwitterionic, based on the presence of a carboxylic acid group and the basic piperazinyl ring. Both groups are affected by the pH of the solution. The most common coordination mode in the quinolone chelates with metal ions is represented by carbonyl and carboxyl ligands in neighboring positions [130]. CFX has been found to form complexes with iron (III) in ratios 1:1 [131], 1:2 [132] and 1:3 [128].

2.8.2 Ascorbic Acid

Vitamin C, also known as ascorbic acid, Figure 6, is a water soluble compound that is regarded as one of the safest and most effective nutrients [133]. It is naturally found in many fruits and vegetables. It must be ingested for human's survival. Vitamin C is dietary and potent water–soluble antioxidant [134], [135]. The powerful electron donor property of ascorbic acid is responsible to its diverse functions [135].

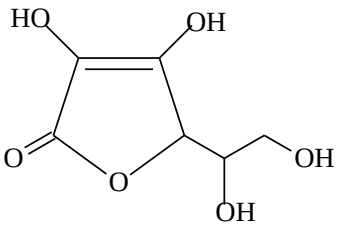

Figure 6: Structure of ascorbic acid

Vitamin C is beneficial in protecting humans against cold [136], cardiovascular disease, stroke [135], cancer [137] and acts to minimize the risk of wheezing symptoms in children [138].

Different methods have been applied for the determination of ascorbic acid in its pure form or in complex matrices. In its pure form, ascorbic acid is determined by titration with iodine in dilute sulfuric acid medium, while different titration is employed for pharmaceutical formulations [139]. Ascorbic acid has been determined in fresh fruit juices [133] and freeze-dried herbal juice [140] by direct titration against iodine. High performance liquid chromatography has been used for the determination of ascorbic acid in fresh fruits like baobab [141], fruit juices [142], beverages and pharmaceutics [143]. This technique achieves low detection limits but requires a bit long sample preparation. Electrochemical methods have been extensively used for the determination of vitamin C. Recently voltammetric methods involving electrodes modified with

nanomaterial such as oxide nanoparticles [144] and carbon nanotubes [145] were reported for food sample analyses. Direct current differential electrolytic Potentiometry has been applied in aqueous titration of ascorbic acid in pharmaceutical preparations employing a couple of platinum indicating electrodes [146], electrodes normally used in oxidation-reduction potentiometric titrations.

In this work, for the first time, Baobab fruit was analyzed, by mark-space bias differential electrolytic potentiometry for the ascorbic acid content by titration against standard potassium iodate solution using silver modified with multiwall carbon nanotubes as indictor electrodes.

Baobab Fruits

Baobab (*Adansonia digitata L.*) is commonly known fruit indigenous to some African countries [147], [148] including Sudan [149]. Baobab fruit pulp has a very high content of ascorbic acid up to 300 mg/100 g or more which is almost six times more than oranges. But unfortunately, the preservation of the fruit pulp, which is originally contained in hard protective outer case, Figure 7, is beyond the control of population leading to undesirable losses of ascorbic acid [148].

Figure 7: Baobab fruits, contained in hard protective outer case, obtained from central Sudan.

2.8.3 Lead (II) Ions

Lead is one of the heavy metals that rank among the priority metals that are of public health significance. The non-natural sources of lead are from human activities, mainly the emission from the industry and transportation. Since it cannot be degraded, it is an environmentally persistent toxin [150]. It was classified as a human carcinogen [151] and has been reported to affect nervous and hematopoietic systems, causes cardiac and vascular damage [152], [153], and genotoxicity [154]. Exposure to lead affects child physical growth [155].

Beside its toxicity to human, lead impact extends to other organisms such as the aquatic biota [156], [157] and plants [158], [159].

Potentiometric titrations of heavy metal ions, including Pb^{+2}, through complex formation reactions with EDTA using silver metal as an indicator electrode has been reported [160]. Selective potentiometric titrations for the determination of Pb^{+2} have been performed using various types of working electrodes modified with diverse ionophores [161]–[165]. Mostly, EDTA was employed as a titrant. In addition to selectivity, graphene was introduced in the electrode composition to increase the surface area and subsequently sensitivity enhancement was achieved [166].

MWCNTs have been incorporated in potentiometric sensors to increase the sensitivity in complexation of heavy metals with EDTA [167], [168] through the improvement of conductivity and, therefore, conversion of the chemical signal to an electrical signal [138].

While normal potentiometry has been extensively investigated for the determination of heavy metal ions especially by complexation with EDTA, a very few research work was devoted to investigate differential electrolytic potentiometry as a technique for this

purpose. DEP has been used to determine mercury (II), copper (II), nickel (II) and bismuth (III) by complex formation reactions with EDTA [139] using electrodes other than the amalgamated gold that used before in this types of reactions [14].

2.8.4 Cyanide

Cyanide is a potent and rapidly-acting asphyxiant to mammals. It prevents live tissue utilization of oxygen through the inhibition of the cellular respiratory enzyme. Inhalation or ingestion of cyanide therefore causes fast death within minutes [171]. Cyanide is a widely used chemical in industry [172]. The main source of cyanide pollution is the effluent from mineral processing operations associated with gold mines [172]. Extraction of gold by cyanide represents a major advance in gold mining because it allowed for higher recoveries than all the other prevailing methods [173].

The high toxicity of cyanide and its widespread industrial applications requires its determination at very low concentration levels. Different detection techniques for cyanide have been developed. These include optical methods [174], chromatography [175], [176], electrochemical [174] and flow injection analysis methods [108], [177], [178]. Potentiometry [179] and differential electrolytic potentiometry [178] were among the electrochemical methods used. Comparative studies of the determination of cyanide at low concentration levels in waste waters by different techniques have been reported [180].

CHAPTER 3

MATERIALS AND METHODS

3.1 Electrode Preparation and Characterization

Ferrocene (98+%, Aldrich) and pure silver metal were used. Growth of carbon nanotube on silver metal was achieved in a chemical vapor deposition reactor. A quartz tube reactor (125 cm length×2.5cm ID) was placed in two separate tube furnaces (Lindburg/Blue M TF55035A-1, USA and OTF 1200X, MTI Corporation, USA) as shown in Figure 8. An amount of 60 mg ferrocene was placed in a ceramic boat in the first heating zone while 0.1 cm diameter and 2 cm long silver wire was held in another boat positioned in the second heating zone.

The operation of the CVD system was started with argon gas being released into the system at a flow rate of 200 standard cubic centimeter per minute (sccm) to free the system from air. When the temperature of the second furnace in which carbon nanotubes grow reached 600, 700, 750 or 800, the ferrocene was then vaporized at 150 °C and the vapor swept into the second furnace for a period of 5min. Argon was then turned off and the mixture of acetylene, carbon source, and hydrogen was turned on at specified flow rates for time ranging from10-30 minutes at 5min intervals. The reactor was then allowed to cool to room temperature under argon environment.

Silver coated with CNTs was collected and characterized using Field Emission Scanning Electron Microscope (FE-SEM, TESCAN VELA3), Transmission Electron Microscope (FE-TEM, JOEL-2100F) and Raman spectrometer (LabRAM HR Evolution, HORIBA Scientific) with an excitation wavelength of 632.8 nm from a tunable He-Ne laser focused on the sample by means of a 50 LWD objective.

Figure 8: Chemical Vapor Deposition, CVD, setup used for CNTs growth on silver metal

3.2 Differential Electrolytic Potentiometry Titration Apparatus

The titration set up used in this work is depicted in Figure 9. The electrodes were prepared for measurement by soldering each of them to a copper wire placed into a glass jacket. These electrodes were placed in the titration cell. The electrodes were polarized using direct current or mark–space bias square wave generator. An oscilloscope was used to monitor the square wave and a potentiometer for measuring the potential difference. The titrant was dispensed from a micro burette.

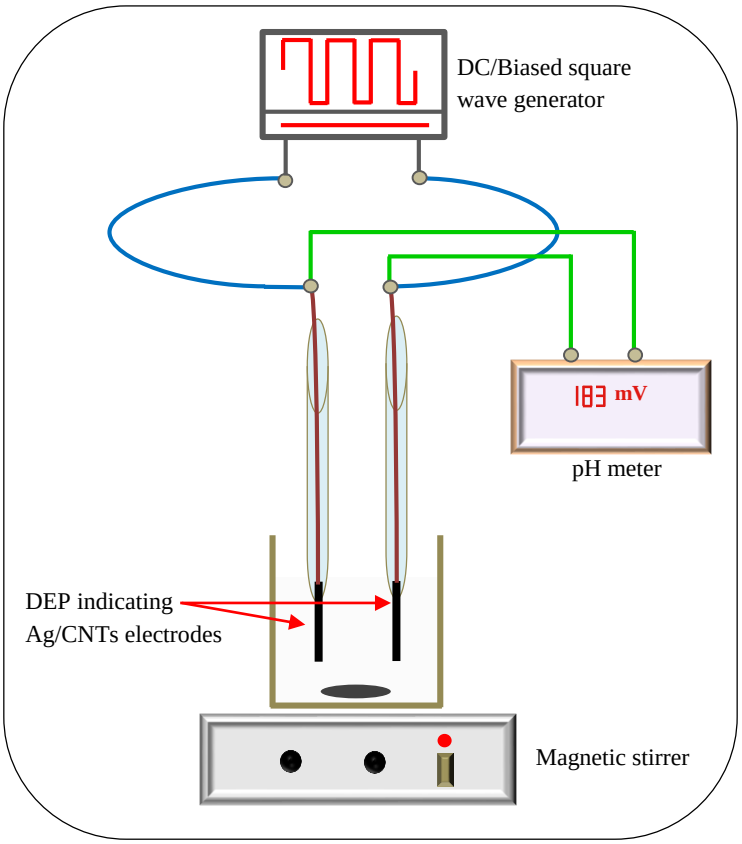

Figure 9: DC/mark–space DEP titration setup using Ag/CNTs indicting electrodes.

3.3 Determination of Ascorbic Acid

3.3.1 Materials, Reagents and Solutions

A solution of 0.02 mol/L ascorbic acid (99.5%, Fluka) was freshly prepared prior to use and then series of standard solutions were prepared by dilution with deionized water. A stock solution of 0.02 mol/L of potassium iodate (min 99.5%, Fisher scientific) was prepared and then used to prepare other diluted solutions as needed. 0.1 mol/L sulfuric acid (Sigma Aldrich) was also prepared. A standard solution of 0.0466 mol/L iodine solution was prepared and standardized against arsenic trioxide prior to use for the direct titration [109]. Redoxon® vitamin C tablets supplied by Bayer were purchased from local pharmacy. Baobab fruits, both contained in hard protective outer case and obtained from broken one, were collected from a market in central Sudan.

3.3.2 Methods

MS-DEP Titrations

A volume of 2.0 ml of 0.02 molar freshly prepared vitamin C was placed in a 50ml beaker, the volume was completed to 20 ml by 0.1 molar sulfuric acid. Two CNTs/Ag electrodes, which are part of the mark-space DEP circuit, were placed in the mixture and polarized by a bias ranging from 0 to 20%. Standard potassium iodate solution was dispensed from micro pipette with stirring the mixture and the potential difference (ΔE) between the two electrodes was recorded. The optimum bias was then fixed for the measurements of other standards of ascorbic acid, each of them was prepared and analyzed three times including the first one used for optimization.

Optimum bias was then applied to determine ascorbic acid in vitamin C tablets and in Baobab fruits using 0.01mol.L^{-1} potassium iodate. For Redoxon analysis, a volume of 2.0 ml of the solution of 0.8g powder/50ml was added to 20ml of 0.1mol.L^{-1} sulfuric

acid and analyzed in the same way. For Baobab, each 2g of the fruit pulp powder was stirred with 20ml of 0.1mol.L^{-1} sulfuric acid for 5 minutes prior to the titration in order to extract all the analyte present and then spiked with 0, 0.002, 0.005, 0.05 and 0.1 mmole of ascorbic acid and then titrated against iodate solution.

Iodimetric Titration

Ascorbic acid standard solutions were analyzed iodimetrically according to US Pharmacopeia procedure for pure vitamin C analysis for comparison [139]. Titrations were performed three times.

Potentiometric Titration

Potentiometric titration with CNTs/Ag working electrode was performed to determine ascorbic acid in 20 ml standard solution (2×10^{-4} mol.L^{-1}) against standard potassium iodate solutions in 0.1mol.L^{-1} sulfuric acid medium. Potentials of the CNTs/Ag working electrode during the titration were recorded against silver/silver chloride reference electrode.

3.4 Determination of Lead (II)

3.4.1 Materials, Reagents and Solutions

All chemicals used were of analytical grade. A stock solution of 0.1 mol/L lead nitrate (Fisher scientific) was prepared then a series of standard solutions were prepared by dilution with deionized water. A stock solution of 0.1 mol/L of Ethylenediaminetetra-acetic acid disodium salt, EDTA, (min 99.5%, BDH) was prepared and then used to prepare other dilute solutions as needed. A volume of 0.1 mol/L of acetate buffer (pH 5.5) was prepared from acetic acid and sodium acetate (Fisher scientific) and 0.1 mol/L borate buffer solution (pH 10, Fluka) was adjusted to pH 9.2 by diluted nitric acid and then used. A standard calcium solution was prepared from nitric acid and calcium carbonate (≥99%, Sigma-Aldrich). A 0.008 mol/L of silver nitrate solution was also prepared from sliver nitrate (99%, BDH).

3.4.2 Methods

MS-DEP Titrations

A volume of 2.00 ml of 5.00×10^{-2} mol/L Pb^{+2} was taken in a 50-ml beaker followed by 20 ml of buffer (acetate pH 5.5) and 50µL of 8×10^{-3} mol/L Ag^{+}. Two CNTs/Ag electrodes, which are part of the mark-space DEP circuit, were placed in the mixture and polarized by a bias ranging from 0 to 30%. EDTA solution (5.00×10^{-2} mol/L) was dispensed from the micro burette with stirring the mixture and the potential difference (ΔE) between the two indicator electrodes recorded. The optimum bias for polarization was selected and then the same procedure applied to titrate (2.00 ml of 1.00×10^{-1}, 5.00×10^{-3}, 5.00×10^{-4} and 1.00×10^{-4} mol/L) of Pb^{+2} with only 10µL of Ag^{+} for the last two solutions. Each solution was prepared and analyzed three times and average volumes of EDTA were obtained.

Back titrations for Pb^{+2} were also performed by adding Pb^{+2} (0.15, 0.015 and 0.0015 mmole) to excess EDTA (0.25, 0.025 and 0.0025 mmole) respectively. 10µL of Ag^{+} and 20 ml of 0.1 mol/L borate buffer (pH 9.2) were then added and the excess EDTA was titrated with Ca^{+2} standard solutions (5.00×10^{-2}, 5.00×10^{-3} and 5.00×10^{-4}) respectively.

Atomic Absorption Analysis of Lead (II)

Standard solutions of 0.1, 5.00×10^{-2}, 5.00×10^{-3} and 5.00×10^{-4} mol/L of Pb^{+2} were analyzed by atomic absorption spectrometer for comparison with the DEP titrations.

3.5 Determination of Cyanide

3.5.1 Reagents and Solutions

All chemicals used were of analytical grade. Distilled, deionized water was used in to prepare the solutions. A stock solution of 0.1 mol/L of potassium cyanide (Fisher Scientific) was prepared. A series of standard solutions of different concentrations were prepared from the stock solution by appropriate dilutions. A stock solution of 0.1 mol/L of silver nitrate (99%, BDH) was prepared and standardized against sodium chloride using Mohr method [181] and then used to prepare other dilute solutions as needed. A 0.1 mol/L solution of potassium nitrate (BDH) was also prepared to be used as a supporting electrolyte.

3.5.2 Direct Current DEP Titrations method

A volume of 5.00 ml of 2.00×10^{-2} mol/L potassium cyanide solution was taken in a 50-ml beaker followed by 20 ml of 0.1 mol/L potassium nitrate. Two Ag /CNTs electrodes, were placed in the mixture and polarized by a direct current ranging from 5 – 20 $\mu A/cm^2$. The mixture was titrated with 5.00×10^{-2} $mol.L^{-1}$ silver nitrate from a micro

burette with continuous stirring while measuring the potential difference (ΔE) between the two indicator electrodes. The optimum current for polarization of the indicating electrodes was then found. The optimum dc current was then fixed to perform a series of titrations for different concentrations of cyanide ions in the range of 4.00×10^{-3} – 1.60×10^{-5} in 0.1 mol/L potassium nitrate.

3.5.3 Mark–Space Bias DEP Titrations method

The same conditions in the dc DEP titrations of cyanide were applied here. Only the polarization of the two electrodes was done by a time biased square wave. The % bias applied was in the range of 0 – 30%. The optimum % bias was selected for further titrations of different concentrations of cyanide ions in the range of 2.00×10^{-2} – 2.00×10^{-5} mol/L.

3.6 Determination of Chloride

3.6.1 Reagents and Solutions

All chemicals used were of analytical grade. Deionized water was used in all preparations. A solution of 0.1 mol/L solution of potassium nitrate (BDH) was prepared.

A stock solution of 0.1 mol/L of sodium chloride (BDH) was prepared then a series of standard diluted solutions were prepared in 0.1 mol/L solution of potassium nitrate. A stock solution of 0.1 mol/L of silver nitrate (99%, BDH) was prepared and standardized against sodium chloride following Mohr method [181] and then used to prepare other dilute solutions as needed. Methods

3.6.2 Direct Current DEP Titrations

A volume of 20.00 ml of 2.50×10^{-3} mol/L of sodium chloride solution was taken in a 50-ml beaker. Two CNTs/Ag electrodes, were placed in the mixture and polarized by a direct current ranging from 2 – 20 $\mu A/cm^2$. The mixture was titrated with 2.50×10^{-2} mol/L silver nitrate from a micro burette with continuous stirring and the potential difference (ΔE) between the two indicator electrodes was measured. The optimum current for polarization of the indicating electrodes was then found. A series of titrations for different concentrations of chloride ions in the range of 5.00×10^{-3} – 2.50×10^{-4} in 0.1 mol/L potassium nitrate was performed at the optimum dc current.

3.6.3 Mark–Space Bias DEP Titrations

The same concentrations used in the dc DEP titrations were applied here by polarizing the indicating electrodes this time by applying a time biased square wave. The bias applied in the range of 0 – 40%. The optimum bias was selected for further titrations.

3.7 Acid Base Titration

3.7.1 Reagents and Solutions

A solution of 0.2 mol/L of sodium hydroxide was prepared and standardized with potassium hydrogen phthalate (99.96, Fisher scientific). The standard sodium hydroxide was then used to standardize a solution of 0.2 mol/L of hydrochloric acid.

3.7.2 Mark–Space Bias DEP Titrations

A 2.00 mL of 5.91×10^{-2} mol/L of hydrochloric acid were added to 20mL of 1×10^{-2} mol/L of potassium nitrate in a 50-ml beaker. Two CNTs/Ag electrodes were placed in the mixture and polarized by a time biased square wave in the range of 0 – 60%. The mixture was then titrated with a solution of 5.42×10^{-2} mol/L of sodium hydroxide and the point was located for each titration.

At the optimum percentage of the square wave bias, lower concentrations of the hydrochloric acid were titrated and the end points were located.

3.8 Flow Injection Analysis Determination of Ciprofloxacin

3.8.1 Chemicals and Reagents

A stock standard solution of 5.0×10^{-3} mol/L of ciprofloxacin hydrochloride monohydrate (99.8 %), was prepared by directly dissolving the drug in water at room temperature. Working standard solutions were prepared by appropriate dilutions of the stock standard solution. A solution of 0.25 mol/L of nitric acid was prepared and used to prepare other diluted solutions.

A 0.1 mol/L standard solution of iron (III) nitrate supplied by BDHs was used. Other iron (III) nitrate solutions were prepared by appropriate dilutions.

3.8.2 Flow Injection Analysis Setup

The flow analysis system used in this work, as depicted in Figure 2 consists of FIAlab Instrument, Inc. USA with a built in peristaltic pump (ALITEA, Sweden), in addition, a syringe pump (model 1250, J–KEM Scientific) with a separate controller attached to the FIA system. The flow cell was fabricated from plexiglass with a canal in the middle and two ports to accommodate the two Ag/CNTs electrodes. One end of the two electrodes are exposed to the solutions that pass through the canal and the other ends are connected to the electrical circuit and to the LabJack–U12 interface that converts the signal to a digital reading using the FIA software. Direct current/mark–space bias was employed for electrode polarization source. The whole system is controlled be a software through a personal computer except the J–KEM syringe pump which has its own controller.

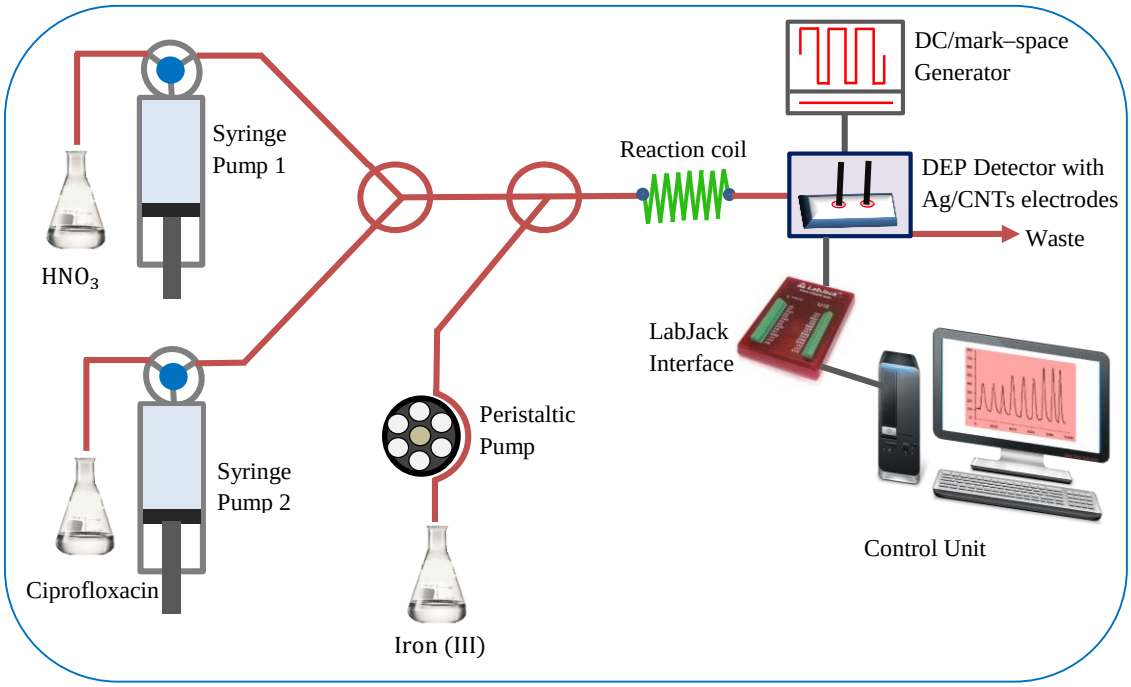

Figure 10: Flow injection analysis – DEP setup used for the determination of ciprofloxacin

3.8.3 Flow Analysis Procedure

The nitric acid solution was passed to the first syringe pump and the CFX solutions to the second one. The peristaltic pump was used to propel the iron (III) solution. At the beginning, the system was flushed with 50 mmol/L nitric for some time.

3.8.4 Method Optimization

The parameters optimized were current density, the percentage of mark–space bias, the flow rate, and the concentrations of nitric acid and iron (III) solutions. Nitric acid solution of 10 mmol/L was dispensed at a constant flow rate of 150 µL/sec. CFX solution of 5.0×10^{-1} mmol/L was introduced at a flow rate of 70 µL/sec. 25 mmol/L iron (III) solution was propelled at a flow rate of 80 µL/sec. The current density was varied from 5 – 40 $\mu A/cm^2$ to find the optimum value. Another experiment was performed by polarization of the indicating electrodes by a biased square wave with different values of percentages of mark–space bias in the range of 0 – 70 %. Triplicate measurements for the potential difference were taken for each run.

After obtaining both the optimum values of the dc current and the % bias, the effects of changing both the concentration of the iron (III) and the flow rate on the measured signal were studied.

3.8.5 Calibration

At optimum conditions of dc current or % bias, the concentrations of nitric acid and iron (III), and the flow rate, signals were measured for a series of standards of CFX solutions. The difference in potential measurements were taken three times for each solution studied.

3.9 Flow Injection Analysis Determination of Ascorbic Acid

3.9.1 Chemicals and Reagents

A solution of 0.5 mol/L ascorbic acid (99.5%, Fluka) was freshly prepared prior to use and then series of standard solutions were prepared by dilution with deionized water. A stock solution of 0.02 mol/L of potassium iodate (min 99.5%, Fisher scientific) was prepared and then used to prepare other diluted solutions as needed. A solution of 0.05 mol/L sulfuric acid (Sigma Aldrich) was also prepared.

3.9.2 Flow Analysis Setup

The flow analysis system used in this work is depicted in Figure 11, the same system used for CFX shown in Figure 10. Only the reagents are different.

3.9.3 Flow Analysis Procedure

The reservoir of 0.05 mol/L sulfuric acid solution was connected to the first syringe pump and the ascorbic acid solutions to the second one. The peristaltic pump was used to propel the KIO_3 solution. At the beginning, the system was flushed with 0.05 mol/L sulfuric for some time.

3.9.4 Method Optimization

The parameters optimized were the current density, the percentage of mark – space bias, the flow rate and the concentration of the analyte. Sulfuric acid solution was dispensed at a constant flow rate of 150 µL/sec. A solution of 0.02 mol/L of iodate was propelled at a flow rate of 100 µL/sec. Ascorbic acid solution of 2.81×10^{-1} mmol/L was introduced at a flow rate of 80 µL/sec. The current density applied for the polarization of the electrodes was varied from 10 – 65 µA/cm^2 to find the optimum value. Another experiment was performed by polarization of the indicating electrodes by a time biased

square wave with different values of % bias in the range of 0 – 50 %. Triplicate measurements for the potential difference were taken for each run.

After obtaining the optimum dc current and the % bias values for polarization, the flow rate of the oxidant was varied in order to find the optimum rate which give the highest signal.

3.9.5 Calibration

All of the values of the optimum parameters were applied to measure the difference in potential (ΔE) for the different concentrations of the standard ascorbic acid solutions in order to stablish a calibration curve. The measured signal was taken three times for each solution.

3.9.6 Analysis of Real Samples

For the analysis of ascorbic acid in vitamin C tablets (Redoxon®), five tablets were ground and then 0.35g of the powder were dissolved in deionized water and the volume made to 1000 mL. This solution was analyzed using the FIA system adjusted to the optimized parameters and applying both dc DEP and m.s.b DEP with both types of electrode polarization.

An amount of 2.01g of Baobab fruit powder was stirred with deionized water for a period of 10 min in a capped flask. The volume was then made up to 100 mL. The suspension was centrifuged at 30×10^3 cpm for 10 min. the clear supernatant was then analyzed at the optimum FIA conditions.

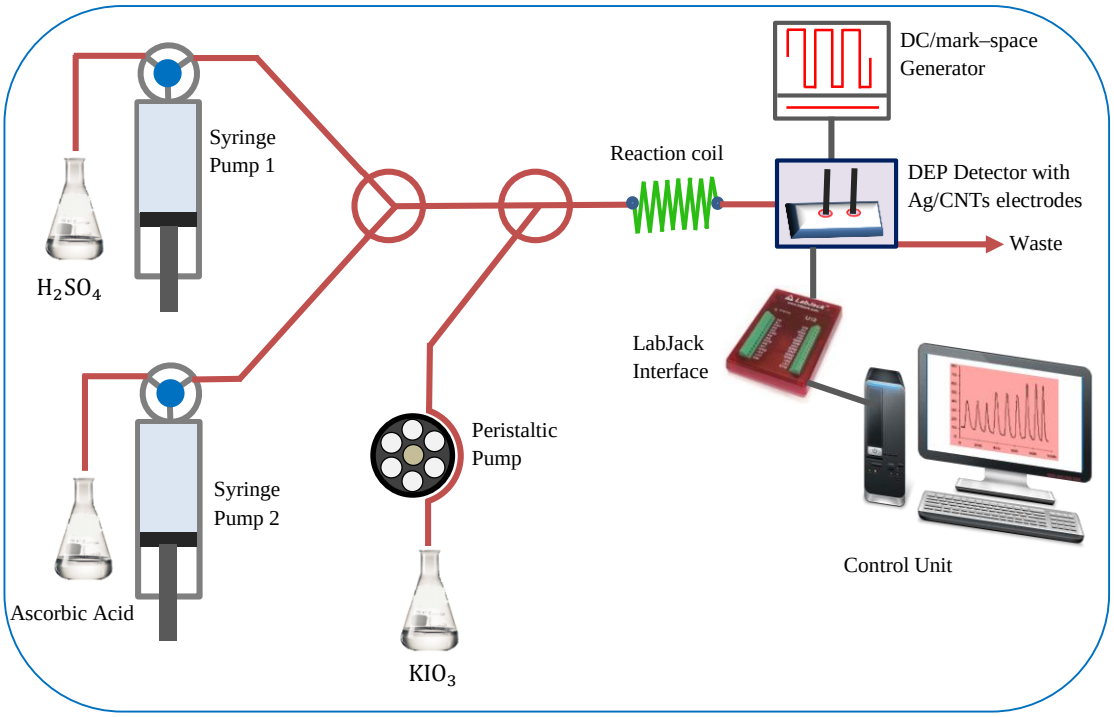

Figure 11: Flow injection analysis – DEP setup used for the determination of ascorbic acid

CHAPTER 4

RESULTS AND DISCUSSION (I)

4.1 Optimization of CNTs Growth on Silver Metal

The preparation of Ag/CNTs electrodes by thermal CVD method requires an investigation of some important parameters that influence the quantity and quality of the nanotube grown. Such parameters include hydrogen gas concentration, temperature and time.

First of all, it should be taken into consideration that the carbon particles other than CNTs reduce the electrical properties of the prepared CNTs/silver electrodes and consequently the sensitivity.

4.1.1 Effect of Hydrogen Concentration

In this study, C_2H_2 flow rate was held constant while varying H_2 flow rate. At 700°C and low H_2 flow rate only amorphous carbon was formed while CNTs growth enhanced by increasing the flow rate as depicted in Figure 12 and Figure 13 up to 90 sccm. However, beyond 100 sccm of H_2 flow rate again amorphous carbon forms. This result was in agreement with that obtained to produce MWCNTs in swirled floating catalyst chemical vapor deposition reactor [140].

C_2H_2 molecules were assumed to decompose at high temperatures according to the following equation

$$C_2H_2 \rightarrow 2C + H_2$$

As the concentration of hydrogen increases, the rate of decomposition is suppressed, which in turn seems to prevent the passivation of the catalyst surface caused by

excessive carbon deposition of carbon atoms and consequently enhances the growth of CNTs [38]. Another mechanism suggested that C_2H_2 is reduced to C_2H_6 in the presence of H_2 and the latter decomposes easier than the former to provide C atoms for CNTs formation [36]. In the above mentioned cases, it is clearly shown that inclusion of H_2 is important for the growth of CNTs from C_2H_2 with high purity. It enhances the graphitization degree of the synthesized CNT and results in lower residual catalyst [141].

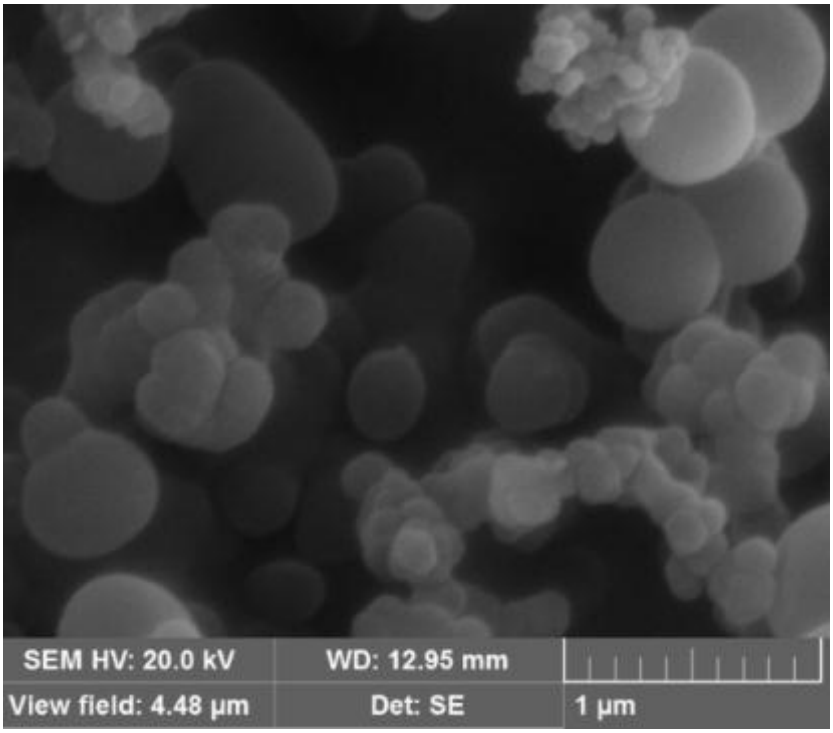

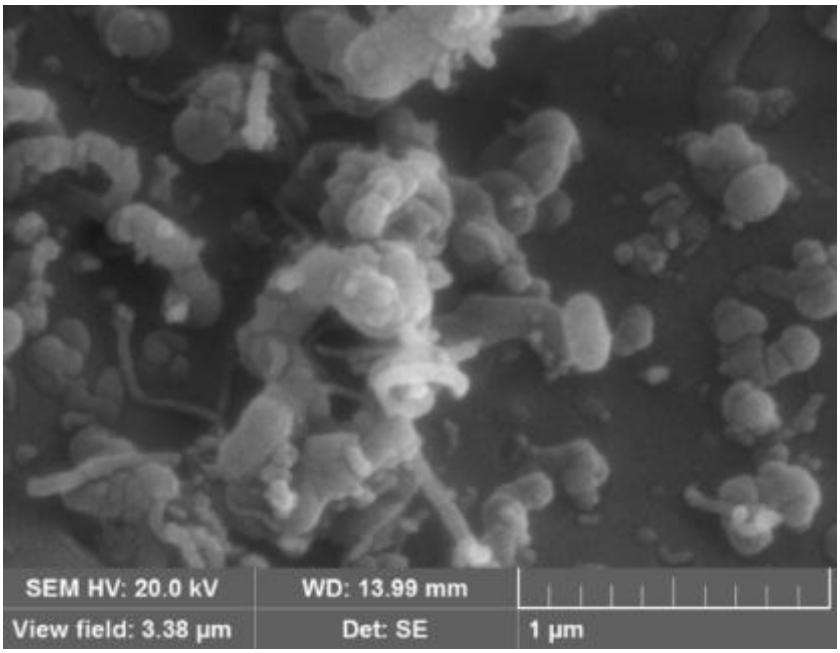

Figure 12: SEM micrographs represent the impact of H_2 flow rate on CNTs grown on silver metal at temperature 700°C for 15 min. C_2H_2 flow rate is 75 sccm with H_2 flow rates 25 (upper) and 50 sccm (lower)

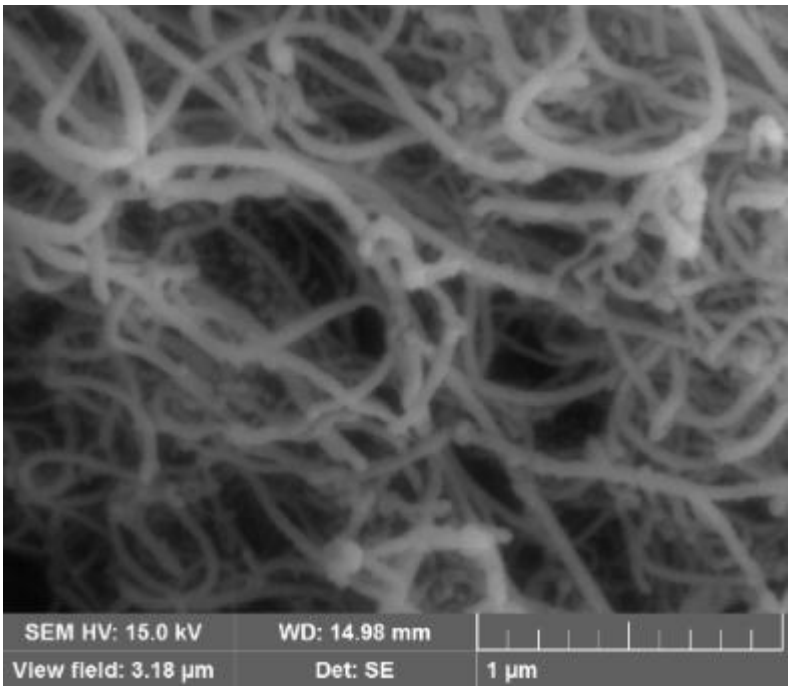

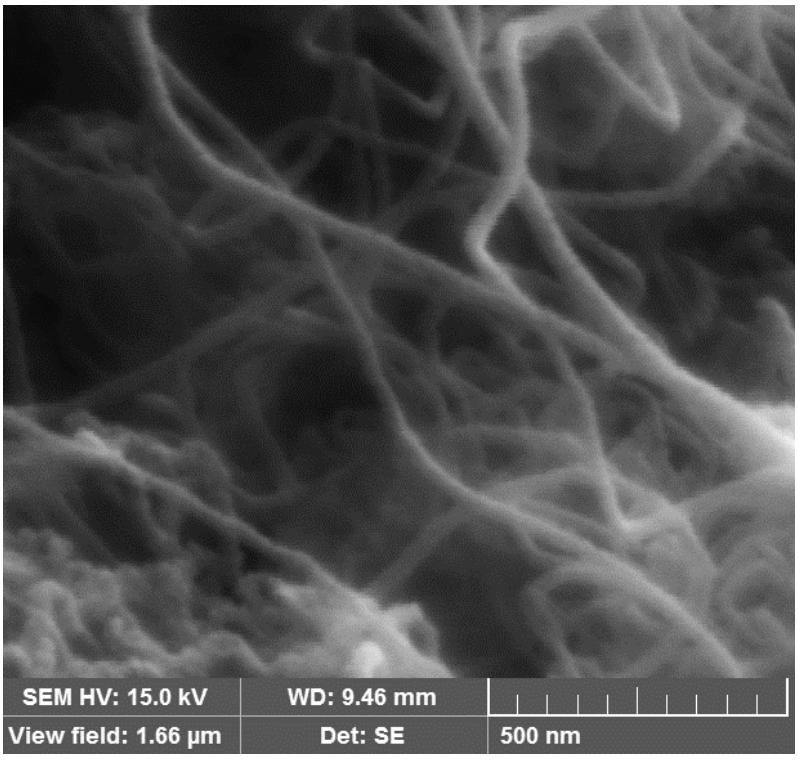

Figure 13: SEM micrographs represent the impact of H_2 flow rate on CNTs grown on silver metal at temperature 700°C for 15 min. C_2H_2 flow rate is 75 sccm with H_2 flow rates 75 (upper) and 90 sccm (lower)

4.1.2 Effect of Temperature

The growth temperature was varied from 600 to 800°C in order to investigate its impact on the CNTs grown on silver metal surface. Figure 14 and Figure 15 show that as the growth temperature increases, the CNTs/silver electrodes get better in term of both quality and surface coverage. At 600°C only amorphous carbon particles were formed. However, at 800°C, maximum amount of CNTs is obtained with least other carbon particles. Moreover, strong adherence to the surface was obtained which enhances the fabricated electrodes properties and keeps them stable for long periods of applications.

The degree of crystalline perfection has increased with the growth temperature. This result is attributed to the increase of the diffusion rate of C atoms in the iron nanoparticles which allows the graphitic sheets to build with a less defect [58], which in turn leads to the increase of the metallic conductivity of the MWCNTs [37].

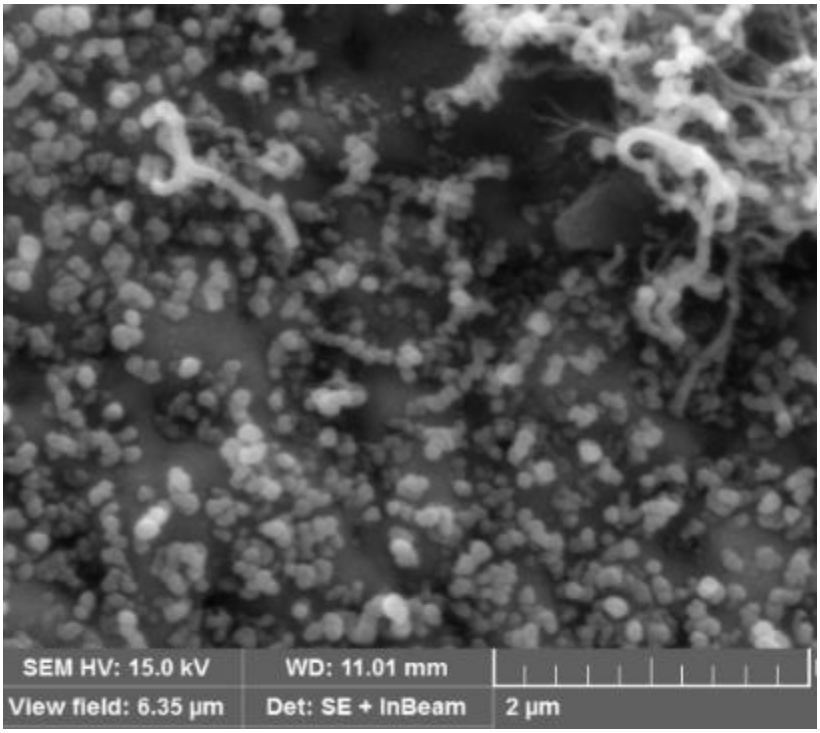

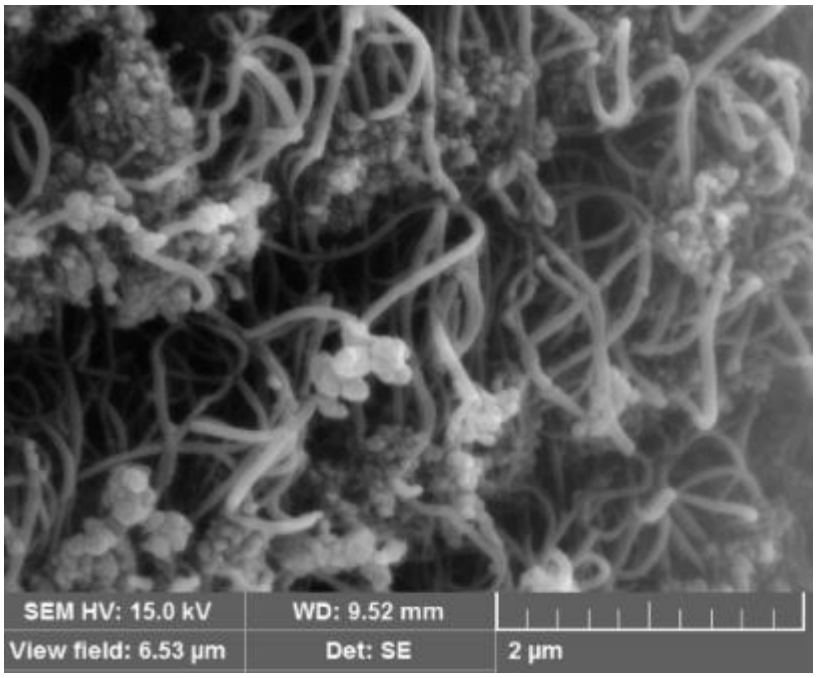

Figure 14: SEM micrographs show CNTs growth on silver metal at temperatures: 600°C (upper) and 700°C (lower).
C_2H_2: H_2 flow rate ratio is 75:90 sccm. Reaction time is 20 min.

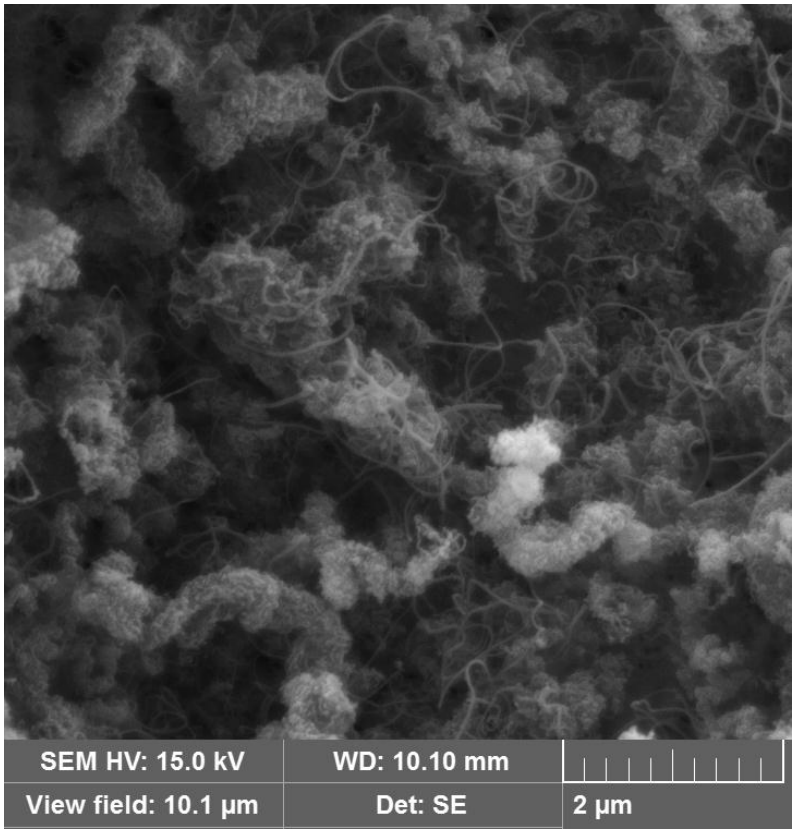

Figure 15: SEM micrographs show CNTs growth on silver metal at temperatures: 750°C (upper) and 800°C (lower).

C_2H_2: H_2 flow rate ratio is 75:90 sccm. Reaction time is 20 min.

4.1.3 Effect of Growth Time

In this work, to fabricate a sensitive electrode, the surface coverage is considered as an important parameter. At short time (10min), CNTs cover parts of the metal while at a longer time (30 min) the surface is totally covered but amorphous carbon particles start to deposit on CNTs, as can be seen from Figure 16, which lead to reduce its degree of graphitization. These results agree with other previous ones [142], [143]. Formation of other carbon materials rather than CNTs can be attributed to the exhaustion of the catalyst with time [144]. A time period of 20 min was found to be optimum time to achieve the required properties.

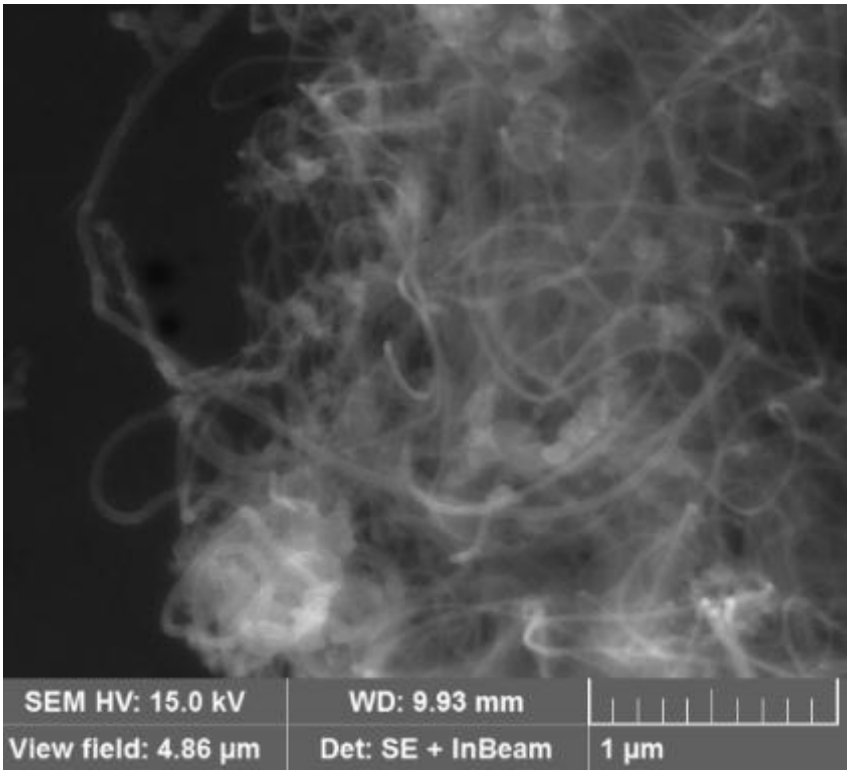

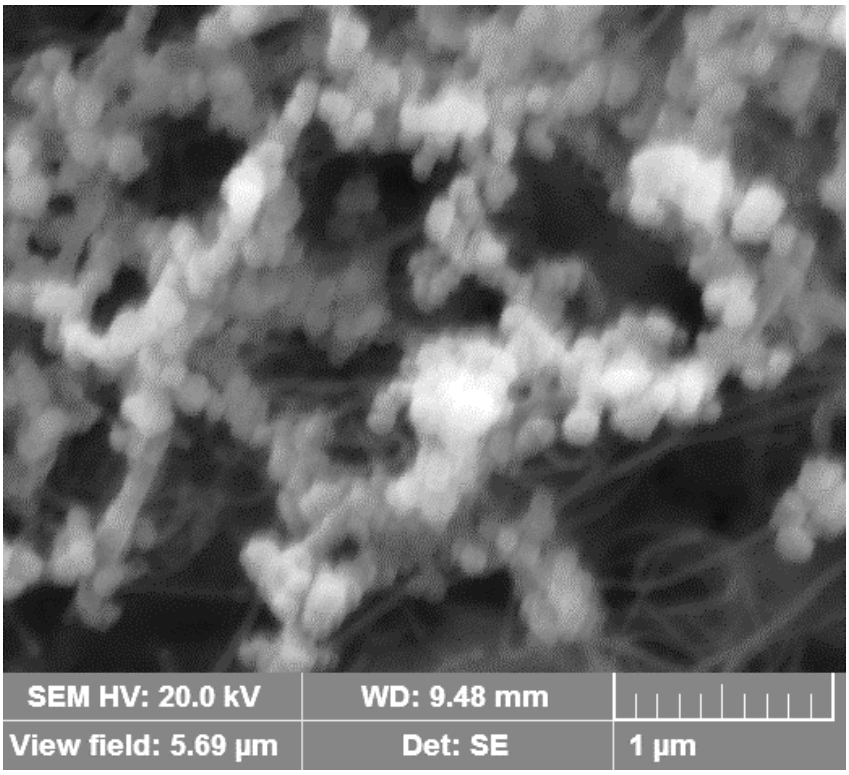

Figure 16: SEM micrographs show CNTs growth on silver metal at for a period of 10 min (upper) and 30 min (lower).
C_2H_2: H_2 flow rate ratio is 75:90 sccm. Reaction temperature is 800°C

4.2 Transmision Electron Microscopic Analysis

Scanning electron microscopy of the carbon nanotubes grown on the silver metal revealed that they are multiwalled with inner and outer diameter of about 10 nm and less than 20 nm respectively as shown in Figure 17.

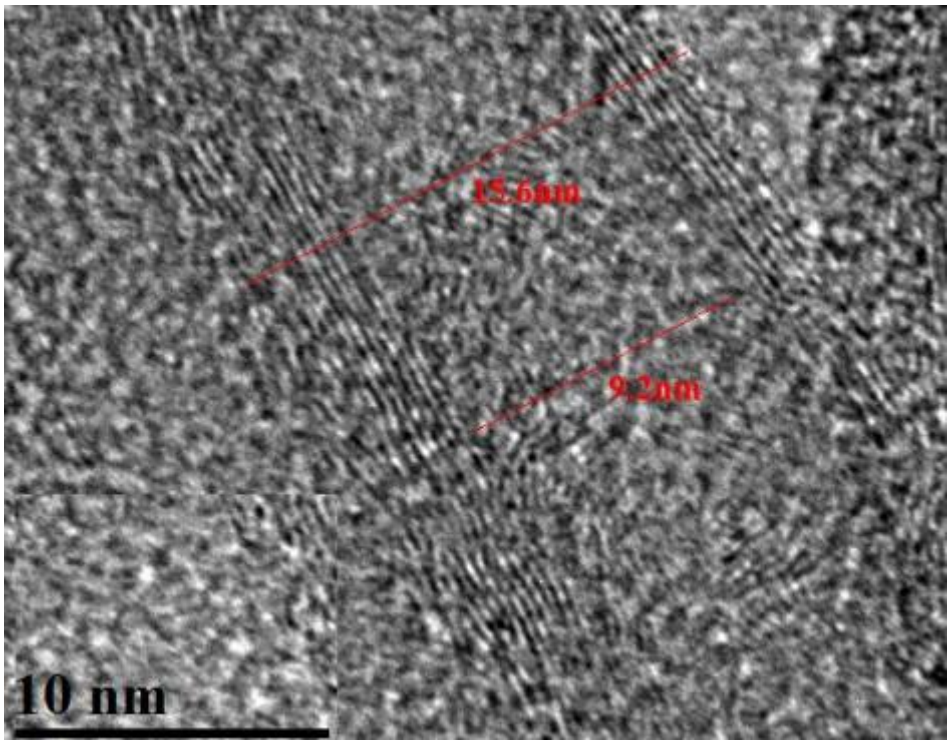

Figure 17: TEM micrograph of multiwall carbon nanotube grown on the silver metal surface

4.3 Raman Study for the Crystallinity of the Grownn CNTs on Silver Metal

Attempts to use Raman spectroscopy for purity assessment have relied upon D-band to G-band peaks ratio to deduce the purity level of CNTs. However, carbon impurities affect the intensity of these two peaks which may result in poor interpretation of the data when there is no reference available for the sake of comparison. So, G′-band peak (~2700 cm^{-1}) may represent a more accurate measurement of MWNT quality or purity, since it is dramatically enhanced by carbon nanotubes [58]. D-band (~1350cm^{-1}) is due to the distorted sp^2 carbon of non-nanotube graphitic components and indicates the presence of impurities [145].

Here, Raman spectra using the 632.8 nm line of a He-Ne laser for CNTs grown on the surface of silver metal at different temperatures are shown in Figure 18 in order to confirm the effect of changing conditions on the quality of the grown CNTs in terms of purity and graphitization. At 700°C, the D-band peak at~1325 cm^{-1} is of high intensity compare to the G-band one at~1580 cm^{-1} while no significant peak around 2655 cm^{-1}. Increasing growth temperature to 750 and 800°C revealed an enhancement of G′-band at~2655cm^{-1} and decrease in the D-peak intensity indicating the formation of CNTs with well graphitization with the least amount of other carbon species. Despite this, even at the optimum conditions there was either some defect in the graphitization of the CNTs or presence of impurities. The incearse of the degree of the graphitization leads to a decrease in resistivity and increase in the metallic conductivity of the multiwalled carbon nanotube [37] which is highly required for electrodes.

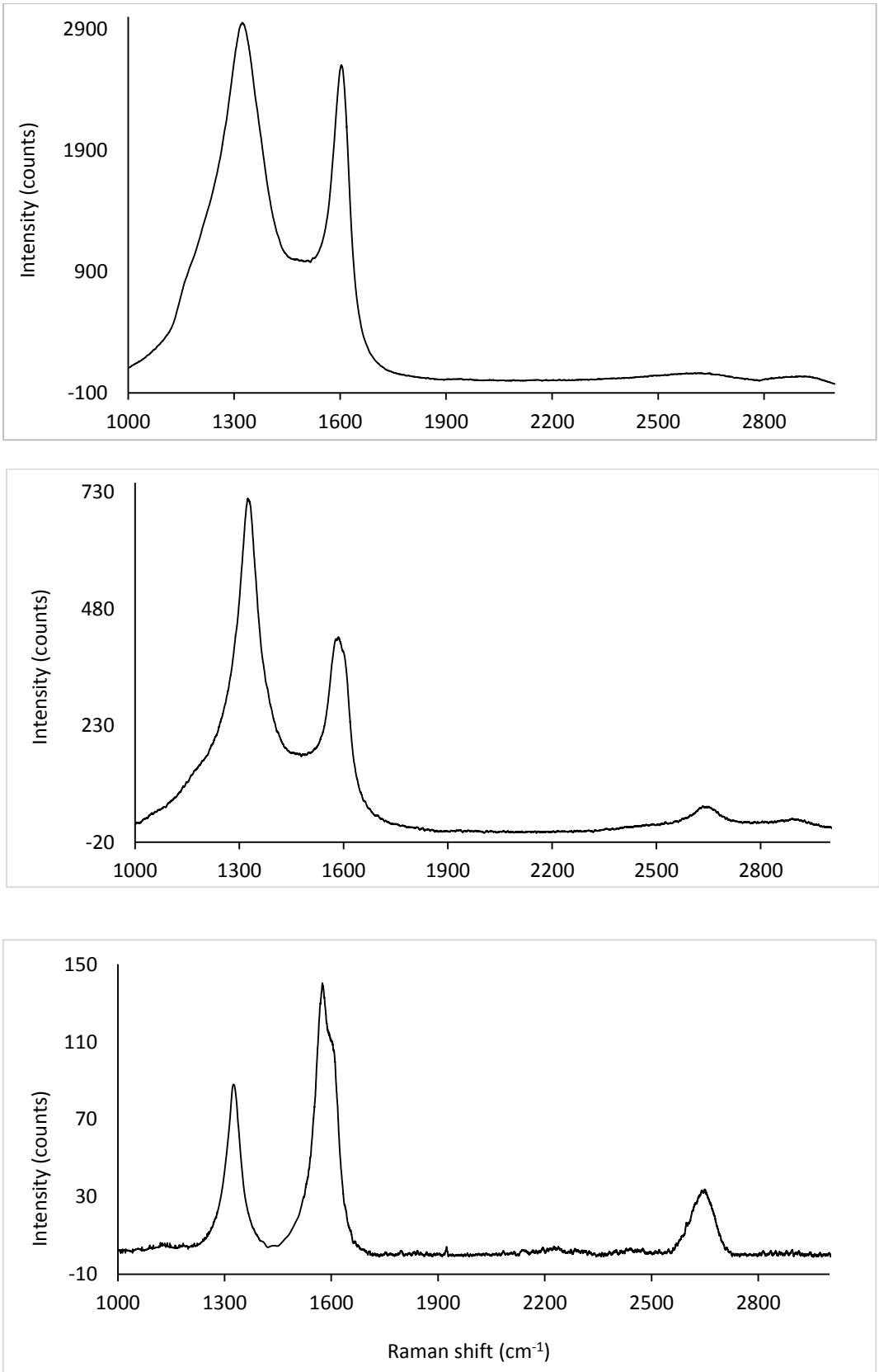

Figure 18: Raman spectra for the surface of the CNTs/silver electrode prepared by CVD at temperatures: 700 (a) 750°C (b) and 800°C (c). C_2H_2: H_2 flow rate ratio is 75:90 sccm. Reaction time is 20 min.

CHAPTER 5

RESULTS AND DICUSSION (II)

5.1 Applications of the Prepared Ag/CNTs Electrodes in Zero Current Potentiometric Titrations

5.1.1 Titration of Ascorbic Acid with Potassium Iodate

Ag/CNTs electrodes were successfully applied and showed excellent response as an indicator electrode to the normal potentiometric titration. Different concentrations of ascorbic acid, in 20ml of 0.1mol/L sulfuric acid, were titrated with potassium iodate. Figure 19 and Figure **20** exhibit the change in potential, during the addition of iodate ions, against silver/silver chloride reference electrode along with the first derivative curve. The plots obtained have a standard sigmoidal shape with a sharp break point demonstrating the expected stoichiometry.

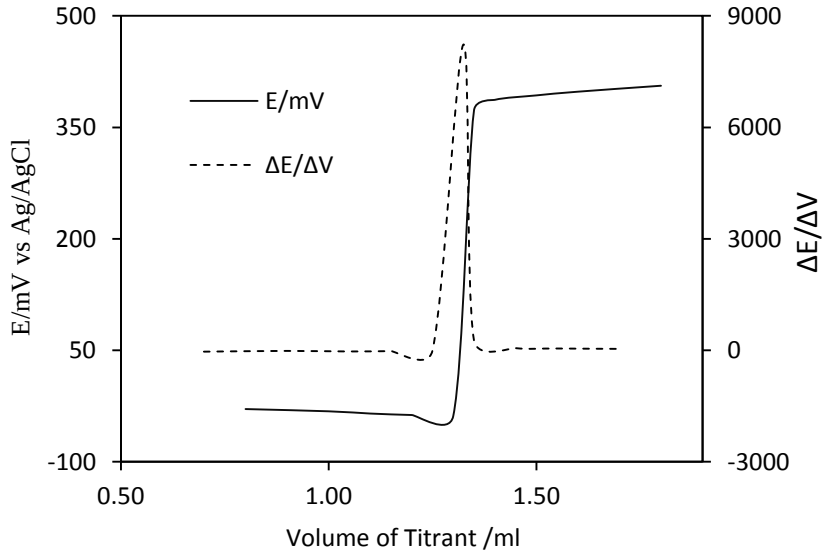

Figure 19: potentiometric titration curve and its first derivative for titration of 2.0 ml of 0.02 mol/L ascorbic acid with 0.01 mol/L potassium iodate in 20 ml of 0.1mol/L sulfuric acid

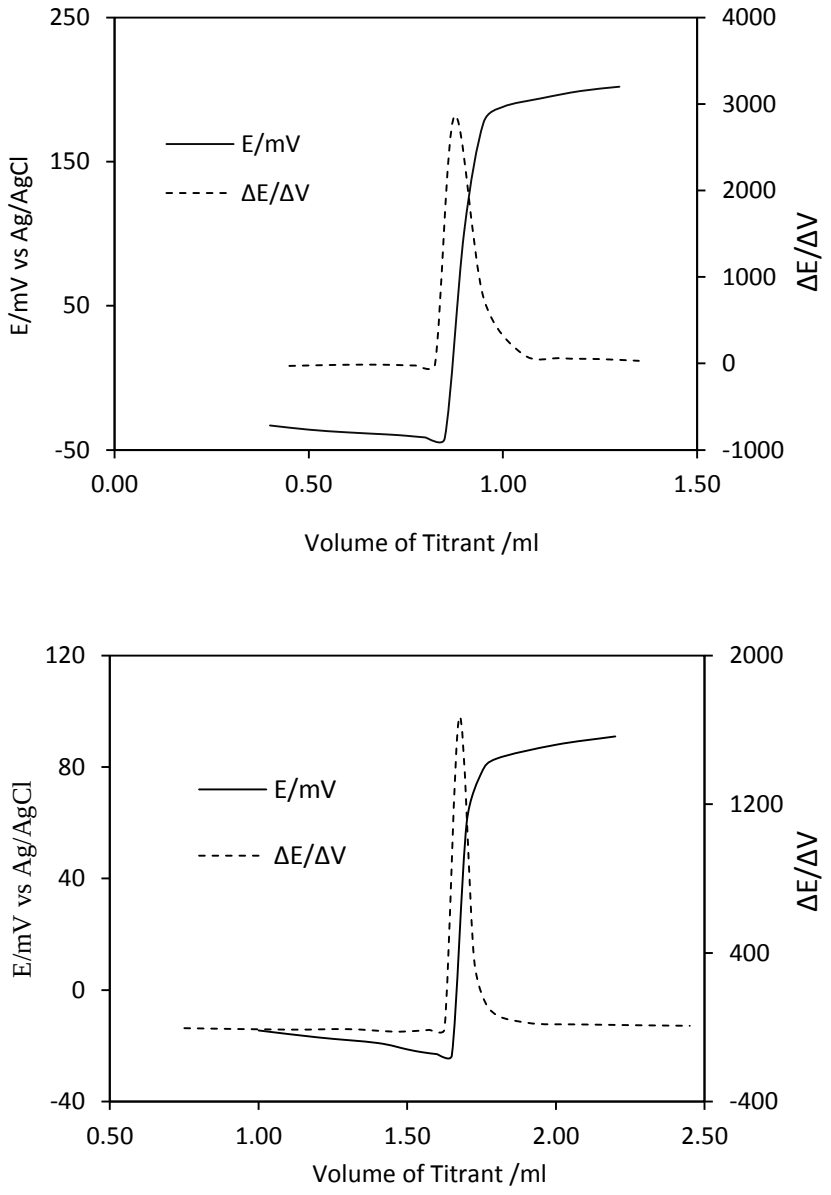

Figure 20: potentiometric titration curve and its first derivative for titration of 0.50 ml of 0.02 mol/L ascorbic acid with 0.01 mol/L potassium iodate (upper) and 0.40 ml of 0.01 mol/L ascorbic acid with 8.0×10^{-4} mol/L potassium iodate (lower), in 20 ml of 0.1mol/L sulfuric

5.1.2 Titration of Calcium Ions with EDTA

Calcium ions were titrated against standard EDTA solutions in borate buffer (pH 9.5) in the presence of trace silver ions, Ag^{+}, using Ag/CNTs as a working electrode. The potential of the working electrode was measured during the titration against the standard silver/silver chloride reference electrode. Different concentrations of calcium ions were titrated. The zero – current potentiometric curves have shown the S shape and the end point was located by finding the first derivative of these curves as shown in Figure 21.

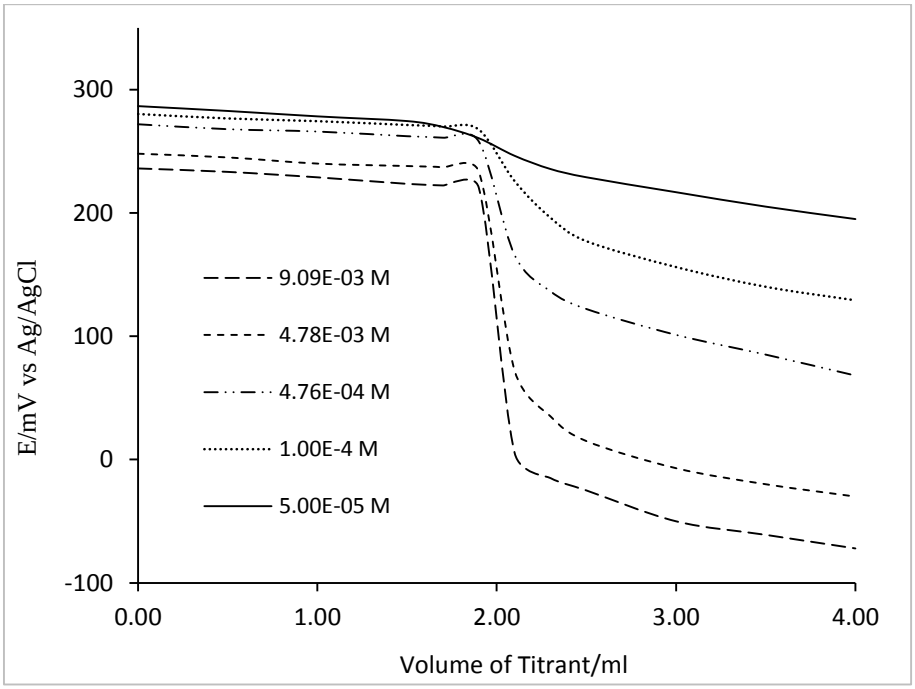

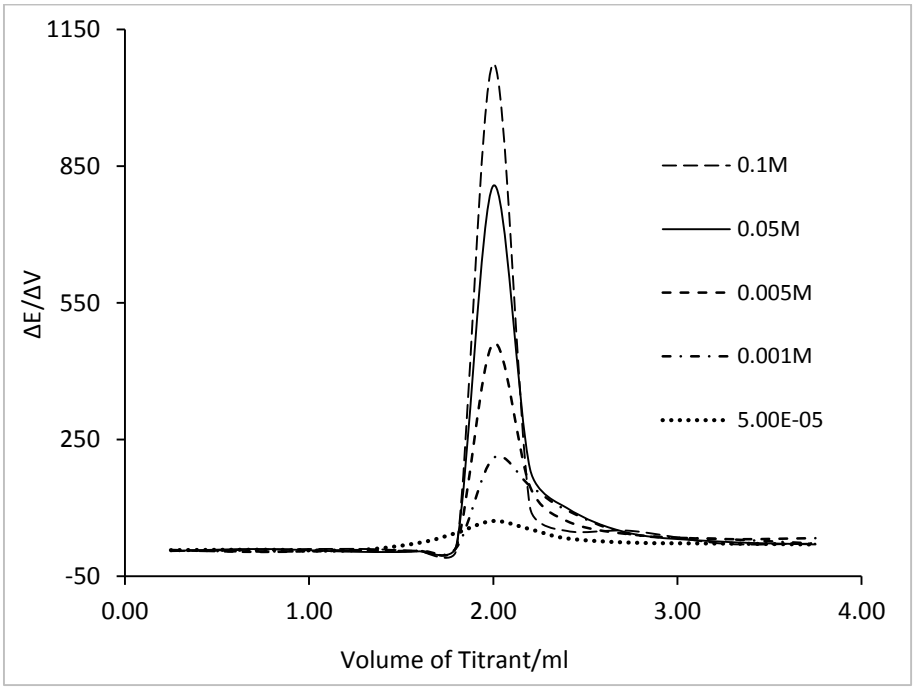

Figure 21: potentiometric titration curves (upper) and their first derivatives (lower) for titration of 20ml of Ca^{+2} with of 10-fold more concentrated EDTA, at pH 10

5.1.3 Titration of Chloride Ions with Silver nitrate

The prepared Ag/CNTs electrode has used in potentiometric titrations of chloride with silver ions in aqueous solutions. The potential of the working electrode was recorded against the silver – silver chloride reference electrode. The end point of the titration was located for different concentration of chloride. The potentiometric curves obtained have the standard S shape and the first derivative curves were obtained for the ease of end point location as they are shown in Figure 22.

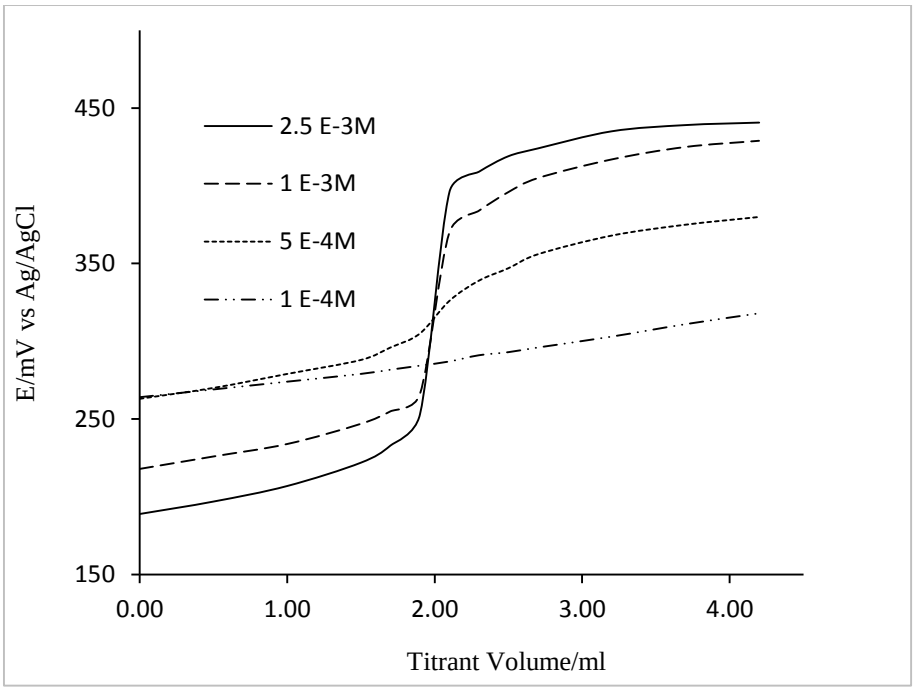

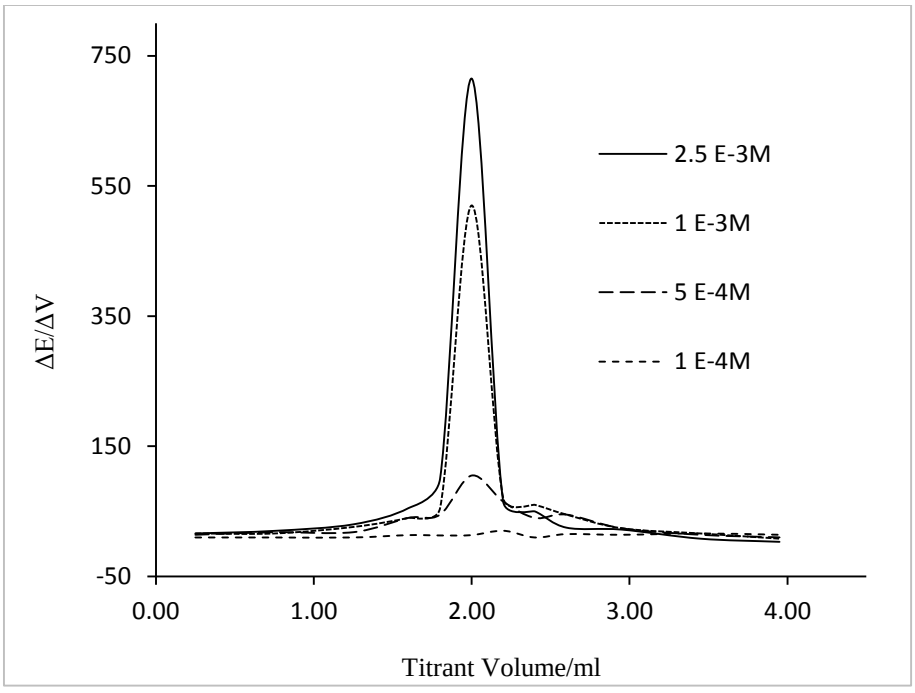

Figure 22: potentiometric titration curves (upper) and their first derivatives (lower) for titration of 20ml of Cl^-, in 0.1mol/L of KNO_3, with of 10-fold more concentrated silver nitrate

CHAPTER 6

RESULTS AND DICUSSION (III)

6.1 Applications of the Prepared Ag/CNTs Electrodes in Mark-Space DEP Titrations

6.1.1 Determination of Ascorbic Acid

The prepared Ag/CNTs electrodes have revealed an excellent performance in the DEP oxidation – reduction determination of ascorbic acid. They have shown fast response and good sensitivity which can be attributed to the CNTs coating that facilitate interfacial electron transfer.

Effect of Bias and Concentration change

A solution of 2.00x×10^{-3} mol.L^{-1} of ascorbic acid in 0.1 mol.L^{-1} sulfuric acid was titrated with 1.00×10^{-2} mol.L^{-1} potassium iodate using the prepared electrodes polarized by different biases ranging from 0 – 20% to find the optimum bias in terms of peak intensity and shape. From the bias optimization, Figure 23, no significant change in the differential peak shape or intensity was obtained. However, a bias of 10% was found to be the best. Different concentrations of standard ascorbic acid were then titrated using the optimum bias conditions. It was found that the peaks become broader as the concentration of ascorbic acid decreases, Figure 24.

DEP Titration Method Validation

Method validation is a process of proving that an analytical method is acceptable for its intended purpose. In pharmaceutical chemistry, method validation requirements for

regulatory submission include studies of method specificity, linearity, accuracy, precision, range, limit of detection, limit of quantitation, and robustness [146].

Linearity

A standard calibration curve was established with standard ascorbic acid solutions containing 4.00×10^{-2}, 1.00×10^{-2}, 2.00×10^{-3}, 1.00×10^{-3} and 5.00×10^{-4} mmole. Triplicate titrations were performed for each calibration point. The linear regression line between the amounts of ascorbic acid added and the amounts measured was obtained using Microsoft Excel while Origin Pro 8 software was employed to locate end points from peaks maxima. The linear regression analysis showed an excellent linearity in terms of the square of the correlation coefficient, R^2, and the y-intercept, Figure 25, [146] and its linear range covers the concentration of the analyte normally found in food and drug samples. Table 1 shows the analytical data.

Precision and Accuracy

Intra-assay and instrument precision were evaluated by analyzing aliquots of standard ascorbic acid solutions for three times. The method showed good reproducibility expressed in term of percent coefficient of variation, CV (%) and also showed high accuracy and recovered good percentage of the standard analyte spiked, Table 1.

The same standard ascorbic acid solutions were analyzed by a normal titration against standardized 0.0466 $mol.L^{-1}$ iodine solution using starch indicator, according to the USP [139], in order to compare with DEP titration for validation. The results obtained, Table 1, agree fairly well with those obtained by DEP titrations.

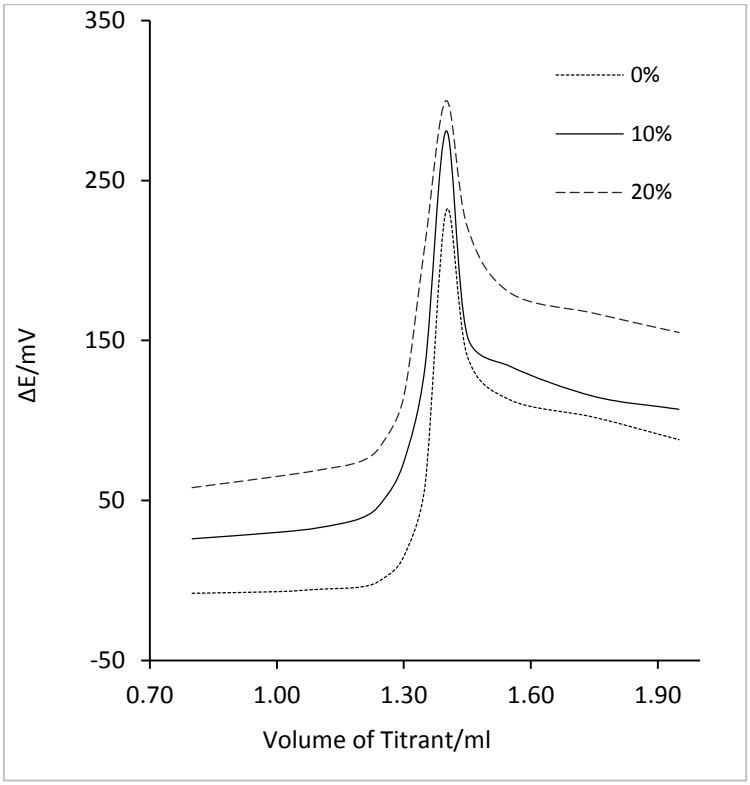

Figure 23: Effect of bias change on the DEP peak intensity for ascorbic acid (0.02 mol.L^{-1}) in 0.1 mol.L^{-1} H_2SO_4 titrated with potassium iodate solution.

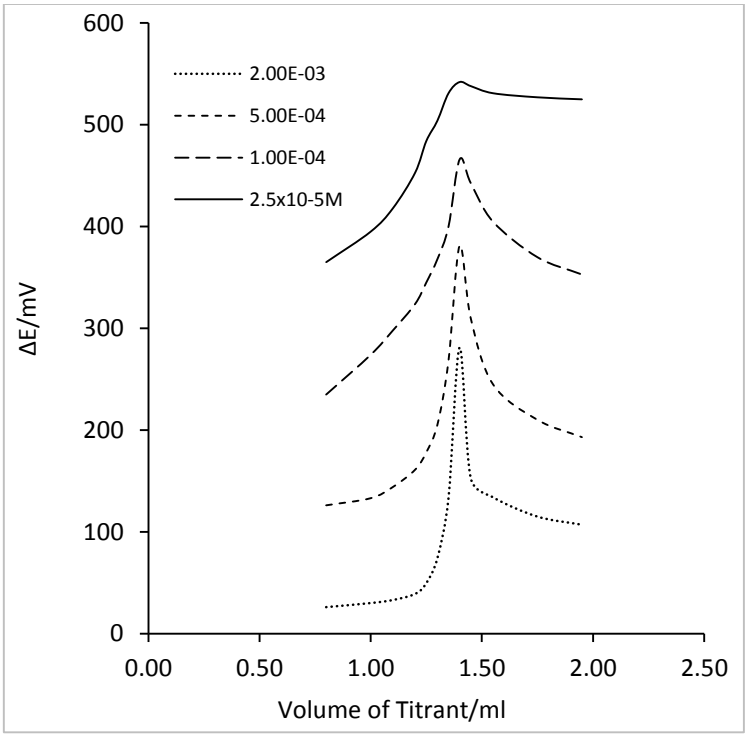

Figure 24: m.s.b DEP titration peaks of different concentration of ascorbic acid.

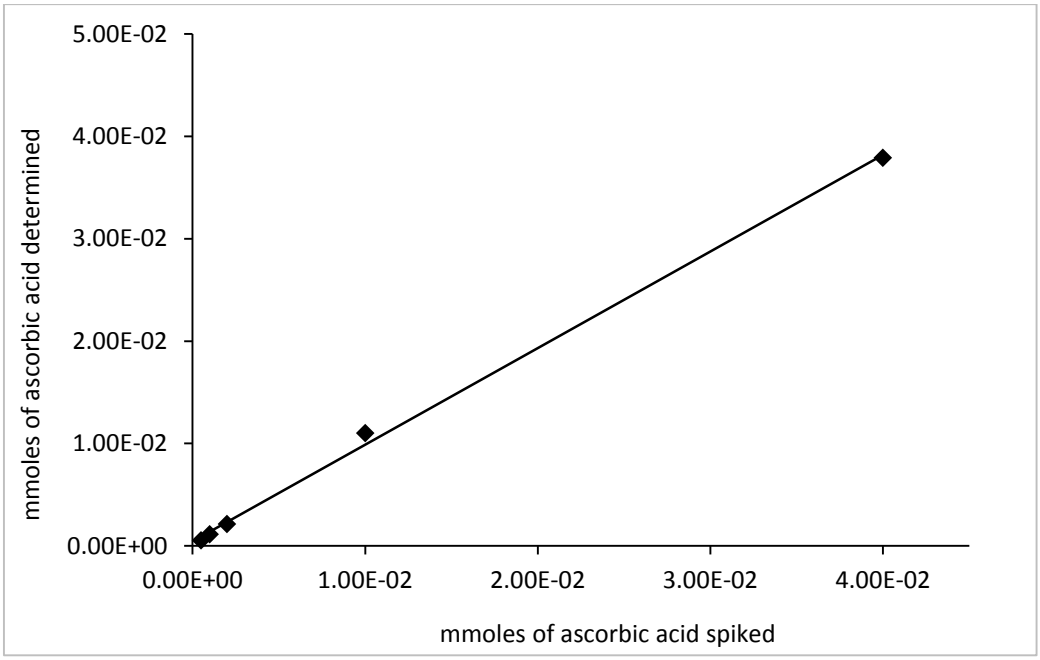

Figure 25: Standard calibration curve of m.s.b DEP titration of ascorbic acid with potassium iodate.

Table 1: Analytical parameters for DEP determination of ascorbic acid in 0.1 mol.L^{-1} sulfuric acid by Ag/CNTs electrodes and comparison against reference iodimetric titration. The number of measurements is 3

Ascorbic acid spiked (mmole)	DEP Titration method						Iodimetric Titration method	
	Ascorbic acid detected (mmole)	Recovery (%)	RSD (%)	Calibration parameters			Ascorbic acid detected (mmole)	Relative error (%)
				Slope	y-intercept	R^2		
4.00×10^{-2}	4.06×10^{-2}	101.4	2.6	0.996	5.00×10^{-5}	0.996	$3.93\text{x}10^{-2}$	3.2
1.00×10^{-2}	1.03×10^{-2}	103.1	2.4				9.73×10^{-3}	4.4
2.00×10^{-3}	2.04×10^{-3}	102.0	2.9				1.98×10^{-3}	3.0
1.00×10^{-3}	1.04×10^{-3}	103.9	4.2				1.01×10^{-3}	2.8
5.00×10^{-4}	4.83×10^{-4}	96.7	3.7				5.05×10^{-4}	-4.4

Determination of ascorbic Acid in Real Samples

(a) In Baobab Fruit

Because of the complex chemical composition of Baobab fruit pulp [118], and in order to perform the analysis of ascorbic acid with minimum interference effect from matrix, the standard addition calibration method was applied. The amounts of analyte spiked into sample solutions were 2.00×10^{-3}, 1.00×10^{-2}, $5.00x\times10^{-2}$ and 1.00×10^{-1} mmol. DEP titration peaks, Figure 26, were obtained from which an excellent linear relation was established as in Figure 27. Other analytical data are shown in Table 2.

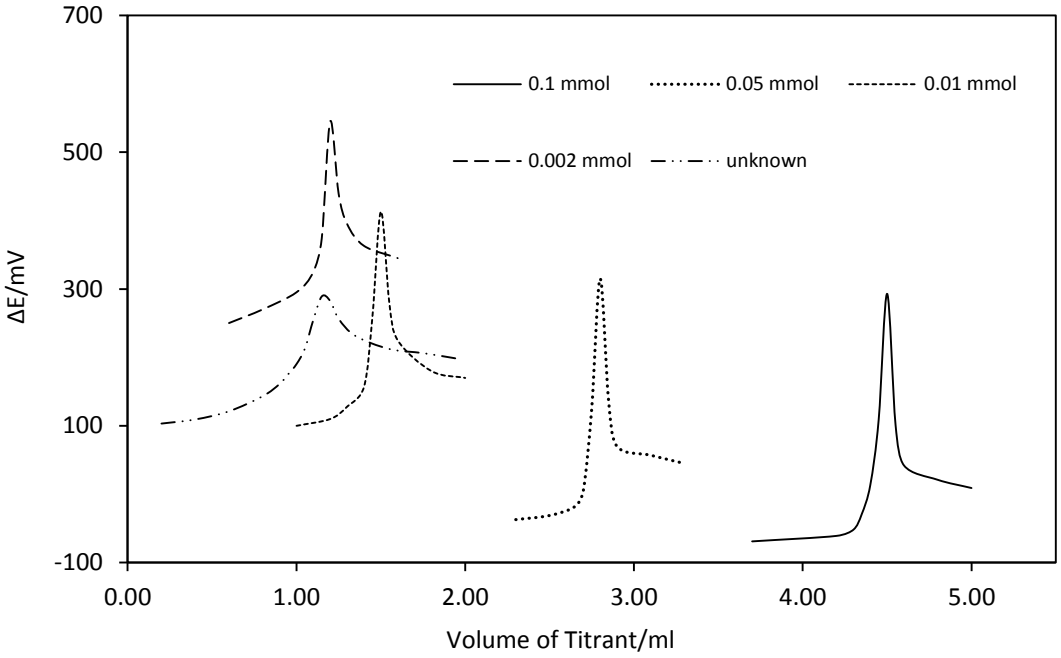

Figure 26: DEP titration peaks for the standard addition calibration for ascorbic acid in Baobab fruits against 0.01mol.L^{-1} potassium iodate.

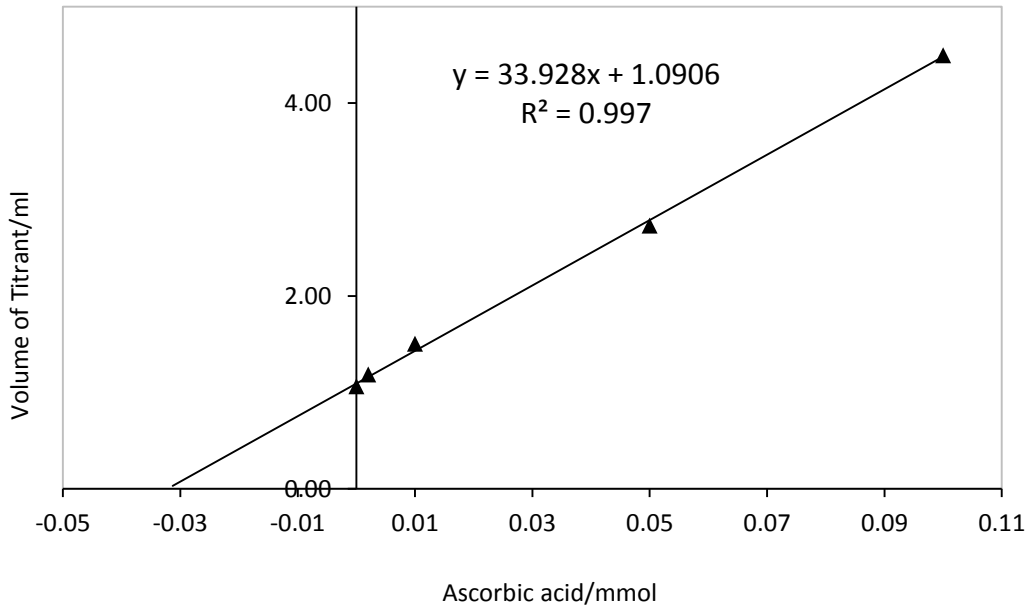

Figure 27: Standard addition calibration for DEP titration of ascorbic acid in Baobab fruits

(b) In Drug Formulation

Ascorbic acid content in Redoxon® tablets was successfully determined by this method as shown in Figure 28. Other data are shown in Table 2.

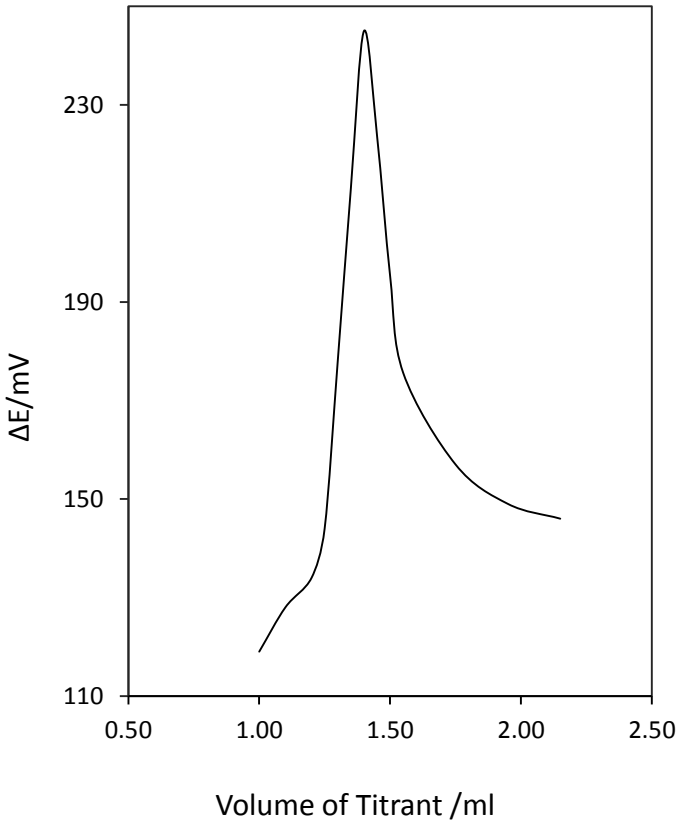

Figure 28: DEP peak for ascorbic acid in Redoxon, titrated with 0.01mol.L^{-1} potassium iodate.

Table 2: Analytical parameters for DEP determination of ascorbic acid in Baobab fruit pulp and in Redoxon tablets by Ag/CNTs electrodes.

Sample	Sample mass (g)	Ascorbic acid spiked (mmole)	Expected amount of ascorbic acid	Detected amount of ascorbic acid	Calibration parameters		
					Slope	y-intercept	R^2
Baobab fruit powder	2.05	0.00	300mg/100g	279mg/100g	33.93	1.09	0.999
		2.00×10^{-3}					
		1.00×10^{-2}					
		5.00×10^{-2}					
		1.00×10^{-1}					
Redoxon® tablets	0.032	0.00	1000mg/tablet	1040mg/tablet	-		

6.1.2 Determination of Lead (II)

Effect of Bias and Concentration change

Different biases ranging from 0 – 30% were applied to a solution of 5.00×10^{-3} Pb^{+2} in 20 ml acetate buffer (pH 5.5) and titrated against 5.00×10^{-2} EDTA. The results obtained revealed that as the % bias increases, the DEP intensity increases, without symmetry loss in the peak shape, up to 20%. However, beyond 20% the peaks tend to be broad, as depicted in Figure 29 which is not good when very dilute solutions are analyzed. So a percentage bias of 20% was selected as an optimum bias for this kind of determination.

Optimum bias was applied to titrate other dilute concentration of Pb^{+2} under the same conditions. Figure 30 exhibits the DEP titration peaks for different concentrations of Pb^{+2}. Titration end points obtained demonstrate the expected reaction stoichiometry between metal ions and EDTA.

Lead (II) ions in aqueous solutions have been successfully determined through back titration of the excess EDTA with standard Ca^{+2} in borate buffer (pH 9.2). This technique is usually employed when the reaction is slow. Figure 31 exhibits the DEP curves for the titration of excess EDTA with Ca^{+2}.

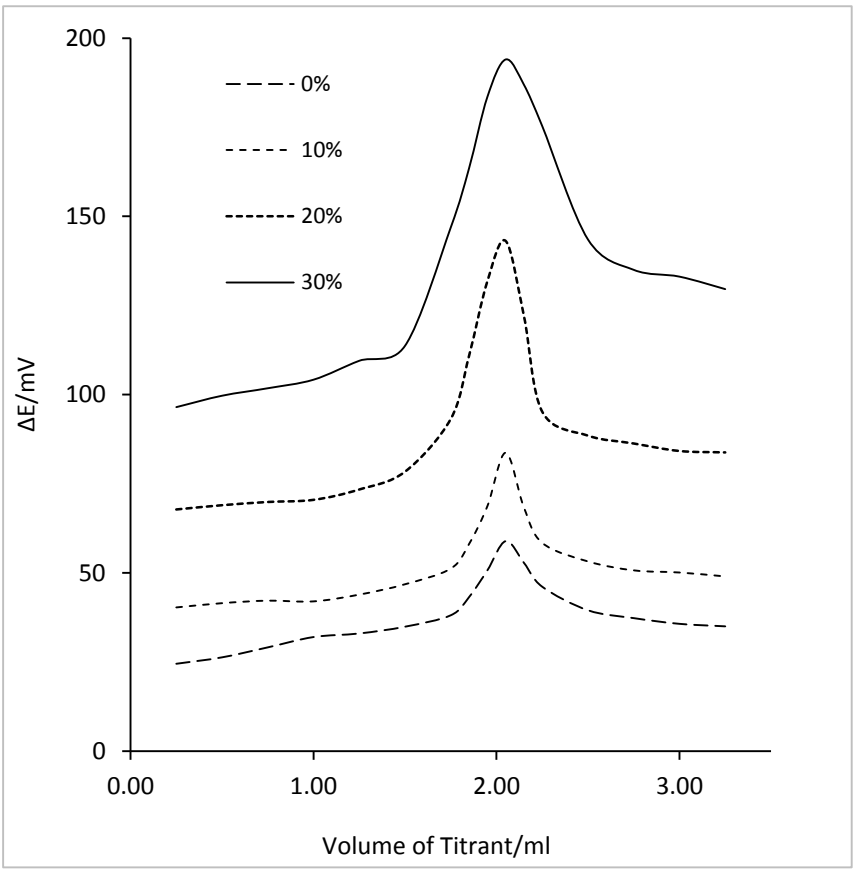

Figure 29**:** Effect of bias change on the DEP peak for $5.00x10^{-3}$ $mol.L^{-1}$ Pb^{+2} titrated with 5.00×10^{-3} $mol.L^{-1}$ EDTA in pH 5.5 (acetate buffer)

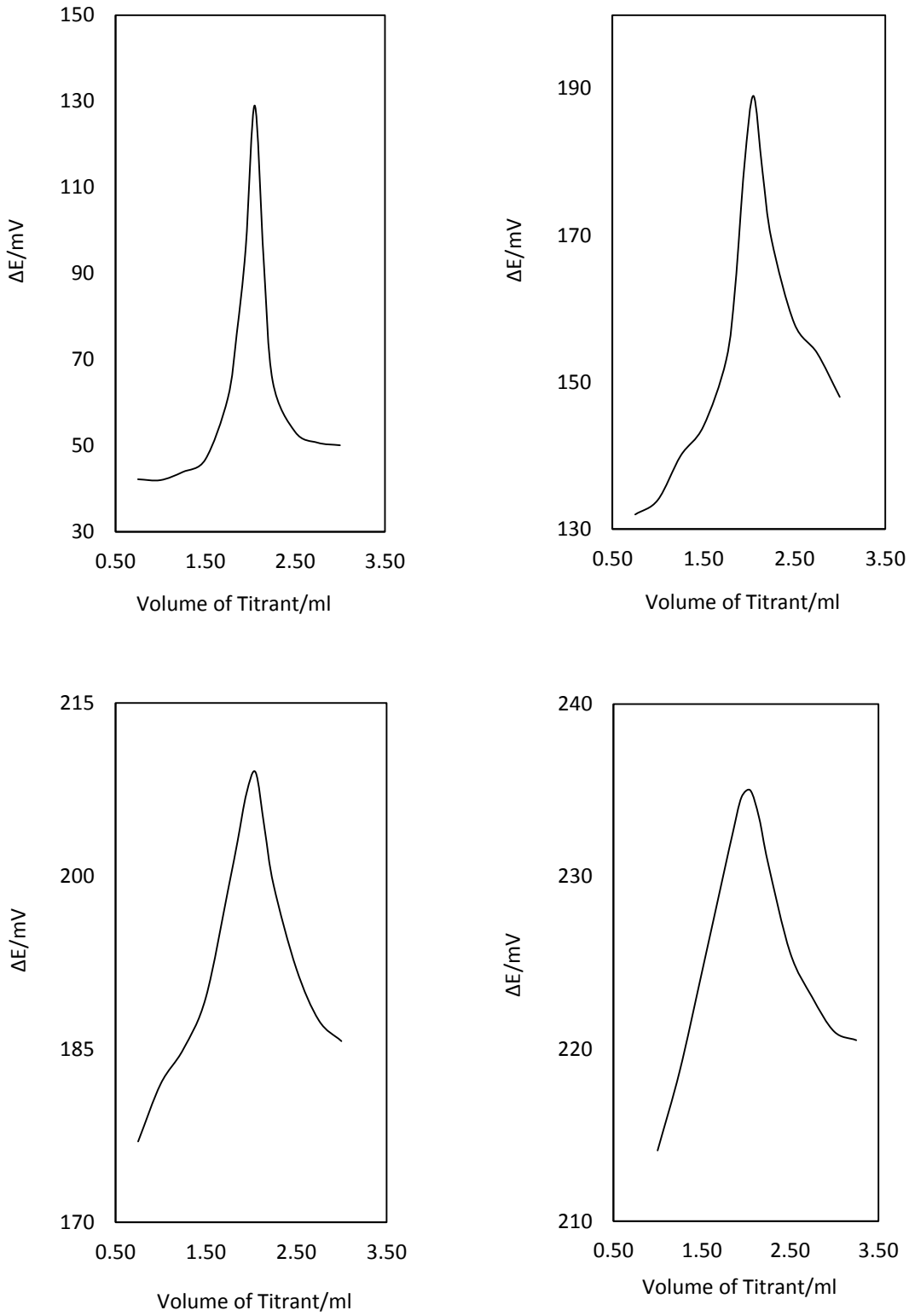

Figure 30: DEP titration curves for 2.00 ml of different concentrations of Pb^{+2}: 1.00×10^{-2} (a), 5.00×10^{-4} (b), 5.00×10^{-5} (c) and 1.00×10^{-5} mol/L (d) against EDTA of 10-fold concentration

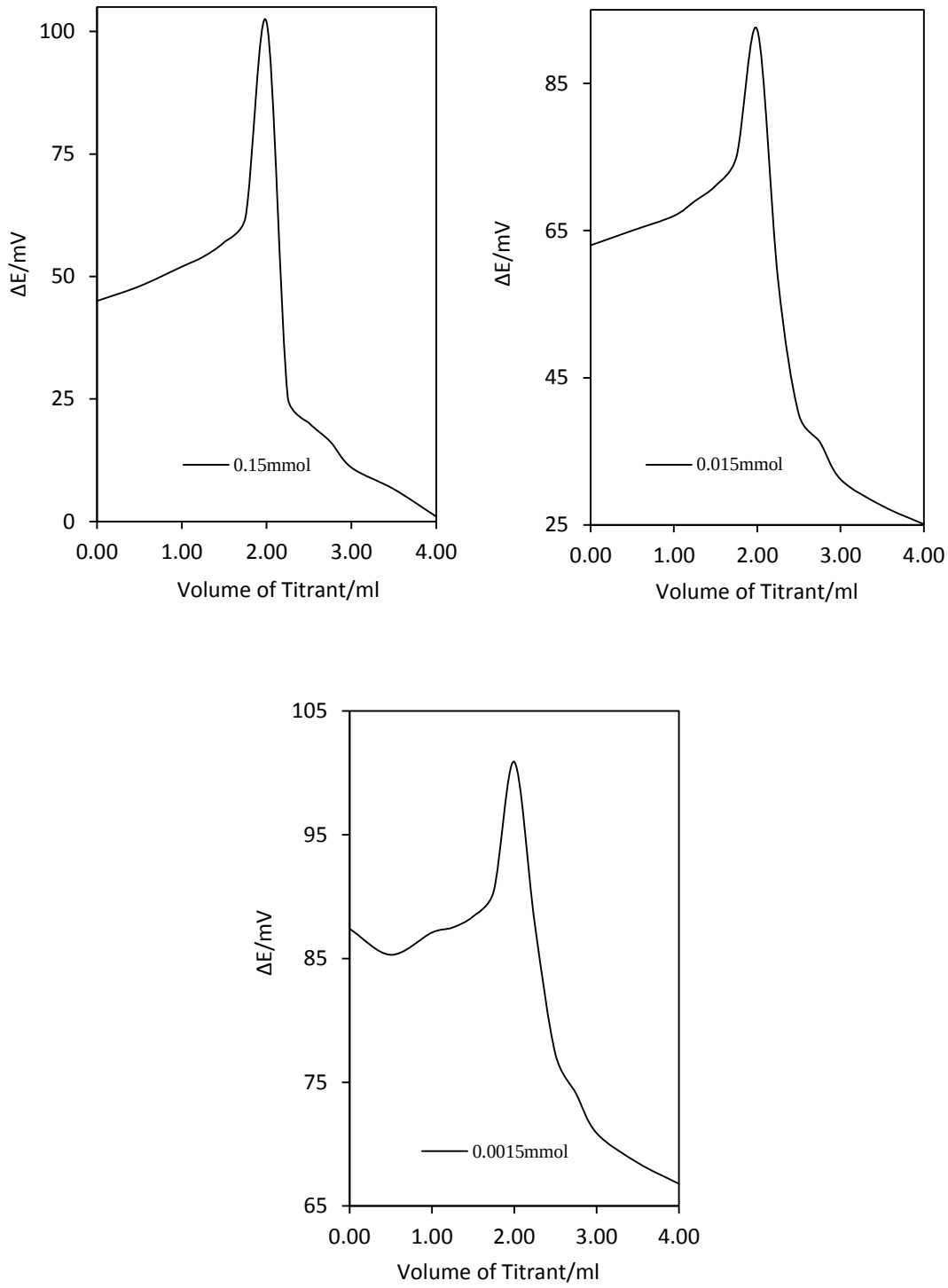

Figure 31: DEP curves for determination of Pb^{+2} by addition excess EDTA and back titration with Ca^{+2} at pH 9.2 (borate buffer). Pb^{+2} amount is shown on the plot. Amount of EDTA added and concentrations of Ca^{+2} as titrant are respectively: 0.25 mmol, 0.05 mol/L (upper left), 0.025 mmol, 0.005 mol/L (upper right) and 0.0025 mmol, 0.0005 mol/L (lower). Total volume in titration vessel ranges between 20.9 and 26.7 ml.

DEP Titration Method Validation

Linearity

A standard calibration curve was established with standard Pb^{+2}. Triplicate titrations were performed for each calibration point. The linear regression line between the concentrations of Pb^{+2} added and concentrations measured was obtained using Microsoft Excel while Origin Pro 8 software was employed to locate the end points from peaks maxima. The linear regression analysis exhibited excellent linearity in terms of the square of the correlation coefficient, R^2, and the y-intercept, Figure 32, [146] and its linear range covered the concentrations 1.00×10^{-2} to 5.00×10^{-5} mol/L. Table 3 shows other analytical data.

Precision and Accuracy

Intra-assay and instrument precision were evaluated by analyzing aliquots of standard Pb^{+2} solutions for three times. The method showed good reproducibility expressed in terms of percent coefficient of variation, CV (%) with good accuracy and good percentage recovery of the standard analyte spiked, Table 3.

The same standard Pb^{+2} solutions were analyzed by atomic absorption spectrometry in order to compare the results obtained with DEP titrations for validation. The results obtained, Table 3, were in agreement with the data obtained by DEP titrations.

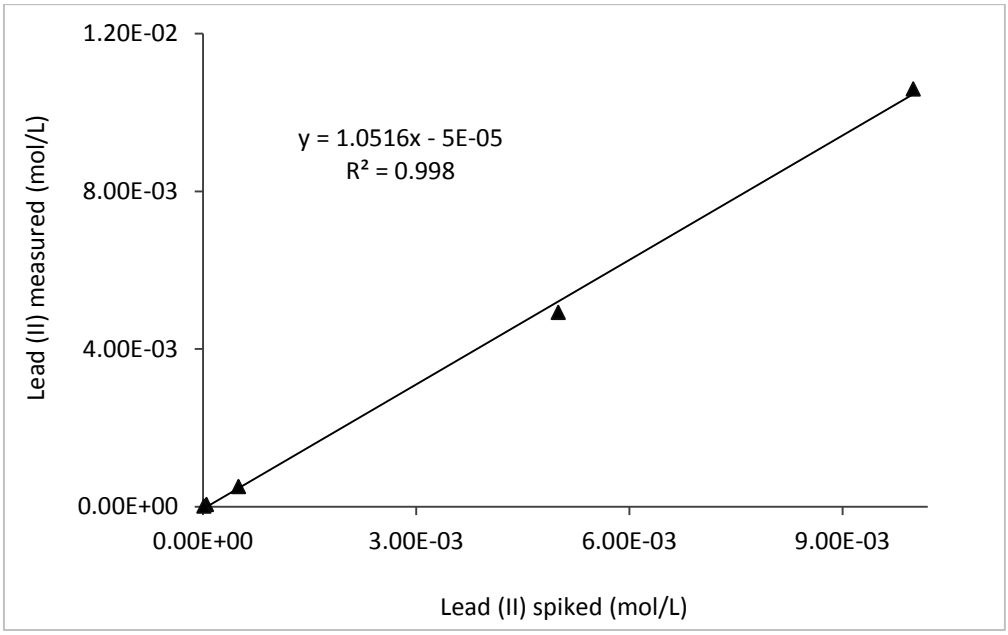

Figure 32: Standard calibration curve of DEP titration of lead (II) against EDTA in acetate buffer (pH 5.5)

Table 3: Analytical parameters for DEP determination of lead (II) in 0.1 mol.L^{-1} acetate buffer (pH 5.5) by Ag/CNTs electrodes and comparison against reference atomic absorption spectrometry. The number of measurements is 3

Pb (II) added (mol/L)	DEP Titration method						AAS method	
	Pb (II) detected (mol/L)	Recovery (%)	RSD (%)	Calibration parameters			Pb (II) detected (mmol/L)	Relative error (%)
				Slope	y-intercept	R^2		
1.00×10^{-2}	1.06×10^{-2}	106.0	2.4	1.06	5.00×10^{-5}	0.998	1.02×10^{-2}	3.9
5.00×10^{-3}	4.93×10^{-3}	98.6	2.9				4.76×10^{-3}	3.6
5.00×10^{-4}	5.09×10^{-4}	101.8	3.5				4.83×10^{-4}	5.4
5.00×10^{-5}	5.21×10^{-5}	104.2	3.2				4.85×10^{-5}	7.4
1.00×10^{-5}	1.09×10^{-5}	109.0	5.1				9.81×10^{-5}	11.1

The Life Time of the Prepared Ag/CNTs Electrode

The lifetime of the fabricated CNT/Ag electrodes was evaluated for a period of 11 weeks through a DEP titration of 5.00×10^{-3} Pb^{+2} with EDTE in pH 5.5. During this period they were used to perform about 60 titrations. Figure 33 indicates the stability of the electrodes for long time and the successful use without any deterioration of the response or shift in the peak location during this period.

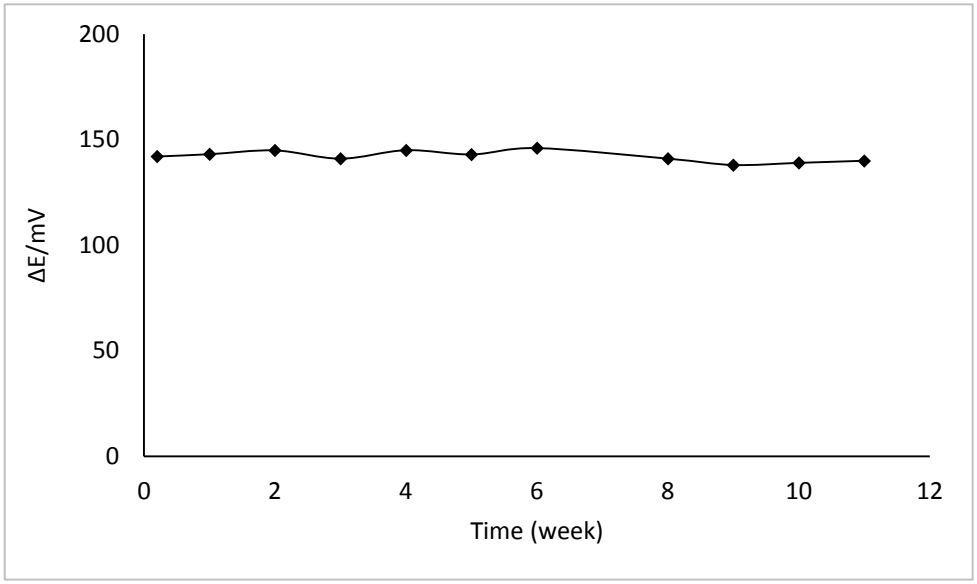

Figure 33: Response of CNT/Ag with time for DEP titration of 5.00×10^{-3} mol/L Pb^{+2} with EDTA at pH 5.5

6.1.3 Determination of Cyanide

Silver ions form a complex with the free cyanide (Eq. 1). Once all the free cyanide has been complexed with silver, further addition of silver ions then results in the precipitation of silver cyanide (Eq. 2). So in the potentiometric titration of free cyanide ions with silver ions, two end–points appear [188].

$$Ag^{+} + 2CN^{-} \rightarrow Ag(CN)_2^{-} \qquad Eq.1$$

$$Ag^{+} + Ag(CN)_2^{-} \rightarrow 2AgCN \qquad Eq.2$$

The first peak represent the complex formation and the second one corresponds to the precipitate formation. It was noticed that the increasing of the value of the polarizing direct current shifts the location of the first peak and the intensity of the second one was decreased as shown in Figure 34.

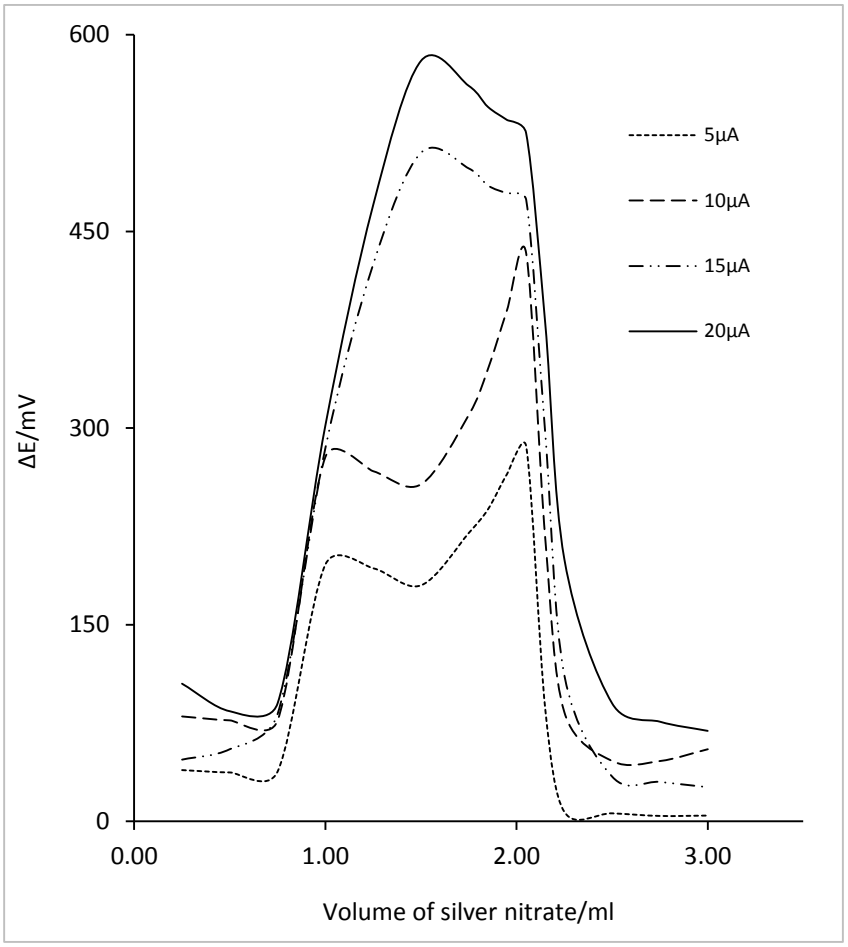

Figure 34: dc effect on the DEP curve for 5.00mL of 2.00x10-2mol.L^{-1} CN^-, in 20mL of 0.1 mol.L^{-1} KNO3, titrated with 5.00×10-2 mol.L^{-1} silver nitrate.

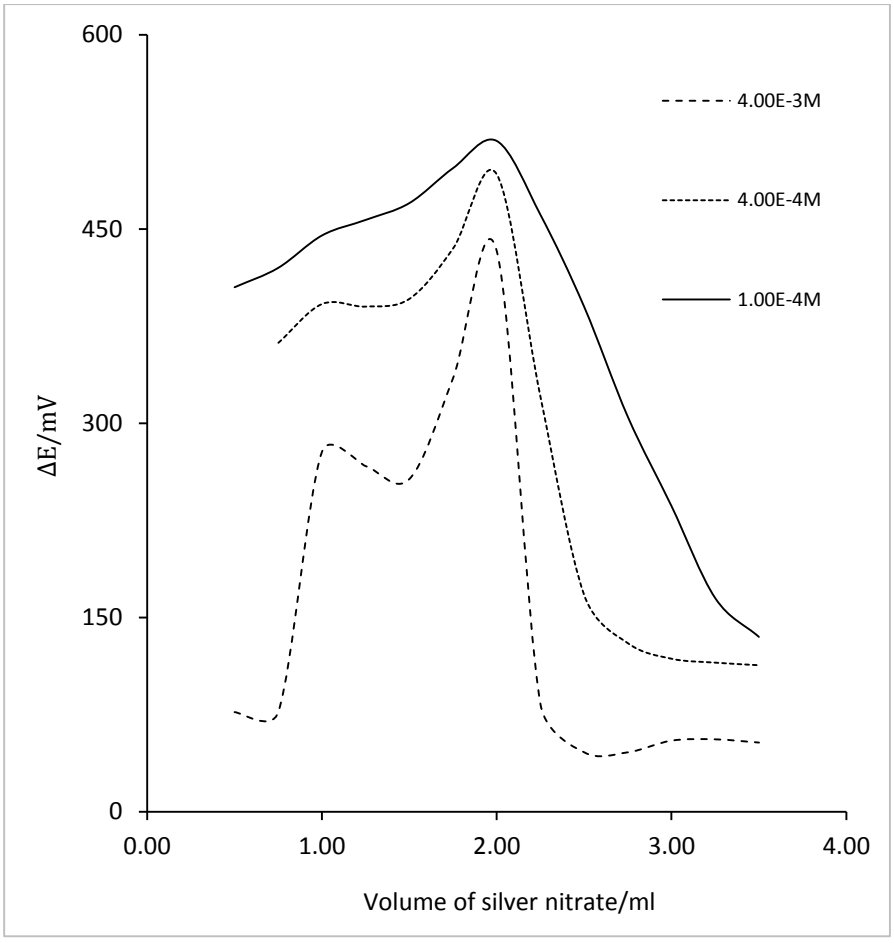

Figure 35: dc DEP curves of different concentration of CN^- in 0.1 $mol.L^{-1}$ KNO_3 titrated with silver nitrate solutions at current density of $10\mu Acm^{-2}$

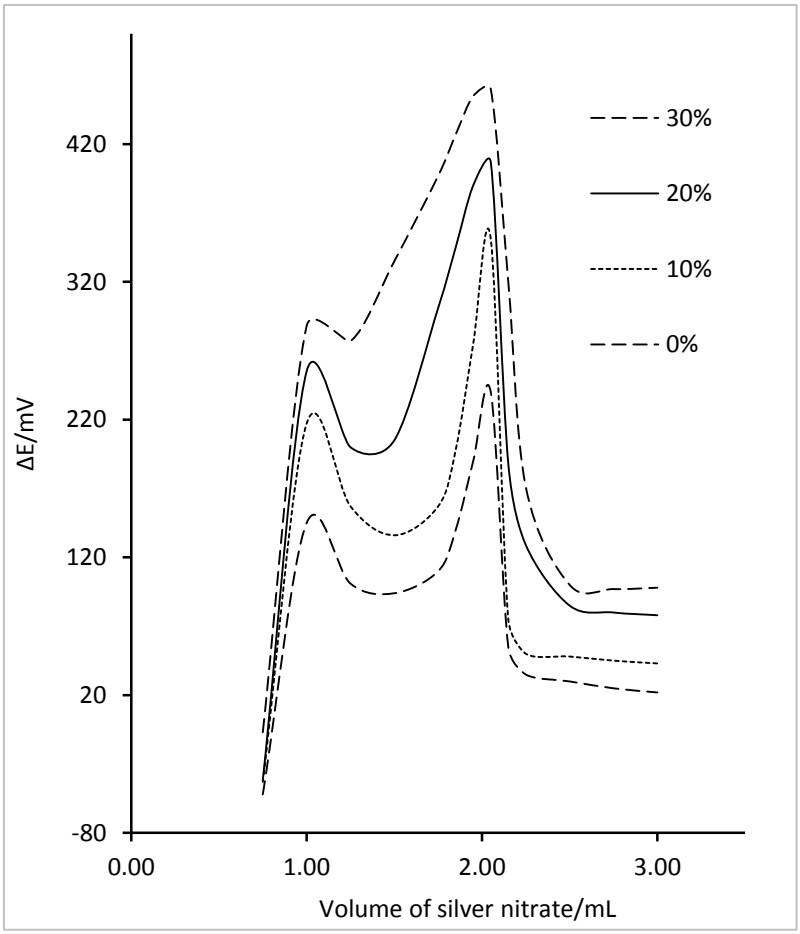

Figure 36: Effect of % bias change on the DEP curves intensity for 5.00 mL of $2.00x10^{-2}$ $mol.L^{-1}$ CN^-, in 20 mL of 0.1 $mol.L^{-1}$ KNO_3, titrated with 5.00×10^{-2} $mol.L^{-1}$ silver nitrate.

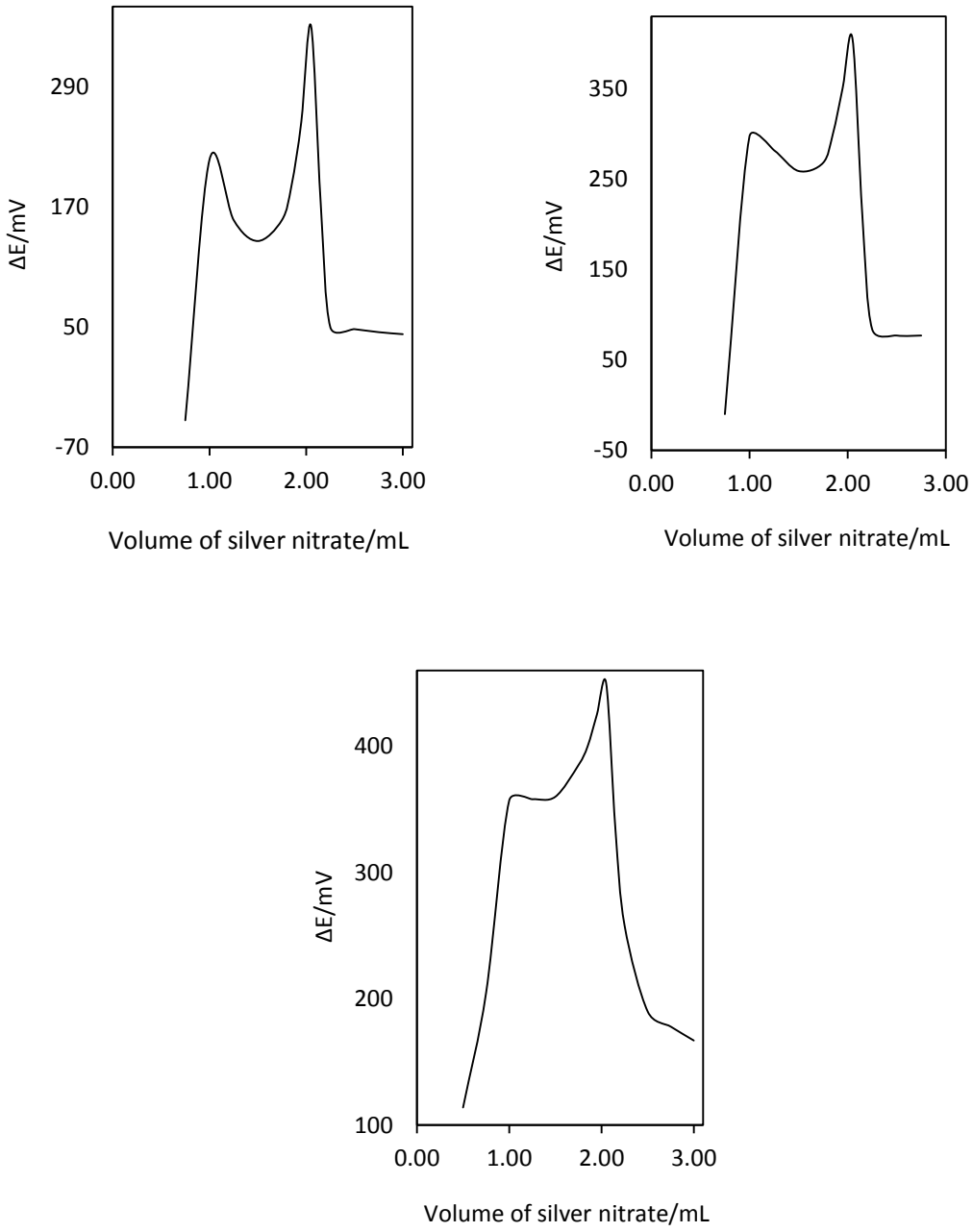

Figure 37: m. s. b. DEP titration curves of 5.00 mL of cyanide ions in 20 mL of 0.1 mol/L potassium nitrate. (1) 2.00×10^{-2} mol/L of CN^- titrated with 5.00×10^{-2} Ag^+ (upper left), (2) 8.00×10^{-3} mol/L of CN^- titrated with 2.00×10^{-2} Ag^+ (upper right) and (3) 8.00×10^{-4} mol/L of CN^- titrated with 2.00×10^{-3} Ag^+ (lower)

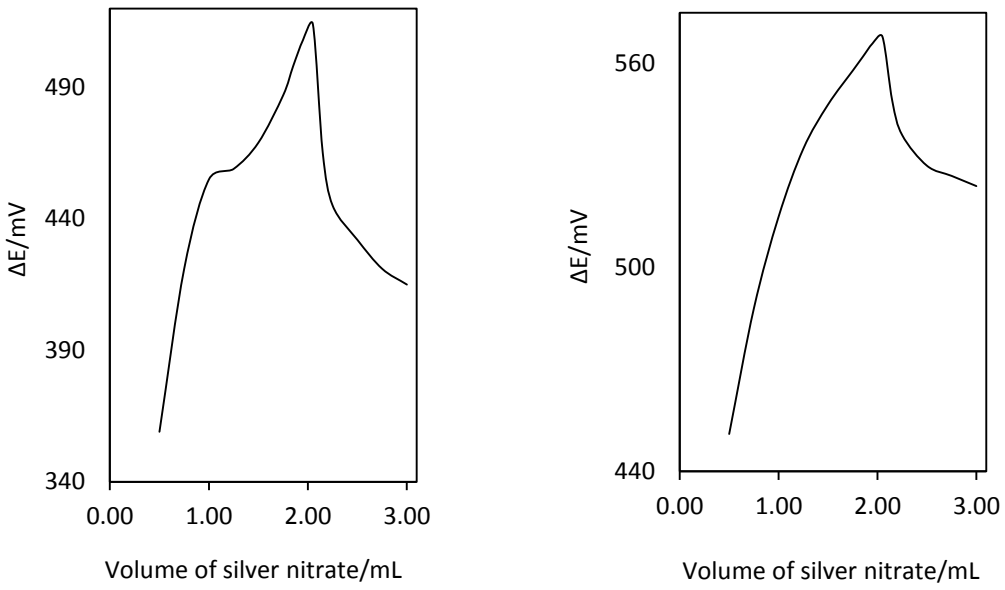

Figure 38: m. s. b. DEP titration curves of 5.00 mL of cyanide ions in 20 mL of 0.1 mol/L potassium nitrate. (1) 8.00×10^{-5} mol/L of CN^- titrated with 2.00×10^{-4} Ag^+ (left) and (2) 2.00×10^{-5} mol/L of CN^- titrated with 5.00×10^{-5} Ag^+ (right)

6.1.4 Acid Base Titration

The Ag/CNTs electrodes were used as an indicating system in the titration of hydrochloric acid with sodium hydroxide. It was found that low values of the percentage of the bias produce symmetrical and sharp peaks. Therefore, the location of the end point can be determined accurately as shown in Figure 39 and Figure 40. So, beyond the value of 20%, the peaks were unsymmetrical, broad and the end point was not accurate, Figure 41 and Figure 42. The optimum % bias was applied to perform a titration at lower concentration Figure 43.

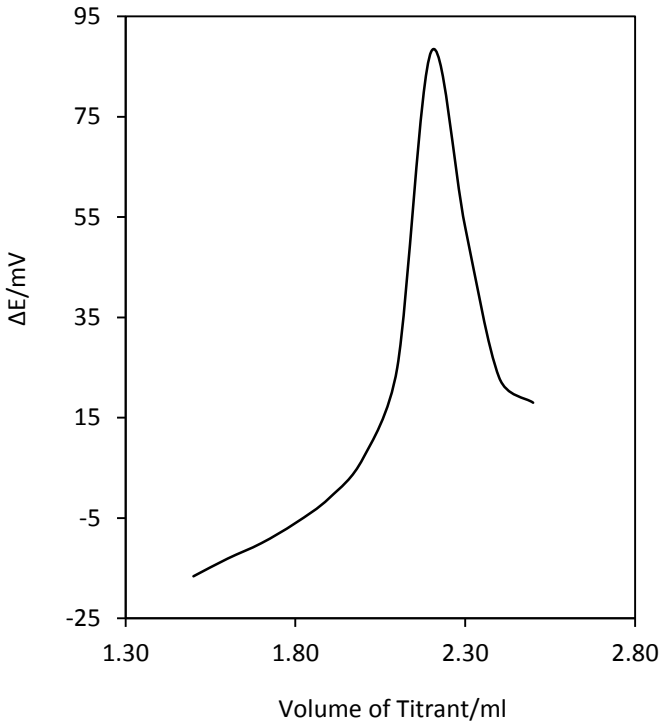

Figure 39: m.s.b DEP titration peak for 2.00ml of hydrochloric acid (5.91×10^{-2} mol/L) vs sodium hydroxide (5.42×10^{-2} mol/L) at 0% bias

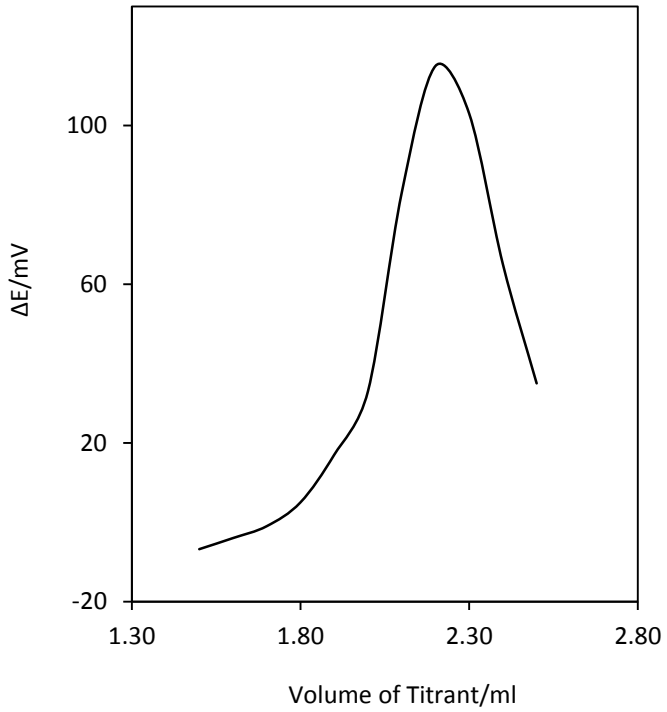

Figure 40: m.s.b DEP titration peak for 2.00ml of hydrochloric acid (5.91×10^{-2} mol/L) vs sodium hydroxide (5.42×10^{-2} mol/L) at 20% bias

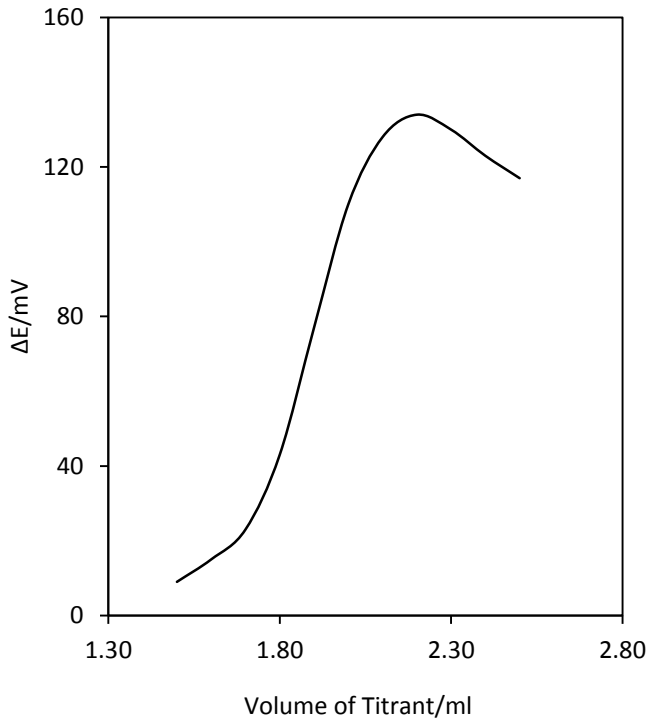

Figure 41: m.s.b DEP titration peak for 2.00ml of hydrochloric acid (5.91×10^{-2} mol/L) vs sodium hydroxide (5.42×10^{-2} mol/L) at 40% bias

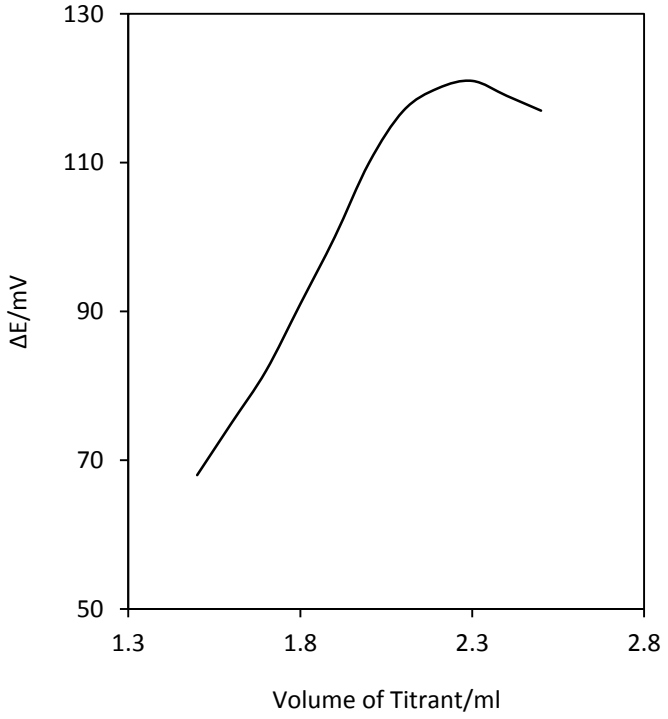

Figure 42: m.s.b DEP titration peak for 2.00ml of hydrochloric acid (5.91×10^{-2} mol/L) vs sodium hydroxide (5.42×10^{-2} mol/L) at 60% bias

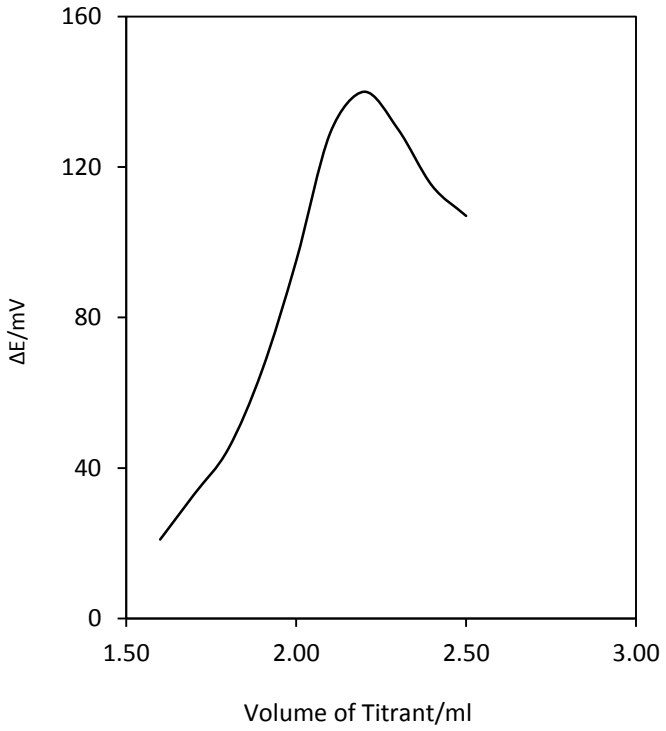

Figure 43: m.s.b DEP titration peak for 2.00ml of hydrochloric acid (1.18×10^{-2} mol/L) vs sodium hydroxide (1.08×10^{-2} mol/L) at 20% bias

6.1.5 Determination of Chloride

DC-DEP Titrations

The most important parameter to be optimized here is the current density. Different values ranging from 2 – 20 μA/cm^2 were examined. Results revealed that no differential curve is obtained at low values while at high ones the curve becomes broad and asymmetric. 15 μA/cm^2 was selected as the optimum value as Figure 44 illustrates. Differential curves for different chloride ion concentrations are shown in Figure 45 and the least concentration detected and quantified was 2.5x10^{-4} mol. dm^{-3}. More details are given table1.

Mark-Space Biased DEP Titration

Here, a square waveform polarizes the indicating electrodes. The time bias was varied in the range 0 – 80 %. Differential curve symmetry and sharpness along with peak height were improved by raising the %bias up to 60% as in Figure 46. However, beyond that, peak broadness increases. Relation between the chloride concentration and shape of the differential curve was depicted in Figure 47. The minimum concentration quantified was 2.5x10-5 which is 10 times less than that in DC case, Table 4.

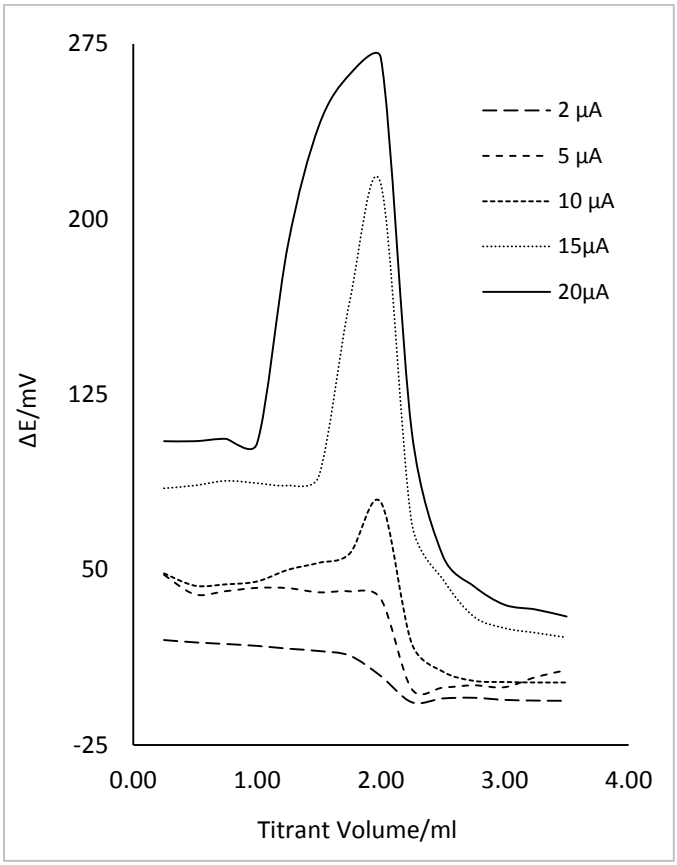

Figure 44: Effect of current densities for titration of 20 ml of $2.5x10^{-3}$ mol/L of chloride in 0.1 mol/L KNO_3, with 0.025 mol/L silver nitrate.

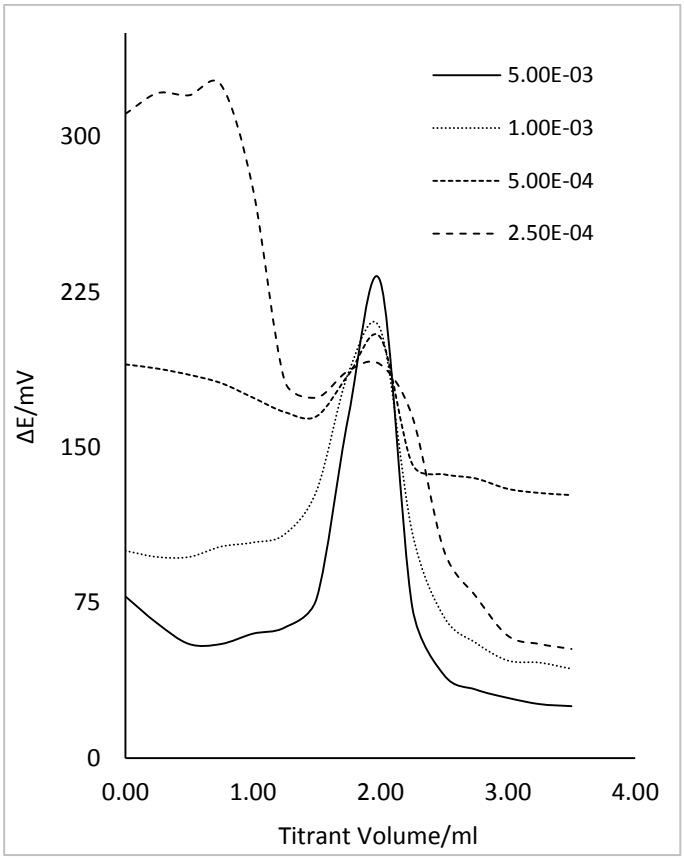

Figure 45: Titration of 20 ml of different concentrations of chloride in 0.1 mol/L KNO_3, with 10-fold more concentrated silver nitrate at current density 15 $\mu A/cm^2$

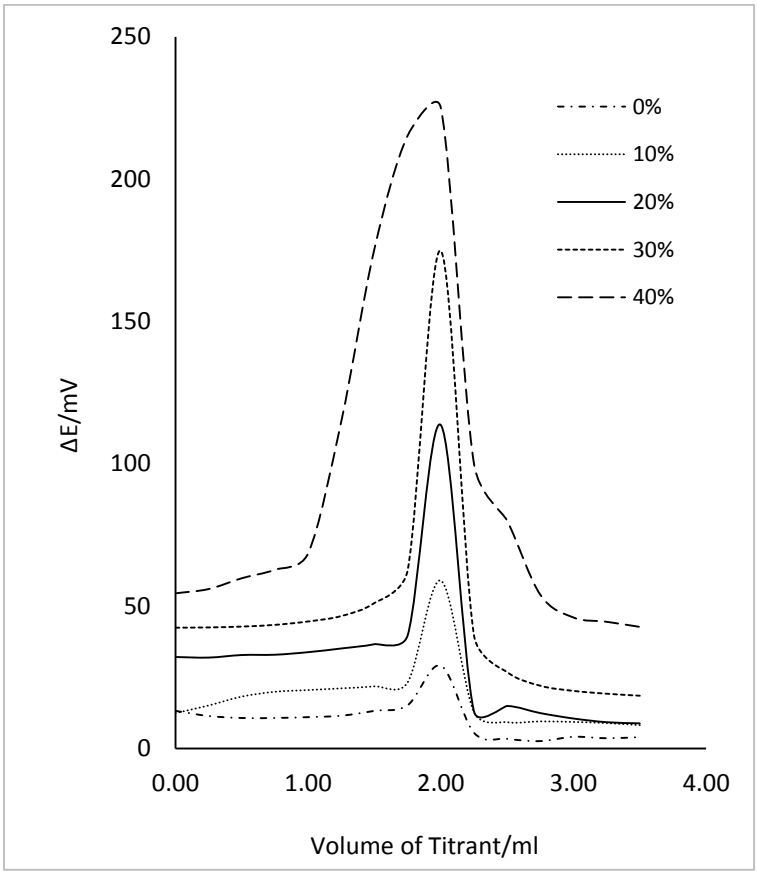

Figure 46: Effect of % time bias on the shape of the curve. Titration of 20 ml of $2.5x10^{-3}$ mol/L chloride in 0.1 mol/L KNO_3, with 0.025 mol/L silver nitrate.

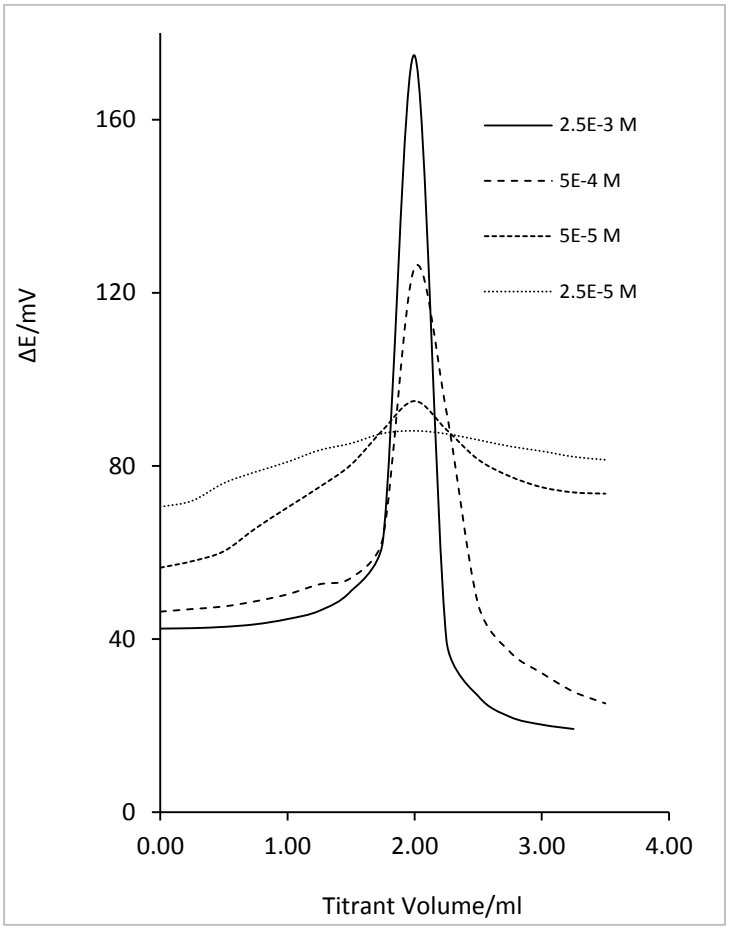

Figure 47: Titration of 20 ml of different chloride concentrations, in 0.1 mol/L KNO3, with 10-fold more concentrated silver nitrate at 60% bias

Table 4: Results obtained by DEP titration of chloride ions with silver ions using CNTs modified silver electrodes

Type of potentiometry	conc. of Cl^- quantified		% recovery + %RSD (n=5)
	mol/L	ppm	
Normal potentiometry	5.0×10^{-4}	18.0	99.3 ± 1.1
Direct current DEP	2.5×10^{-4}	9.0	98.6 ± 0.6
Time biased square wave DEP	5.0×10^{-5}	1.8	99.4 ± 1.0
	2.5×10^{-5}	0.9	98.8 ± 2.9

6.2 Applications of the Ag/CNTs Electrodes with Both Direct Current and Mark-Space DEP as a Detector in FIA

6.2.1 Determination of Ciprofloxacin

DEP technique with both dc and m.s.b polarization has been applied successfully as a detection system in a FIA system for the determination of ciprofloxacin hydrochloride using Ag/CNTs electrodes.

Effect of Current Density and Square Wave Bias

The Ag/CNTs indicator electrodes were polarized by a dc current and by a time biased square wave. The effect of increasing current density on the signal strength is shown in Figure 48 and Figure **49**. It was found that the signal increases as the current density increases. However, beyond a current density of 20 $\mu A/cm^2$, the resulting peaks are broad. Figure 48 and Figure **49** show the FIA peaks at certain current densities while the effect of different current densities on the values of the measured DEP potential is shown in Figure 50 from which the optimum current density was selected.

Polarization with a time biased square wave has shown that the value of the potential difference (ΔE) increases as the percentage of the bias increased as shown in Figure 51. Figure 52 shows that a bias of 70% produced a potential signal less than a bias of 50%. From Figure 53, it clear that the optimum response is at a bias of 40%. Below this value, peaks of low heights were obtained while beyond it, the height decreased rather than increase.

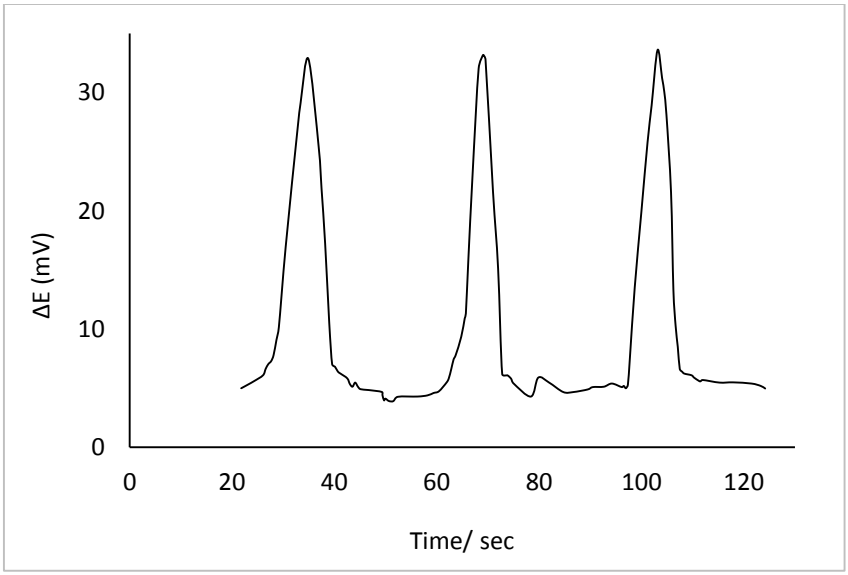

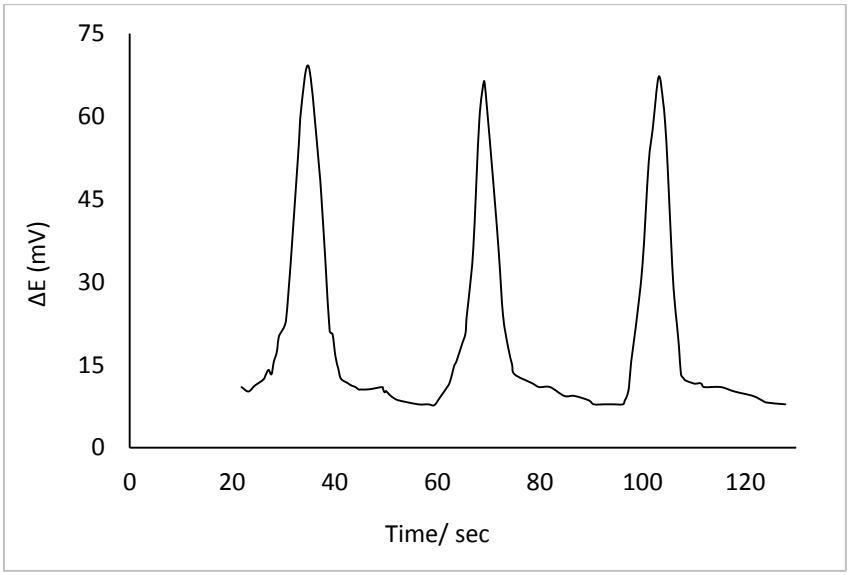

Figure 48: FIA triplicates of 5.0×10^{-1} mmol/L of CFX at current density 10.5µA/cm^2 (upper) and 21µA/cm^2 (lower).

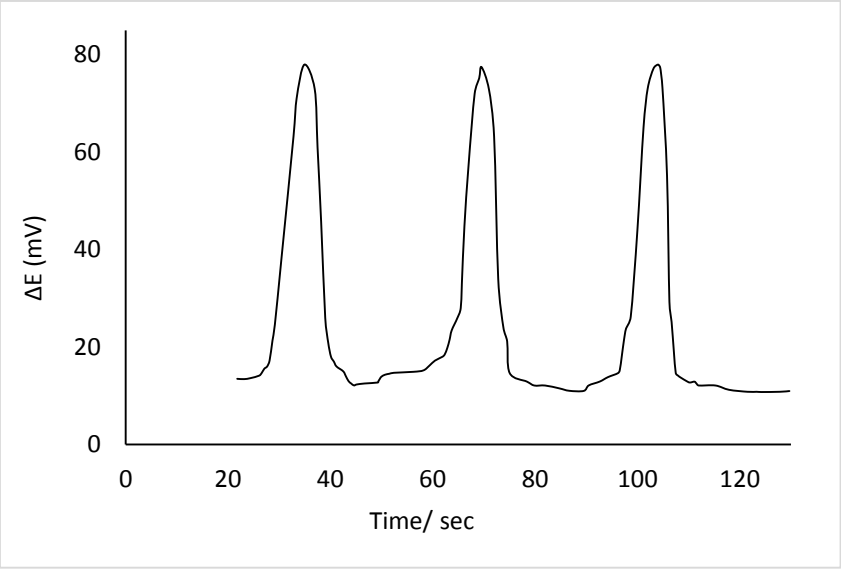

Figure 49: FIA triplicates of a solution of 5.0×10^{-1} mmol/L of CFX at current density 31.6µA/cm^2

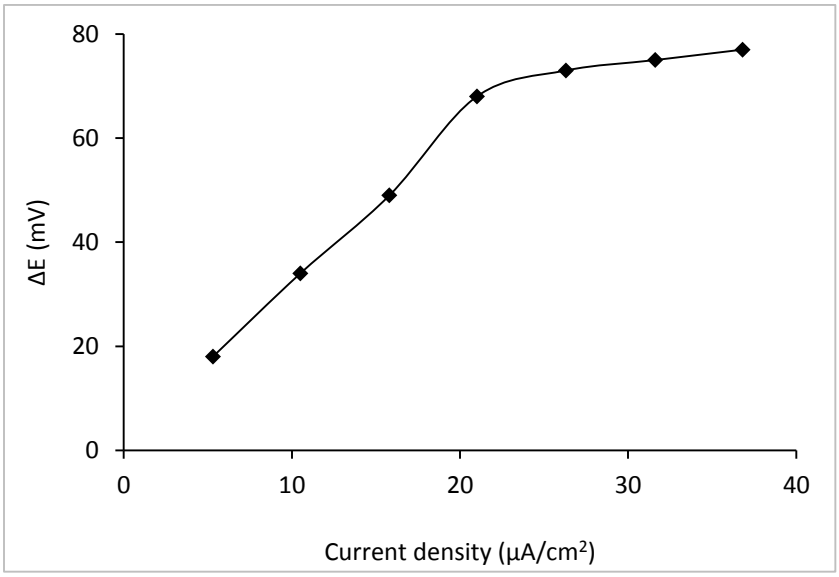

Figure 50: Effect of current density on the FIA–DEP potantial values of 5.0×10^{-1} mmol/L of CFX solution

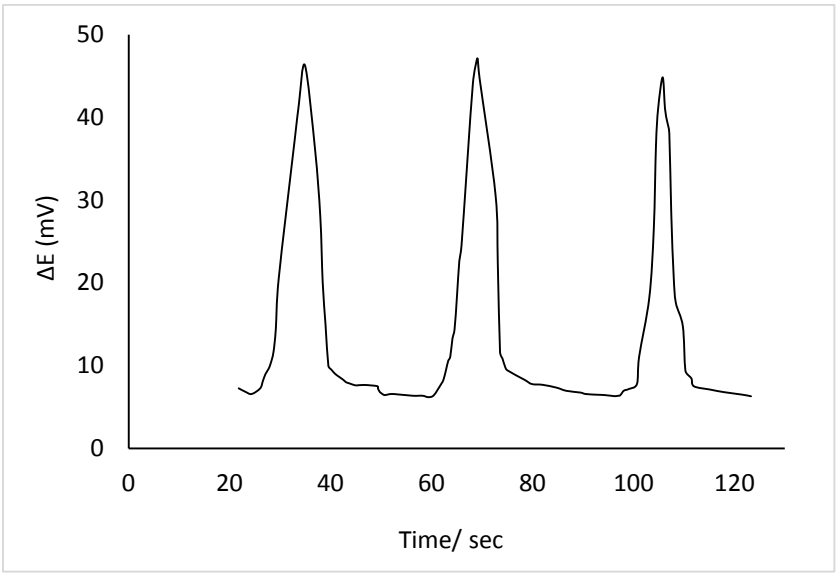

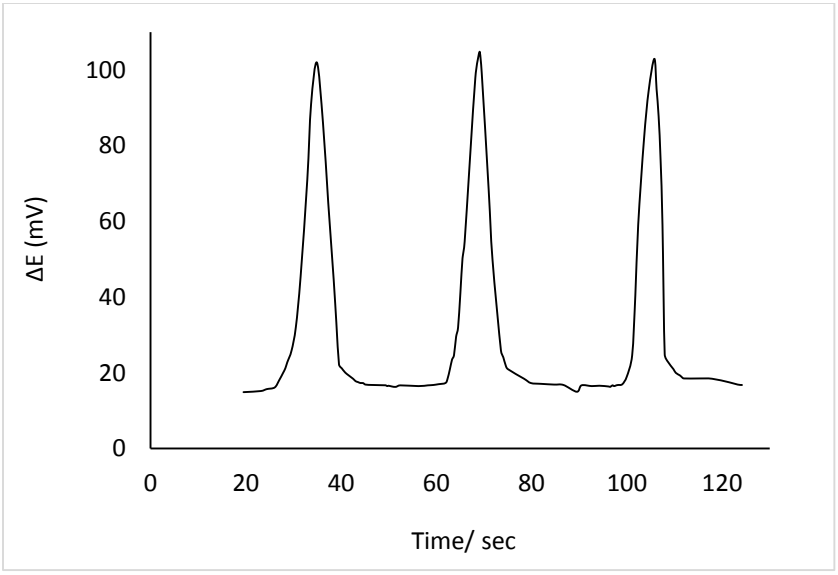

Figure 51: FIA triplicates of a solution of 5.0×10^{-1} mmol/L of CFX at a time bias of 10% (upper) and 50% (lower).

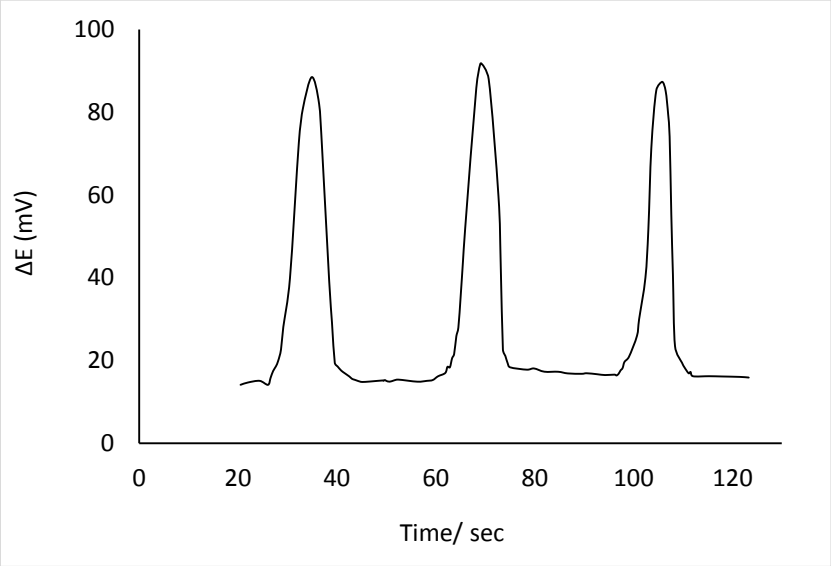

Figure 52: FIA triplicates of a solution of 5.0×10^{-1} mmol/L of CFX at a time bias of 70%.

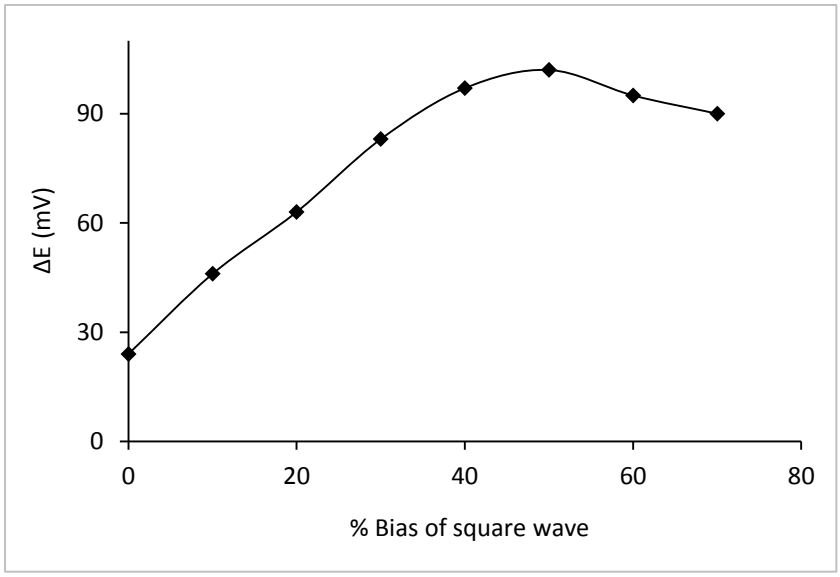

Figure 53: Effect of the % bias on the FIA–DEP signal of 5.0×10^{-1} mmol/L of CFX solution

Effect of the Flow Rate

The flow rate is one of the most important parameters to be optimized in FIA because the dispersion of the analyte in the reagent stream depends on it this parameter.

In case of both dc DEP and m.s.b DEP during for the determination of CFX, no significant change in the potential signal was noted when a flow rate of the iron (III) solution closed to 90µL/sec was applied as is shown in Figure 54.

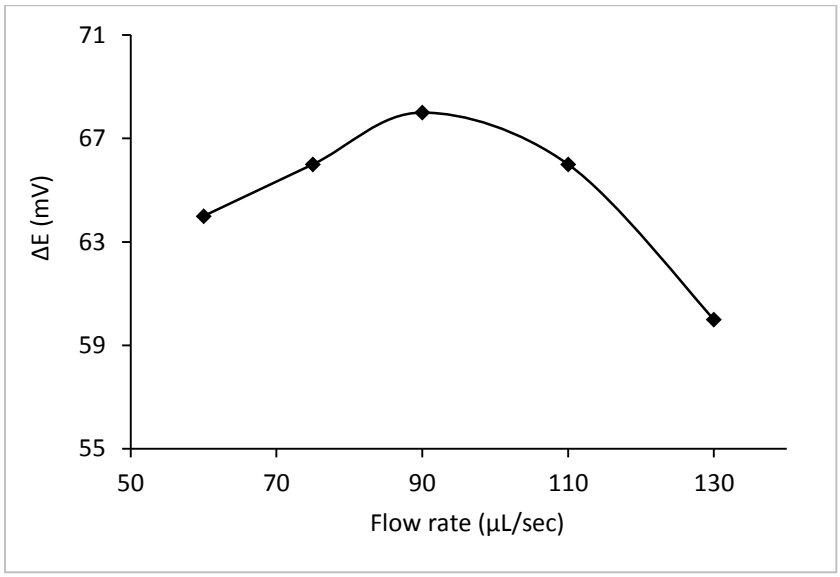

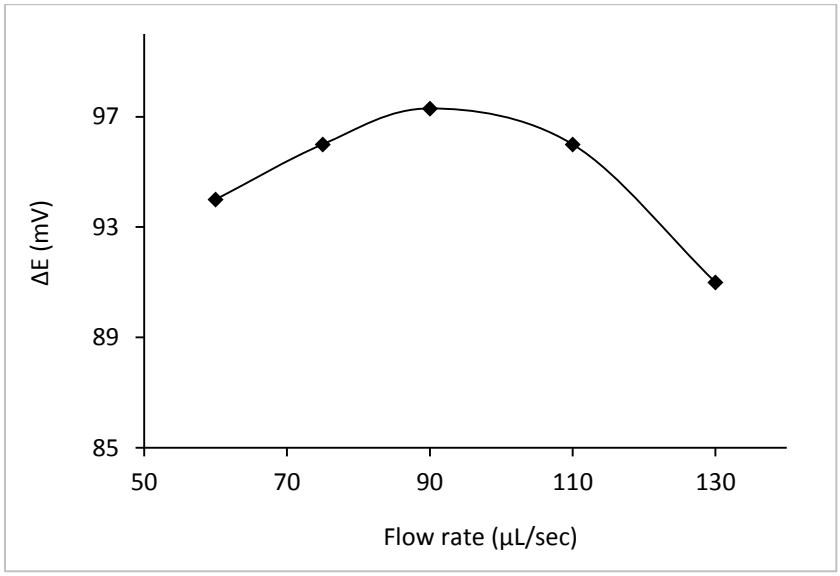

Figure 54: The effect of the flow rate of iron (III) solution on the potential values for both types of polarization; d.c DEP (upper) and m.s.b DEP (lower).

Effect of Nitric Acid Concentration

Nitric acid was used as carrier/supporting electrolyte and also to provide the suitable pH for the complexation between the iron (III) and CFX. Different concentrations of nitric acid in the range of 1 – 250 mmol/L were tested. No significant change in the potential difference (ΔE) was noticed in range of 1 – 25 mmol/L for both d.c. and m.s.b DEP. At a higher concentration, 250 mmol/L, appreciable decrease in the potential signal has taken place. This decrease in the potential value may be attributed to the decrease of the stability of the complex or to the formation of the complex in another ratio. The effect of the pH on the complexation reaction is sown in Figure 55.

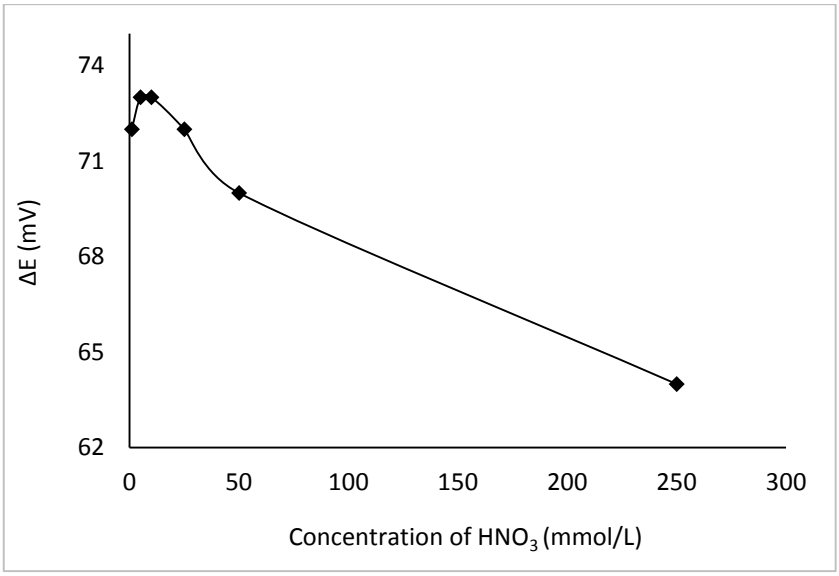

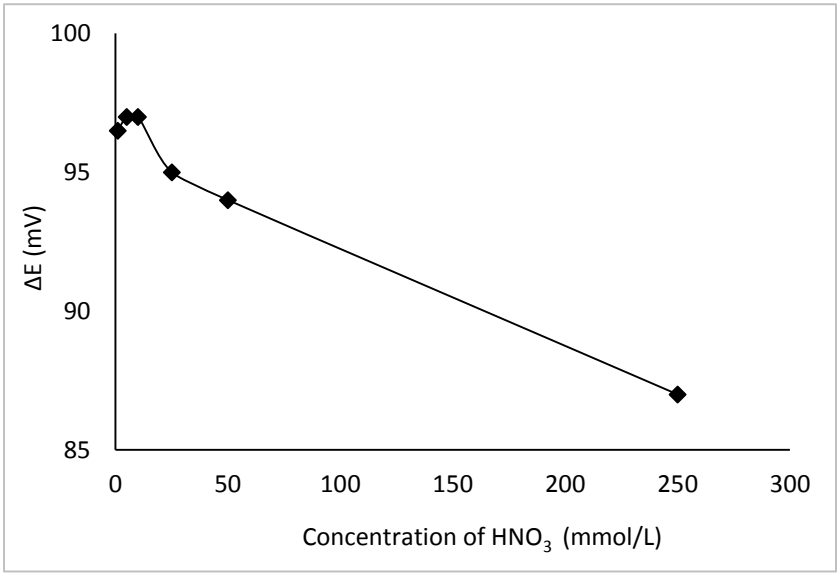

Figure 55: The effect of nitric acid concentration on the potential signal for CFX complexation with iron (III). d.c DEP (upper) and m.s.b DEP (lower)

Analytical Appraisals

The dc DEP and m.s.b DEP methods were calibrated by triplicate running of a series of standard solutions of CFX at the optimum conditions obtained. CFX was determined in the concentration range of 0.06 – 1 mmol/L. Good linear relationship was obtained for both techniques. The m.s.b DEP method was found to be more sensitive than the dc DEP one. This increase in the sensitivity when using a biased square wave is attributed to the continuous reversing of the signal that prevents buildup of films on the electrode surface which keeps the electrodes fully active for long periods of time [17]. Figure 56 and Figure 57 show the dc and m.s.b DEP calibrations respectively. Analytical data are given in Table **5**.

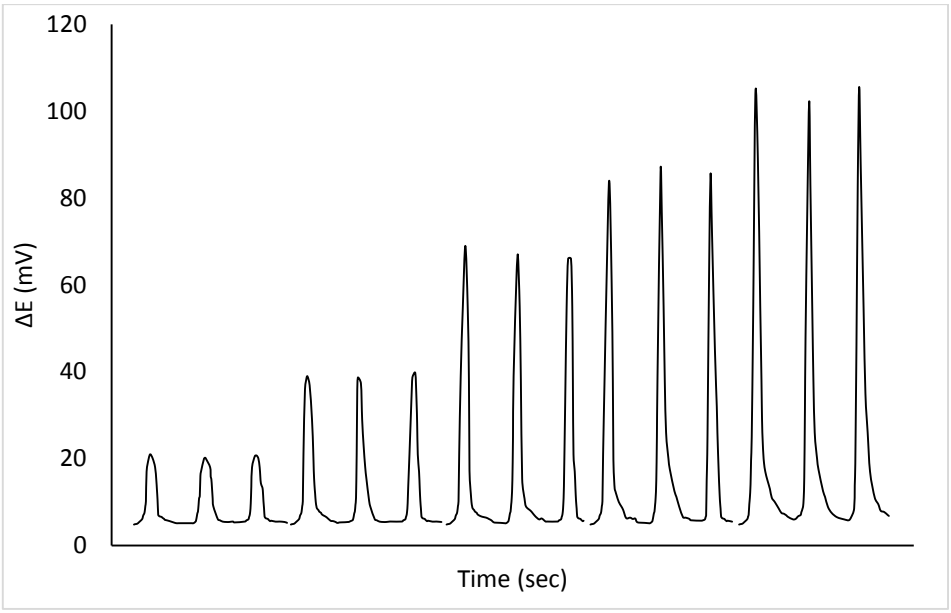

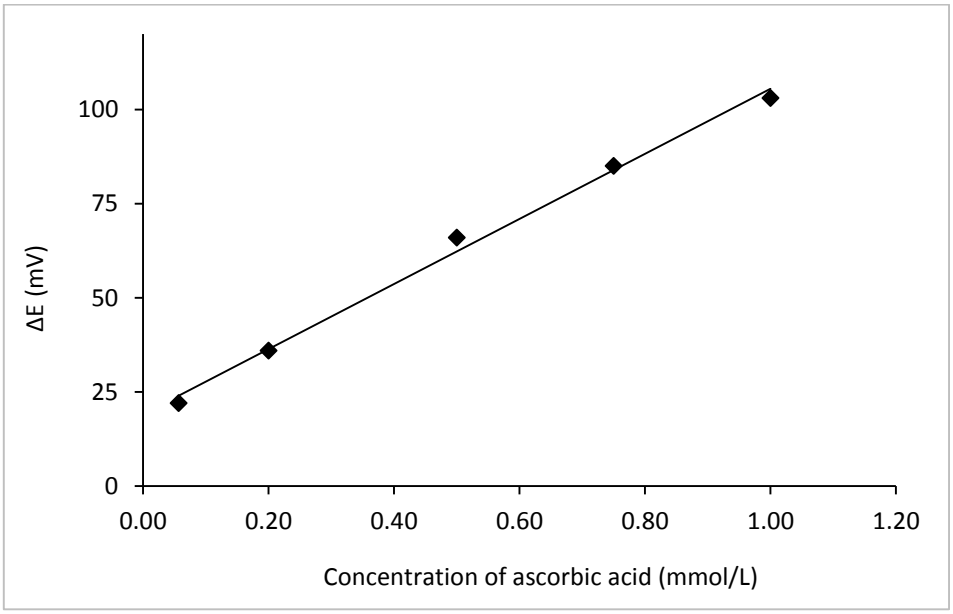

Figure 56: FIA triplicates of d.c-DEP peaks for CFX standard solutions 0.06, 0.20, 0.50, 0.75 and 1.00 mmol/L (upper) and the calibration curve (lower).

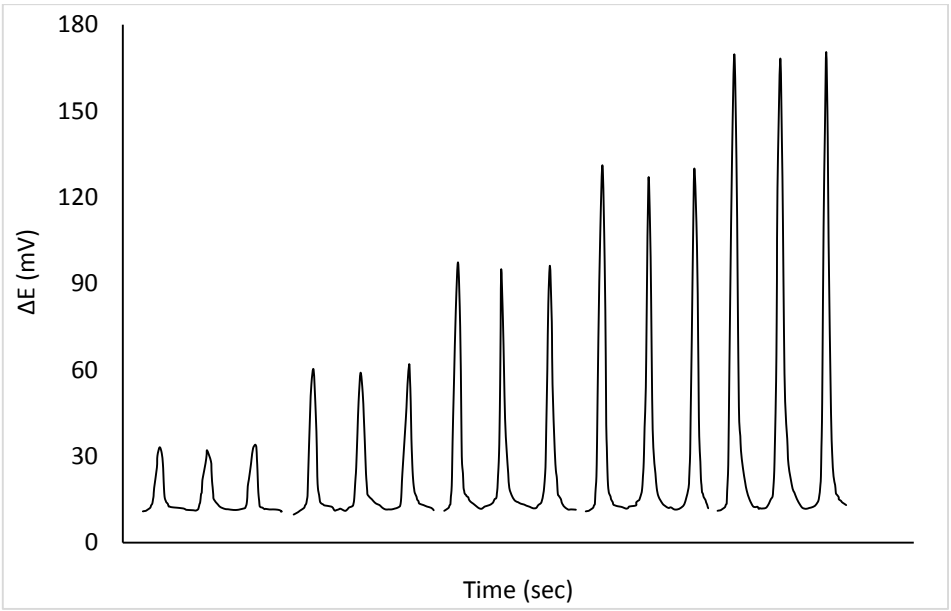

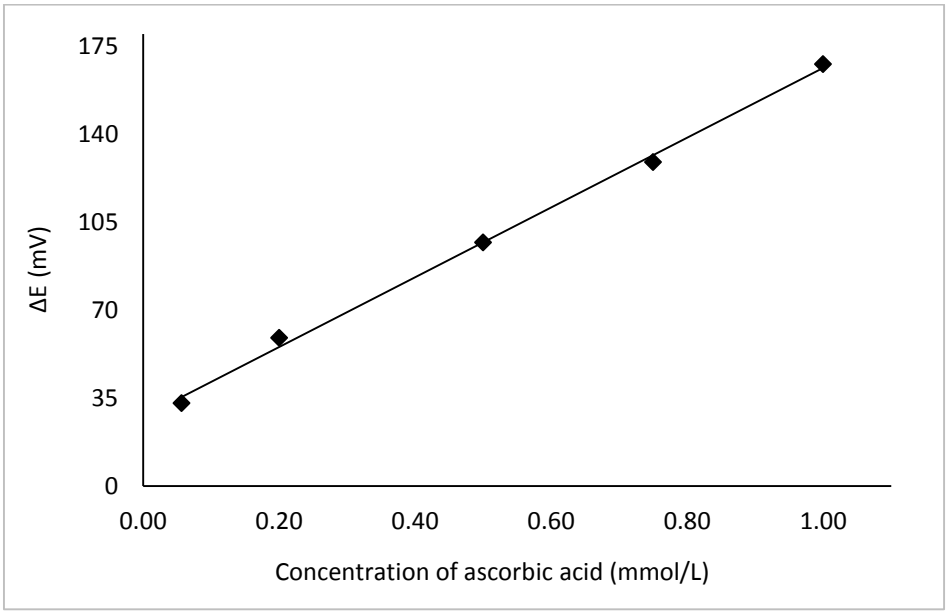

Figure 57: FIA triplicates of m.s.b-DEP peaks for CFX standard solutions 0.06, 0.20, 0.50, 0.75 and 1.00 mmol/L (upper) and the calibration curve (lower).

Table 5: Analytical parameters for FIA – DEP determination of ciprofloxacin by Ag/CNTs electrodes for triplicate measurements

CFX conc. (mmol/L)	d.c – DEP				m.s.b – DEP			
	%RSD	Slope	y-intercept	R^2	%RSD	Slope	y-intercept	R^2
0.06	2.4	86.5	19.1	0.994	3.0	139.0	27.5	0.998
0.20	2.2				2.5			
0.50	2.3				1.2			
0.75	1.2				2.1			
1.00	1.6				0.8			

6.2.2 Determination of Ascorbic Acid

Both dc DEP and m.s.b DEP techniques have been applied successfully as a detection system using FIA for the analysis of ascorbic acid. The reagent used was potassium iodate.

Ascorbic acid reacts with potassium iodate according to the following equation:

$$KIO_3 + 3C_6H_8O_6 \rightarrow 3C_6H_6O_6 + I^- + 3H_2O$$

Effect of Current Density and Square Wave Bias

The Ag/CNTs indicator electrodes were polarized by a dc current and by a time biased square wave. Figure 62 shows the effect of increasing the current density on the signal strength. It was found that the signal increases as the current density increases. However, not only the peak height is considered in this regard, the peak shape is also an important factor. Beyond 42 µA/cm2 the peaks start to broaden with less significant increase in the height, so, this value of the current density was considered to be optimum, Figure 58 and Figure **59**.

In case of mark–space bias polarization, a 20% bias, Figure 60, was found to be an optimum value. Below this value, Figure 61, the peak height was low. Beyond this value, no increase in the peak intensity was observed, Figure 62.

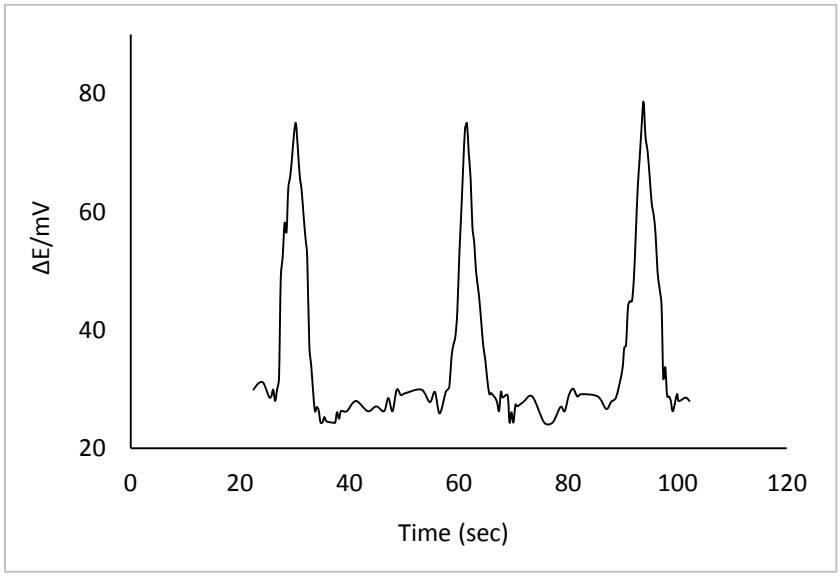

Figure 58: FIA triplicates of a solution of 2.8×10^{-1} mmol/L of ascorbic acid at current density of $21\mu A/cm^2$.

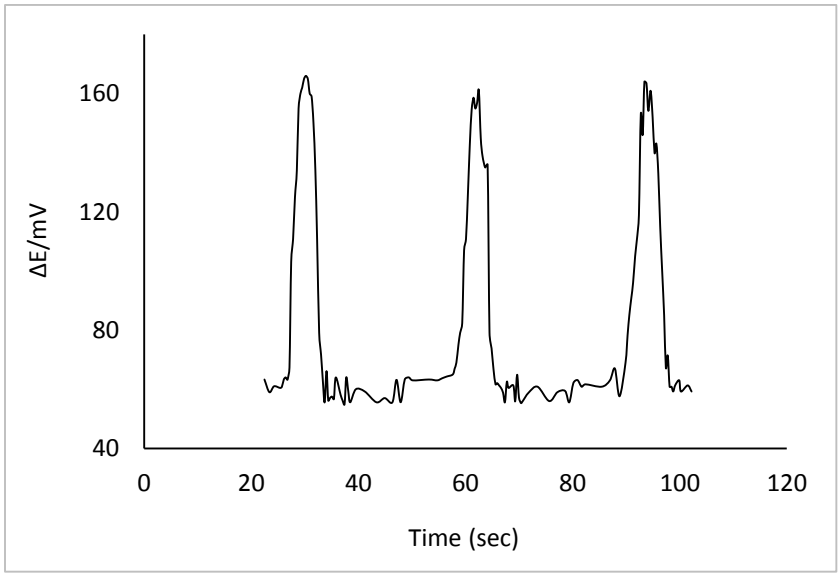

Figure 59: FIA triplicates of a solution of 2.8×10^{-1} mmol/L of ascorbic acid at current density of 63µA/cm^2.

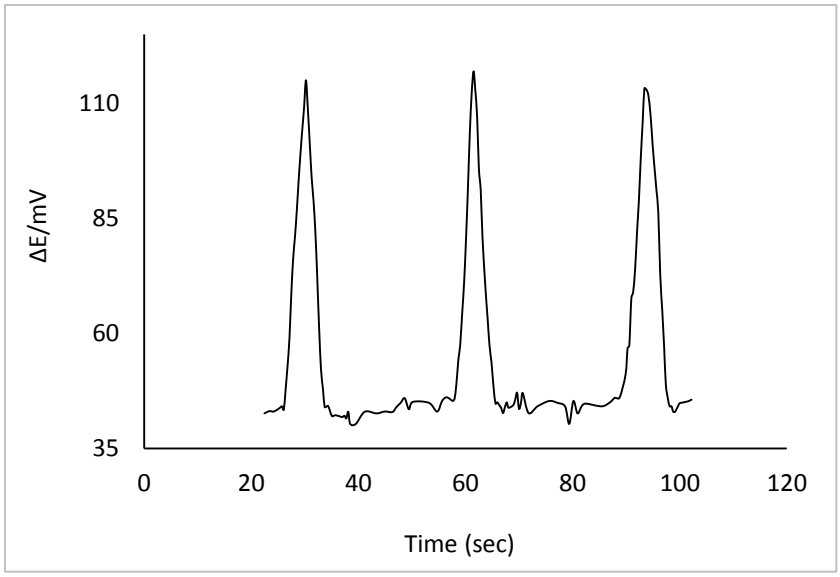

Figure 60: FIA triplicates of a solution of 2.8×10^{-1} mmol/L of ascorbic acid at a time bias of 10%.

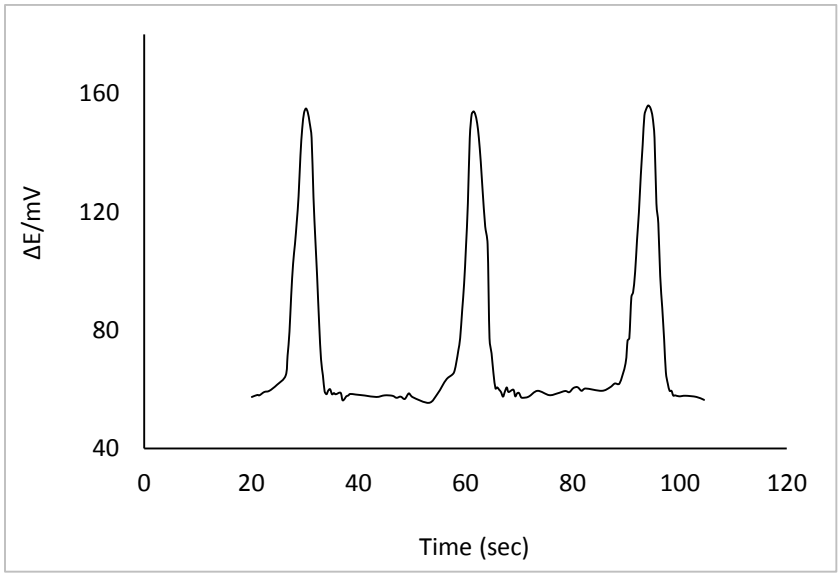

Figure 61: FIA triplicates of a solution of 2.8×10^{-1} mmol/L of ascorbic acid at a time bias of 20%

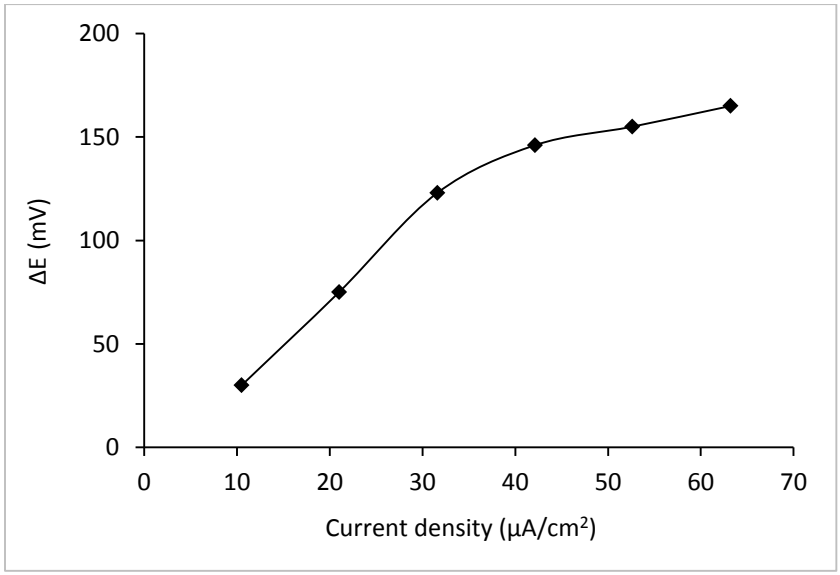

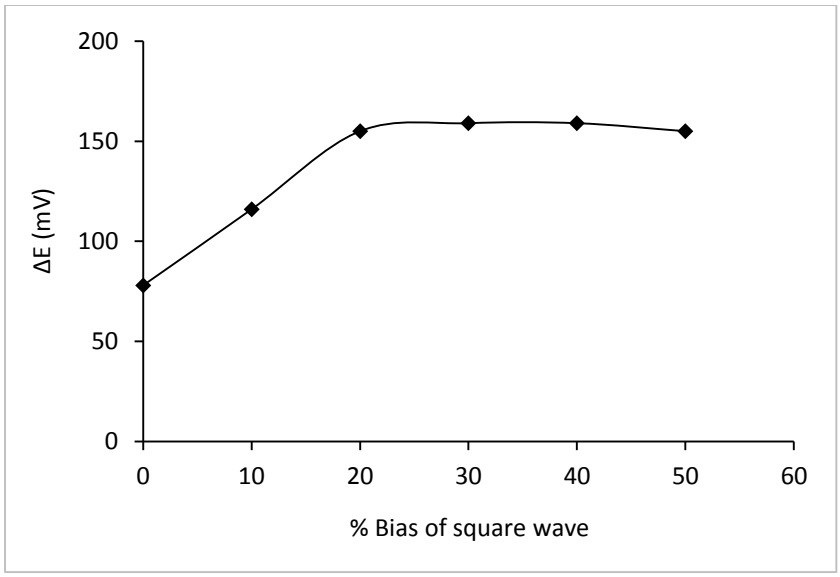

Figure 62: Effect of different current densities (upper) % bias (lower) on the FIA – DEP peaks of 2.8×10^{-1} mmol/L of ascorbic acid.

Effect of the Flow Rate

One of the most important parameters to be studied in FIA is the flow rate. The analyte dispersion consequently and its reaction with the reagent depends on the flow rate in addition to other parameters and hence the signal strength.

For both dc DEP and m.s.b DEP as a detection techniques in FIA system for ascorbic acid determination, the optimum KIO_3 flow rate was in the range of 75 – 90 µL/sec as shown in Figure 63. Below this range, the decrease in the potential signal is attributed to less sample dispersion and less amount of product. Beyond this range, increasing of the flow rate may allow the solution components to reach the flow through detector in a shorter time before appreciable amounts react.

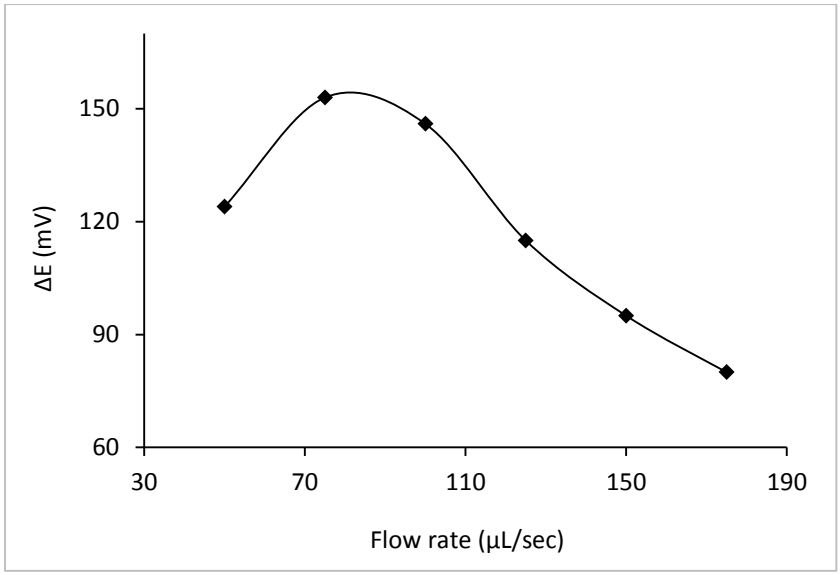

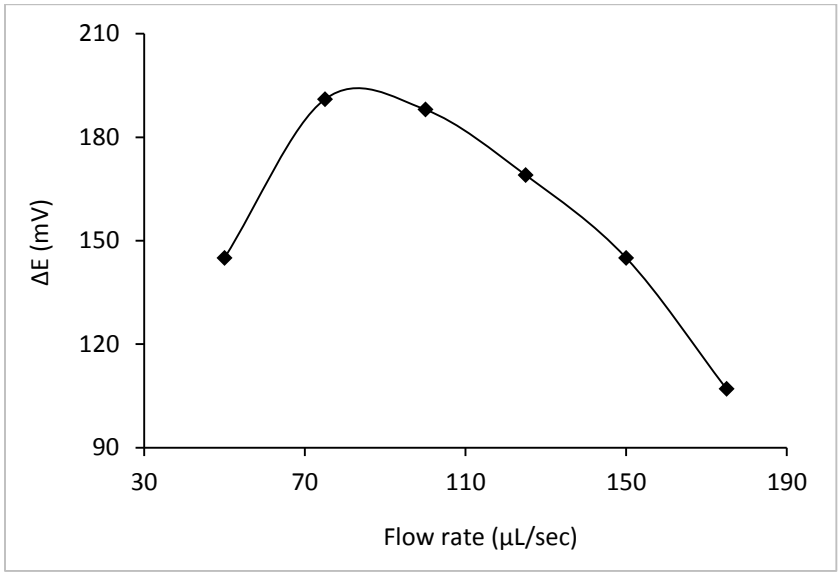

Figure 63: Effect of the flow rate on the DEP peak height for both types of polarization; dc (upper) and m.s.b (lower).

Analytical Appraisals

The dc DEP and m.s.b DEP methods were calibrated by triplicate running of series of standard solutions of ascorbic acid by applying the optimum conditions. Ascorbic acid was determined in the concentration range of 0.06 – 0.85 mmol/L. Good linear relationship was obtained for both types of polarization, in terms of the square of the correlation coefficient as depicted in . The m.s.b DEP method was found to be more sensitive than the dc DEP one. This increase in the sensitivity can be attributed to the continuous reversing of the signal that prevents buildup of films on the electrode surface which keeps the electrodes fully active for long periods of time[17]. Analytical parameters are given in Table 6.

Application

Both methods were applied for the determination of ascorbic acid in vitamin C and in Baobab fruit. The results of analysis were compared with that of the same batch of samples with the USP method [139]. Analytical data are given in Table **6**.

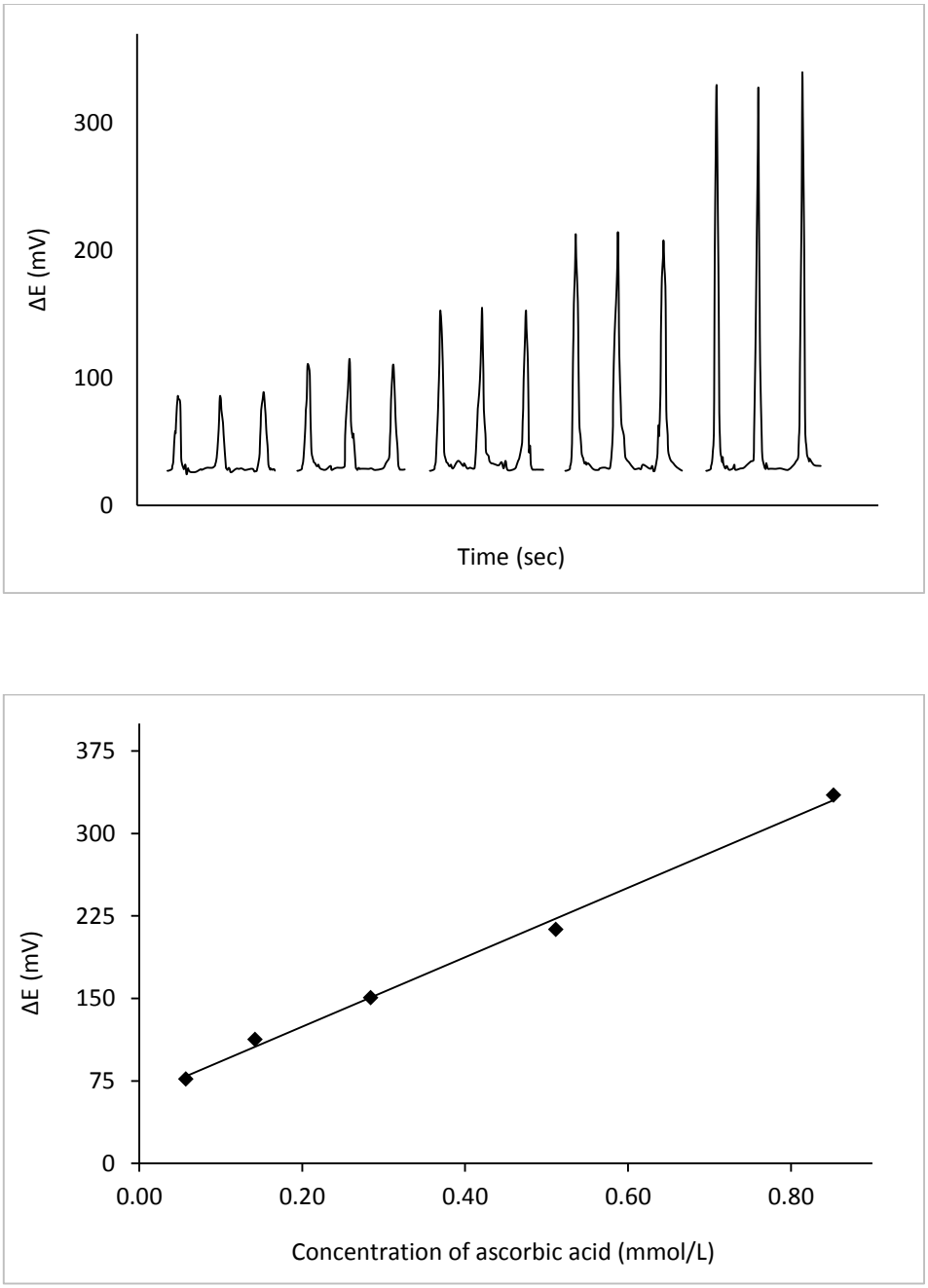

Figure 64: d.c-DEP – FIA triplicates (upper) and the calibration (lower) of ascorbic acid ascorbic acid standard solutions (0.06, 0.14, 0.28, 0.51 and 0.85 mmol/L) at the optimum conditions.

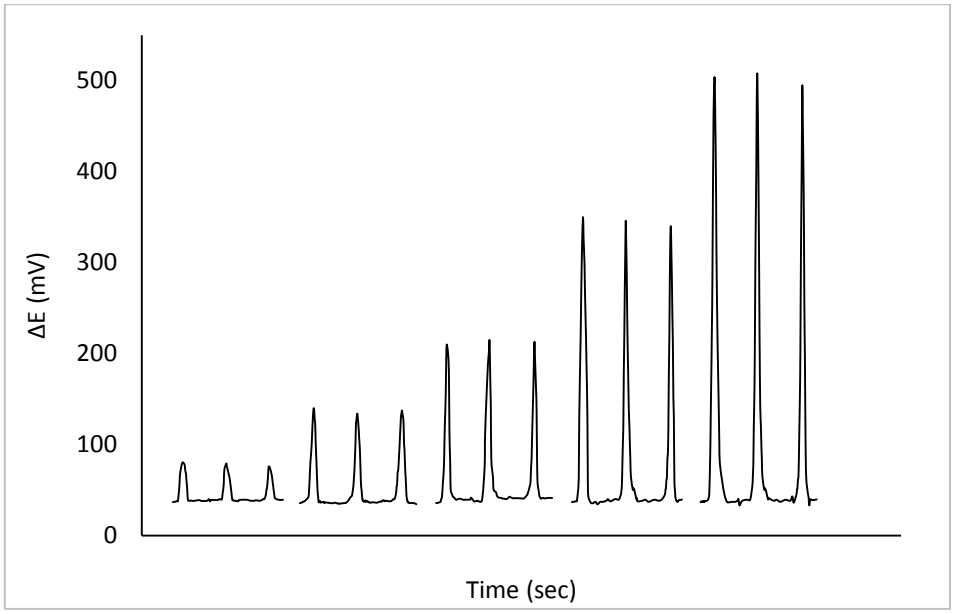

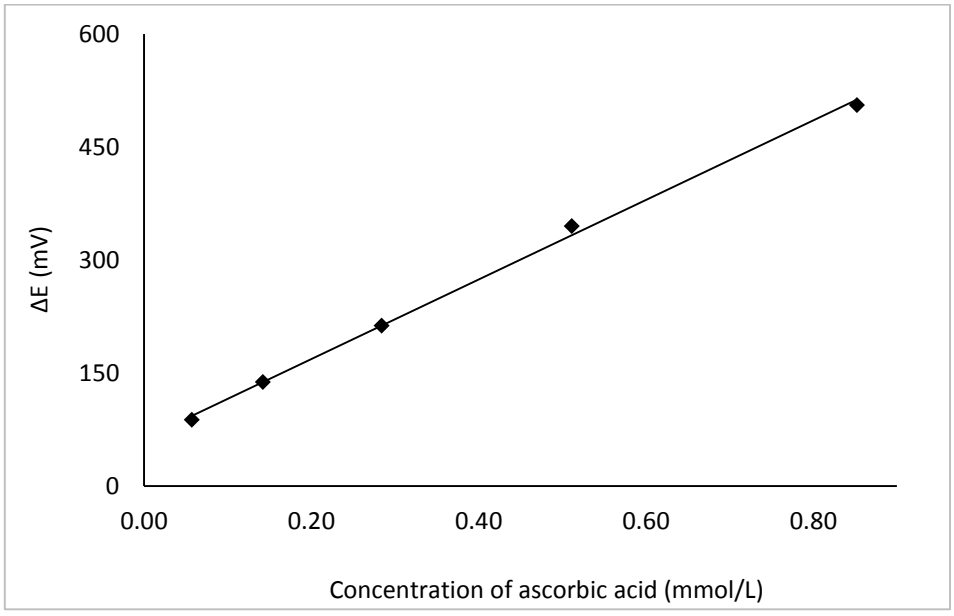

Figure 65: m.s.b-DEP – FIA triplicates (upper) and the calibration (lower) of ascorbic acid ascorbic acid standard solutions (0.06, 0.14, 0.28, 0.51 and 0.85 mmol/L) at the optimum conditions.

Table 6: Analytical parameters for FIA – DEP determination of ascorbic acid by Ag/CNTs electrodes for triplicate measurements

Ascorbic acid conc. (mmol/L)	d.c – DEP				m.s.b – DEP			
	%RSD	Slope	y-intercept	R^2	%RSD	Slope	y-intercept	R^2
0.06	3.9	315.8	61.2	0.996	3.0	527.9	63.1	0.998
0.14	2.7				2.2			
0.28	1.1				1.2			
0.51	1.5				1.5			
0.85	1.9				1.3			

CONCLUSION

Carbon nanotubes (CNTs) have been successfully grown on the surface of silver wire in a chemical vapor deposition reactor through the thermal decomposition of acetylene gas and in the presence of ferrocene as a catalyst source and hydrogen gas. Both acetylene and hydrogen flow rates, carbon nanotubes growth temperature and growth time were optimized. The CNTs grown on the surface of silver wire were characterized by scanning electron microscopy, Raman spectrometry and transmission electron microscopy. The surface was completely covered with a well graphitized CNTs.

The silver wires coated with CNTs have been polarized be a mark space – biased square wave and used as indicating systems in the differential electrolytic potentiometric titrations, DEP, for the determination of different analytes. These electrodes have been found to work in different types of ion – combination reactions in addition to the oxidation – reduction reactions. They succeed to detect accurately the end points for the different titrations. The prepared electrodes have shown high sensitivity, low detection limit, fast response and high stability for long time.

The prepared electrodes have been also used as indicating system in the flow injection analysis for the determination of some drugs. They were polarized with both direct current and time biased square wave. The results obtained showed good linearity, high precision and low detection limit. The polarization with a biased square wave revealed higher sensitivity than the one with direct current in all analyses.

These electrodes can be considered as universal detection systems in the DEP techniques.

RECOMMENDATIONS

For the future work, the following studies are recommended:

- More investigation of the electrochemistry taking place at the Ag/CNTs electrodes surface to explain their ability to work in different types of reactions.
- Since these electrodes have shown a good performance, they may be modified with other materials in order to make them selective toward specific analytes.
- Investigation of these electrodes in the classical potentiometry, since the preliminary study revealed good results in this field.

REFERENCES

[1] E. Bishop, “Ultramicro Potentiometric Titrimetric Analysis. Differential Electrolytic Potentiometry in Redox Systems,” *Microchim. Acta*, vol. 44, pp. 619–629, 1956.

[2] A. Abdennabi, “Differential Electrolytic Potentiometric Titrimetry in Non-aqueous Media.,” Exeter, 1979.

[3] A. M. S. Abdennabi and E. Bishop, “Differential Electrolytic Potentiometry with Periodic Polarisation. Part XXVII. Precipitation and Complexation Titrations in Anhydrous Acetic Acid,” *Analyst*, vol. 108, no. 1292, pp. 1227–1234, 1983.

[4] S. Fraihat and A. Abulkibash, “Differential Electrolytic Potentiometry: A Detector for Flow Injection/Sequential Analysis in Complexation Reactions,” *Asian J. Chem.*, vol. 24, no. 11, pp. 4847–4850, 2012.

[5] C. Hu and S. Hu, “Carbon Nanotube-Based Electrochemical Sensors: Principles and Applications in Biomedical Systems,” *J. Sensors*, pp. 1–40, 2009.

[6] I. Dumitrescu, P. R. Unwin, and J. V Macpherson, “Electrochemistry at Carbon Nanotubes: Perspective and Issues,” *Chem. Commun.*, vol. 7345, no. 45, pp. 6886–901, Dec. 2009.

[7] J. Nugent, K. Santhanam, A. Rubio, and P. Ajayan, “Fast Electron Transfer Kinetics on Multiwalled Carbon Nanotube Microbundle Electrodes,” *Nano Lett.*, vol. 1, no. 2, pp. 87–91, 2001.

[8] Y. Lan, Y. Wang, and Z. F. Ren, “Physics and Applications of Aligned Carbon Nanotubes,” *Adv. Phys.*, vol. 60, no. 4, pp. 553–678, 2011.

[9] A. Merkoçi, M. Pumera, X. Llopis, B. Pérez, M. del Valle, and S. Alegret, “New Materials for Electrochemical Sensing VI: Carbon Nanotubes,” *Trends Anal. Chem.*, vol. 24, no. 9, pp. 826–838, 2005.

[10] J. Ŗužička and E. H. Hansen, “Flow Injection Analyses, Part I. A New Concept of Fast Continuous Flow Analysis,” *Anal. Chim. Acta*, vol. 78, no. 1, pp. 145–

157, Aug. 1975.

[11] M. Trojanowicz and K. Kolacinska, “Recent Advances in Flow Injection Analysis,” *Analyst*, pp. 1–128, 2016.

[12] A. Abulkibash, S. Fraihat, and B. EL ALI, “Flow Injection Determination of Vitamin C in Pharmaceutical Preparations by Differential Electrolytic Potentiometry,” *J. Flow Inject. Anal.*, vol. 26, no. 2, pp. 121–125, 2009.

[13] A. Taufiq and A. Abulkibash, “Differential Electrolytic Potentiometric Detector in Flow Injection Analysis for Cyanide Determination,” *J. Flow Inject. Anal.*, vol. 24, no. 1, pp. 9–12, 2007.

[14] C. N. Reilley, W. D. Cooke, and N. H. Furmlk, “Derivative Polarographic Titrations,” *Anal. Chem.*, vol. 23, no. 9, pp. 1223–1226, 1951.

[15] H. Willard and F. Fenwick, “Bimetallic Electrode Systems in Electrometric Analysis. I. Systems Comprising Two Dissimilar Metals,” *J. Am. Chem. Soc.*, vol. 44, no. 11, pp. 2504–2515, 1922.

[16] G. D. Short and E. Bishop, “Differential Electrolytic Potentiometry. Part VII. The Interpretation of Current-Potential-Temperature Relationships of Antimony Electrodes in Neutral Solution,” *Analyst*, vol. 87, no. 1038, p. 724, 1962.

[17] E. Bishop, “Differential Electrolytic Potentiometry with Periodic Polarisation Part XXII. Symmetrical Periodic Current Differential Electrolytic Potentiometry in Oxidation - Reduction Titrimetry,” *Analyst*, vol. 98, no. 1172, pp. 712–724, 1973.

[18] A. M. S. Abdennabi and E. Bishop, “Differential Electrolytic Potentiometry with Periodic Polarisation. Part XXV. Direct and Mark-space Biased Periodic Polarisation in Acid - Base Titrimetry in Acetic Anhydride- Acetic Acid,” *Analyst*, vol. 107, no. 1278, pp. 1032–1039, Jan. 1982.

[19] E. Bishop and A. M. S. Abdennabi, “Differential Electrolytic Potentiometry with Periodic Polarisation. Part XXIX. Precipitation and Complexation Titrations in Anhydrous Acetic Acid,” *Analyst*, vol. 108, no. 1292, pp. 1349–1356, 1983.

[20] E. Bishop, “Differential Electrolytic Potentiometry. Part II. Precision and

Accuracy of Applications to Redox Titrimetry," *Analyst*, vol. 83, no. 985, pp. 212–222, 1958.

[21] E. Bishop and G. D. Short, "Differential Electrolytic Potentiometry. Part VI. The Precision and Accuracy of Applications to Acid-Base Titrations with Antimony Electrodes," *Analyst*, vol. 87, no. 1035, pp. 467–477, 1962.

[22] R. G. D. E. Bishop, "Differential Electrolytic Potentiometry. Part V. The Precision and Accuracy of Applications to Argentimetry," *Analyst*, vol. 87, no. 1032, pp. 207–213, 1962.

[23] R. G. D. E. Bishop, "Differential Electrolytic Potentiometry . Part VIII. The Behaviour and Energetics of Current-carrying Silver and Silver Halide Electrodes in the Semi-micro Scale Titration of Nanogram Amounts of Halides at Extreme Dilution," *Analyst*, vol. 87, no. 1040, pp. 845–859, 1962.

[24] E. Bishop and R. Dhaneshwar, "Diff erentiaI Electrolytic Potentiometric Determination of Nanogram Quantities of Halides at Extreme Dilution by Constant Current Coulometry," *Anal. Chem.*, vol. 36, no. 4, pp. 726–730, 1964.

[25] E. Bishop and G. D. Short, "Differential Electrolytic Potentiometry. Part XV. The Macro- and Microcoulometry of Acid-Base Reactions," *Analyst*, vol. 89, no. 1062, pp. 587–593, 1964.

[26] E. Bishop and G. D. Short, "Differential Electrolytic Potentiometry. Part XIV. An Examination of Electrode Parameters and Electrode Systems in Acid-Base Titrimetry," *Analyst*, vol. 89, no. 1059, pp. 415–420, 1964.

[27] R. G. Monk and K. C. Steed, "Microchemical Methods in Radiochemical Analysis. Determination of Chemical Yields by Micro-Coulometry," *Anal. Chim. Acta*, vol. 26, pp. 305–315, 1962.

[28] J. N. A. and F. P. Bowden, "The Kinetics of Electrode Reactions. I and II on JSTOR," *Proc. R. Soc. Lond. A. Math. Phys. Sci.*, vol. 169, no. 937, pp. 206–234, 1938.

[29] I. M. Kolthoff and N. Tanaka, "Rotated and Stationary Platinum Wire Electrodes," *Anal. Chem.*, vol. 26, no. 4, pp. 632–636, 1954.

[30] S. Glasstone, H. Eyring, and K. Laidler, *The Theory of Rate Processes*. McGraw-Hill, 1941.

[31] E. Bishop, "Coulometric Analysis," in *Comprehensive Analytical Chemistry*, 1st editio., vol. 2D, D. W. Wilson, C.L. Wilson, Ed. Amsterdam: Elsevier, 1975.

[32] S. Iijima, "Helical Microtubules of Graphitic Carbon," *Nature*, vol. 354, no. 6348, pp. 56–58, 1991.

[33] E. T. Thostenson, Z. Ren, and T.-W. Chou, "Advances in the Science and Technology of Carbon Nanotubes and their Composites: A Review," *Compos. Sci. Technol.*, vol. 61, no. 13, pp. 1899–1912, 2001.

[34] J. Fischer, H. Dai, A. Thess, and R. Lee, "Metallic Resistivity in Crystalline Ropes of Single-Wall Carbon Nanotubes," *Phys. Rev. B*, vol. 55, no. 8, pp. 4921–4924, 1997.

[35] M. Nihei, A. Kawabata, D. Kondo, M. Horibe, S. Sato, and Y. Awano, "Electrical Properties of Carbon Nanotube Bundles for Future via Interconnects," *Jpn. J. Appl. Phys.*, vol. 44, no. 4A, pp. 1626–1628, 2005.

[36] Z. Yao, C. L. Kane, and C. Dekker, "High-Field Electrical Transport in Single-Wall Carbon Nanotubes," pp. 2–5, 1999.

[37] J. W. Jang, D. K. Lee, C. E. Lee, T. J. Lee, C. J. Lee, and S. J. Noh, "Metallic Conductivity in Bamboo-shaped Multiwalled Carbon nanotubes," *Solid State Commun.*, vol. 122, no. 11, pp. 619–622, 2002.

[38] D. Tekleab, R. Czerw, D. L. Carroll, and P. M. Ajayan, "Electronic Structure of Kinked Multiwalled Carbon Nanotubes," *Appl. Phys. Lett.*, vol. 76, no. 24, p. 3594, 2000.

[39] J. Wang, "Carbon-Nanotube Based Electrochemical Biosensors: A review," *Electroanalysis*, vol. 17, no. 1, pp. 7–14, 2005.

[40] N. Zhao and J. Kang, "Direct Growth of Carbon Nanotubes on Metal Supports by Chemical Vapor Deposition," in *Carbon Nanotubes - Synthesis, Characterization, Applications*, S. Yellampalli, Ed. Croatia and Shanghai, 2011, pp. 99–120.

[41] K. Hernadia, A. Fonseca, J. B. Nagya, D. Bernaertsb, and A. A. Lucasa, "Fe-Catalyzed Carbon Nanotube Formation," *Carbon N. Y.*, vol. 34, no. 10, pp. 1249–1257, 1996.

[42] Y. Y. Wei, G. Eres, V. I. Merkulov, and D. H. Lowndes, "Effect of Catalyst Film Thickness on Carbon Nanotube Growth by Selective Area Chemical Vapor Deposition," *Appl. Phys. Lett.*, vol. 78, no. 10, pp. 1394–1396, 2001.

[43] C. Emmenegger, J. M. Bonard, P. Mauron, P. Sudan, A. Lepora, B. Grobety, A. Züttel, and L. Schlapbach, "Synthesis of Carbon Nanotubes over Fe Catalyst on Aluminum and Suggested Growth Mechanism," *Carbon N. Y.*, vol. 41, no. 3, pp. 539–547, 2003.

[44] S. Esconjauregui, C. M. Whelan, and K. Maex, "The Reasons Why Metals Catalyze the Nucleation and Growth of Carbon Nanotubes and Other Carbon Nanomorphologies," *Carbon N. Y.*, vol. 47, no. 3, pp. 659–669, 2009.

[45] M. Pumera, "Carbon Nanotubes Contain Residual Metal Catalyst Nanoparticles even after Washing with Nitric Acid at Elevated Temperature Because these Metal Nanoparticles are Sheathed by Several Graphene Sheets," *Langmuir*, vol. 23, no. 22, pp. 6453–6458, 2007.

[46] F. Banhart, "Interactions between Metals and Carbon Nanotubes: At the Interface between Old and New Materials," *Nanoscale*, vol. 1, no. 2, pp. 201–13, Nov. 2009.

[47] S. Talapatra, S. Kar, S. K. Pal, R. Vajtai, L. Ci, P. Victor, M. M. Shaijumon, S. Kaur, O. Nalamasu, and P. M. Ajayan, "Direct Growth of Aligned Carbon Nanotubes on Bulk Metals," *Nat. Nanotechnol.*, vol. 1, no. 2, pp. 112–6, Nov. 2006.

[48] M. Kumar and Y. Ando, "Chemical Vapor Deposition of Carbon Nanotubes: A Review on Growth Mechanism and Mass Production," *J. Nanosci. Nanotechnol.*, vol. 10, no. 6, pp. 3739–3758, Jun. 2010.

[49] J. Robertson, "Heterogeneous Catalysis Model of Growth Mechanisms of Carbon Nanotubes, Graphene and Silicon Nanowires," *J. Mater. Chem.*, vol. 22, no. 37, p. 19858, 2012.

[50] M. Kumar, “Carbon Nanotube Synthesis and Growth Mechanism,” in *Carbon Nanotubes - Synthesis, Characterization, Applications*, S. Yellampalli, Ed. Croatia and Shanghai: INTECH, 2011, pp. 147–170.

[51] G. H. Dong, Lifeng; Jiao, Jun; Foxley, Sean; Tuggle, David W.; Mosher, Catherine L.; Grathoff, “Effects of Hydrogen on the Formation of Aligned Carbon Nanotubes by Chemical Vapor Deposition,” *J. Nanosci. Nanotechnol.*, vol. 2, no. 2, pp. 155–160, 2002.

[52] C. Reynolds, B. Duong, and S. Seraphin, “Effects of Hydrogen Flow Rate on Carbon Nanotube Growth,” *... Res. Physics, http//www. jurp. ...*, 2010.

[53] M. Jung, K. Y. Eun, J. Lee, and Y. Baik, “Growth of Carbon Nanotubes by Chemical Vapor Deposition,” *Diam. Relat. Mater.*, vol. 10, pp. 1235–1240, 2001.

[54] C.-M. Chen, Y.-M. Dai, J. G. Huang, and J.-M. Jehng, “Intermetallic Catalyst for Carbon Nanotubes (CNTs) Growth by Thermal Chemical Vapor Deposition Method,” *Carbon N. Y.*, vol. 44, no. 9, pp. 1808–1820, Aug. 2006.

[55] C. Singh, M. S. P. Shaffer, and A. H. Windle, “Production of Controlled Architectures of Aligned Carbon Nanotubes by an Injection Chemical Vapor Deposition Method,” *Carbon N. Y.*, vol. 41, no. 2, pp. 359–368, 2003.

[56] Y. Wang, X. Gao, H.-J. Qian, Y. Ohta, X. Wu, G. Eres, K. Morokuma, and S. Irle, “Quantum Chemical Simulations Reveal Acetylene-Based Growth Mechanisms in the Chemical Vapor Deposition Synthesis of Carbon Nanotubes,” *Carbon N. Y.*, vol. 72, pp. 22–37, Jun. 2014.

[57] C. Jin, J. Park, Y. Huh, J. Yong, C. Lee, and J. Y. Lee, “Temperature Effect on the Growth of Carbon Nanotubes Using Thermal Chemical Vapor Deposition,” *Chem. Phys. Lett.*, vol. 343, no. July, pp. 33–38, 2001.

[58] K.-E. Kim, K.-J. Kim, W. S. Jung, S. Y. Bae, J. Park, J. Choi, and J. Choo, “Investigation on the Temperature-Dependent Growth Rate of Carbon Nanotubes Using Chemical Vapor Deposition of Ferrocene and Acetylene,” *Chem. Phys. Lett.*, vol. 401, pp. 459–464, 2005.

[59] Y. T. Lee, J. Park, Y. S. Choi, H. Ryu, and H. J. Lee, “Temperature-Dependent Growth of Vertically Aligned Carbon Nanotubes in the Range 800-1100°C,” *J. Phys. Chem. B*, vol. 106, no. 100, pp. 7614–7618, 2002.

[60] Y. T. Lee, N. S. Kim, J. Park, J. B. Han, Y. S. Choi, H. Ryu, and H. J. Lee, “Temperature-Dependent Growth of Carbon Nanotubes by Pyrolysis of Ferrocene and Acetylene in the Range between 700 And 1000°C,” *Chem. Phys. Lett.*, vol. 372, no. 5–6, pp. 853–859, May 2003.

[61] S. Y. Lim, M. M. Norani, and S. Suriati, “Effect of Parameters on Carbon Nanotubes Grown by Floating Catalyst Chemical Vapor Deposition,” vol. 242, pp. 242–254, 2012.

[62] A. A. Muataz, F. Ahmadun, C. Guan, E. Mahdi, and A. Rinaldi, “Effect of Reaction Temperature on the Production of Carbon Nanotubes,” *Nano*, vol. 01, no. 03, pp. 251–257, Nov. 2006.

[63] X. Zou, J. & Cheng, “Temperature Effects on Preparation of Multi-Walled Carbon Nanotubes by Floating Catalytic Chemical Vapor Deposition,” *Adv. Mater. Res.*, vol. 264–265, pp. 837–842, 2011.

[64] S. K. Pal, S. Talapatra, S. Kar, L. Ci, R. Vajtai, T. Borca-Tasciuc, L. S. Schadler, and P. M. Ajayan, “Time and Temperature Dependence of Multi-Walled Carbon Nanotube Growth on Inconel 600.,” *Nanotechnology*, vol. 19, p. 045610, 2008.

[65] S. Porro, S. Musso, M. Giorcelli, A. Chiodoni, and A. Tagliaferro, “Optimization of a Thermal-CVD System for Carbon Nanotube Growth,” *Phys. E Low-dimensional Syst. Nanostructures*, vol. 37, no. 1–2, pp. 16–20, Mar. 2007.

[66] M. E. Itkis, D. E. Perea, R. Jung, S. Niyogi, and R. C. Haddon, “Comparison of Analytical Techniques for Purity Evaluation of Single-Walled Carbon Nanotubes,” *J. Am. Chem. Soc.*, vol. 127, no. 11, pp. 3439–3448, 2005.

[67] K. Safarova, A. Drovak, and R. Kubinek, “Usage of AFM, SEM and TEM for the research of carbon nanotubes,” *Mod. Res. Educ. Top. Microsc.*, pp. 513–519, 2007.

[68] S. Maruyama, R. Kojima, Y. Miyauchi, S. Chiashi, and M. Kohno, “Low-

Temperature Synthesis of High-Purity Single-Walled Carbon Nanotubes from Alcohol," *Chem. Phys. Lett.*, vol. 360, no. 3–4, pp. 229–234, 2002.

[69] C. Hong, Y. You, and C. Pan, "Article Synthesis of Water-Soluble Multiwalled Carbon Nanotubes with Grafted Temperature-Responsive Shells by Surface RAFT Polymerization Synthesis of Water-Soluble Multiwalled Carbon Nanotubes with Grafted Temperature-Responsive Shells by Surface RAFT Po," *Chem. Mater.*, vol. 17, no. 13, pp. 2247–2254, 2005.

[70] T. Belin and F. Epron, "Characterization Methods of Carbon Nanotubes: A Review," *Mater. Sci. Eng. B*, vol. 119, no. 2, pp. 105–118, May 2005.

[71] L. Bokobza, "Raman Spectroscopic Characterization of Multiwall Carbon Nanotubes and of Composites," *Express Polym. Lett.*, vol. 6, no. 7, pp. 601–608, 2012.

[72] a I. López-Lorente, B. M. Simonet, and M. Valcárcel, "Raman Spectroscopic Characterization of Single Walled Carbon Nanotubes: Influence of the Sample Aggregation State.," *Analyst*, vol. 139, no. 1, pp. 290–8, 2014.

[73] R. A. DiLeo, B. J. Landi, and R. P. Raffaelle, "Purity Assessment of Multiwalled Carbon Nanotubes by Raman Spectroscopy," *J. Appl. Phys.*, vol. 101, no. 6, p. 064307, 2007.

[74] S. C. Colindres, K. Aguir, F. C. Sodi, L. V. Vargas, J. M. Salazar, and V. G. Febles, "Ozone Sensing Based on Palladium Decorated Carbon Nanotubes," *Sensors (Switzerland)*, vol. 14, no. 4, pp. 6806–6818, 2014.

[75] K. G. Ong, Y. Y. An, M. Z. Hang, S. U. Lei, S. X. Iong, and L. M. Ao, "Electrochemistry and Electroanalytical Applications of Carbon Nanotubes : A Review," *Anal. Sci.*, vol. 21, pp. 1383–1393, 2005.

[76] M. Trojanowicz, "Analytical Applications of Carbon Nanotubes: A Review," *Trends Anal. Chem.*, vol. 25, no. 5, pp. 480–489, 2006.

[77] P. Yáñez-Sedeño, J. M. Pingarrón, J. Riu, and F. X. Rius, "Electrochemical Sensing Based on Carbon Nanotubes," *Trends Anal. Chem.*, vol. 29, no. 9, pp. 939–953, Oct. 2010.

[78] W. Liang and Y. Zhuobin, “Direct Electrochemistry of Glucose Oxidase at a Gold Electrode Modified With Single-Wall Carbon Nanotubes,” *Sensors*, vol. 3, pp. 544–554, 2003.

[79] B. Zeng and F. Huang, “Electrochemical Behavior and Determination of Fluphenazine at Multi-Walled Carbon Nanotubes/ (3-Mercaptopropyl) Trimethoxysilane Bilayer Modified Gold Electrodes,” *Talanta*, vol. 64, pp. 380–386, 2004.

[80] F. Zhao, F. Huang, Q. Yan, and B. Zeng, “Characterization of Dodecanethiol SAM and Multi-Walled Carbon Nanotube Modified Gold Electrodes, and Voltammetric Determination of Prochlorperazine,” *Microchim. Acta*, vol. 150, no. 2, pp. 179–185, 2005.

[81] S. Wei, F. Zhao, and B. Zeng, “Electrochemical Behavior and Determination of Uric Acid at Single-Walled Carbon Nanotube Modified Gold Electrodes,” *Microchim. Acta*, vol. 150, no. 3–4, pp. 219–224, 2005.

[82] C. E. Banks and R. G. Compton, “New Electrodes for Old: From Carbon Nanotubes to Edge Plane Pyrolytic Graphite,” *Analyst*, vol. 131, no. 1, p. 15, 2006.

[83] H. Wang, Y. Wu, and J.-F. Song, “Interface Potential Sensing From Adsorption of Human Serum Albumin (HSA) On Carbon Nanotube (CNT) Monitored By Zero Current Potentiometry for HSA Determination,” *Biosens. Bioelectron.*, vol. 72, pp. 225–229, 2015.

[84] E. Jaworska, K. Maksymiuk, and A. Michalska, “Carbon Nanotubes Based Potentiometric Bio-Sensors for Determination of Urea,” *Chemosensors*, vol. 3, pp. 200–210, 2015.

[85] T. S. Anirudhan and S. Alexander, “Design and Fabrication of Molecularly Imprinted Polymer-Based Potentiometric Sensor from the Surface Modified Multiwalled Carbon Nanotube for the Determination of Lindane (γ-Hexachlorocyclohexane), an Organochlorine Pesticide,” *Biosens. Bioelectron.*, vol. 64, pp. 586–593, 2015.

[86] A. Darroudi, AbolfazlEshghi, Hossein; Rezaeian, Shima; Chamsaz, Mahmoud;

Bakavoli, MehdiHaghbeen, KamahldinHosseiny, “A Novel Carbon Paste Electrode for Potentiometric Determination of Vanadyl Ion,” *Iran. J. Chem. Chem. Eng*, vol. 34, no. 4, pp. 89–96, 2015.

[87] H. Khani, M. K. Rofouei, P. Arab, V. K. Gupta, and Z. Vafaei, “Multi-Walled Carbon Nanotubes-Ionic Liquid-Carbon Paste Electrode as a Super Selectivity Sensor: Application to Potentiometric Monitoring Of Mercury Ion (II),” *J. Hazard. Mater.*, vol. 183, no. 1–3, pp. 402–9, Nov. 2010.

[88] A. Shirzadmehr, A. Afkhami, and T. Madrakian, “A New Nano-Composite Potentiometric Sensor Containing an Hg2+ Ion Imprinted Polymer for the Trace Determination of Mercury Ions in Different Matrices,” *J. Mol. Liq.*, vol. 204, pp. 227–235, 2015.

[89] O. R. Shehab and A. M. Mansour, “Potentiometric Multi-Walled Carbon Nanotube Zn-Sensor Based on a Naphthalocyanine Neutral Carrier: Experimental and Theoretical Studies,” *RSC Adv.*, vol. 5, no. 72, pp. 58416–58427, 2015.

[90] M. Cuartero, A. Crespo, and E. Bakker, “Tandem Electrochemical Desalination − Potentiometric Nitrate Sensing for Seawater Analysis,” *Anal. Chem.*, vol. 87, pp. 8084–8089, 2015.

[91] F. Mohammadabadi, H. A. Zamani, and F. Joz-yarmohammadi, “Fabrication of a Tb3+ Carbon Paste Ion Selective Electrode by Using Nanosilica and Multi-Walled Carbon Nanotubes (MWCNTs),” *Int. J. Electrochem. Sci.*, vol. 10, pp. 2791–2800, 2015.

[92] J. Ruzicka and E. H. Hansen, “Peer Reviewed: Flow Injection Analysis: From Beaker to Microfluidics.,” *Anal. Chem.*, vol. 72, no. 5, p. 212 A–217 A, 2000.

[93] J. Růžička and E. H. Hansen, “Flow injection analysis Part X. Theory, Techniques and Trends,” *Anal. Chim. Acta*, vol. 99, pp. 37–76, 1978.

[94] B. Karlberg, “Flow Injection Analysis,” in *Chemical Derivatization in Analytical Chemistry*, R. Lawrence and J. Frei, Eds. New York and London: Springer, 1982, pp. 1–42.

[95] J. Růžička, E. H. Hansen, and E. a. Zagatto, “Flow Injection Analysis,” *Anal. Chim. Acta*, vol. 88, pp. 1–16, 1977.

[96] L. A. Pradela-Filho, B. C. Oliveira, R. M. Takeuchi, and A. L. Santos, “A Prussian Blue-Carbon Paste Electrode for Selective Cathodic Amperometric Determination of Nitrite Using a Flow-Injection Analysis System with Carrier Recycling,” *Electrochim. Acta*, vol. 180, pp. 939–946, 2015.

[97] P. Salazar, M. Martín, J. L. González-Mora, and A. R. González-Elipe, “Application of Prussian Blue electrodes for amperometric detection of free chlorine in water samples using Flow Injection Analysis,” *Talanta*, vol. 146, pp. 410–416, 2016.

[98] B. C. Lourencao, R. A. Medeiros, S. Scherrer, A. Gilberto, R. C. Rocha-filho, and O. Fatibello-filho, “Amperometric Flow-Injection Determination of the Anthelmintic Drugs Ivermectin and Levamisole Using Electrochemically Pretreated Boron-Doped Diamond Electrodes,” *Sensors Actuators B. Chem.*, vol. 222, pp. 181–189, 2016.

[99] J. R. Santos and A. O. S. S. Rangel, “Development of a Chromatographic Low Pressure Flow Injection System: Application to the Analysis of Methylxanthines in Coffee,” *Anal. Chim. Acta*, vol. 715, pp. 57–63, 2012.

[100] M. Amatatongchai, W. Sroysee, S. Chairam, and D. Nacapricha, “Simple Flow Injection for Determination of Sulfite by Amperometric Detection Using Glassy Carbon Electrode Modified with Carbon Nanotubes-PDDA-Gold Nanoparticles.,” *Talanta*, vol. 133, pp. 134–41, 2015.

[101] V. K. Gupta, P. Norouzi, H. Ganjali, F. Faridbod, and M. R. Ganjali, “Flow Injection Analysis of Cholesterol Using FFT Admittance Voltammetric Biosensor Based on MWCNT–ZnO Nanoparticles,” *Electrochim. Acta*, vol. 100, pp. 29–34, Jun. 2013.

[102] J. S. Stefano, D. S. Cordeiro, M. C. Marra, E. M. Richter, and R. A. A. Munoz, “Batch-Injection versus Flow-Injection Analysis Using Screen-Printed Electrodes: Determination of Ciprofloxacin in Pharmaceutical Formulations,” *Electroanalysis*, vol. 27, pp. 1–9, 2015.

[103] G. Liu and Y. Lin, “Biosensor Based on Self-Assembling Acetylcholinesterase on Carbon Nanotubes for Flow Injection/Amperometric Detection of Organophosphate Pesticides and Nerve Agents,” *Anal. Chem.*, vol. 78, no. 3, pp. 835–843, 2006.

[104] V. B. Kandimalla and H. Ju, “Binding of Acetylcholinesterase to Multiwall Carbon Nanotube-Cross-Linked Chitosan Composite for Flow-Injection Amperometric Detection of an Organophosphorous Insecticide.,” *Chemistry*, vol. 12, no. 4, pp. 1074–80, Jan. 2006.

[105] J. Upan, P. Reanpang, O. Chailapakul, and J. Jakmunee, “Flow Injection Amperometric Sensor with a Carbon Nanotube Modified Screen Printed Electrode for Determination of Hydroquinone,” *Talanta*, vol. 146, pp. 766–771, 2015.

[106] A. M. . Abdennabi, M. . Koken, and M. . Khaled, “Application of Differential Electrolytic Potentiometry for Detection in Flow Injection Analysis,” *Anal. Chim. Acta*, vol. 360, no. 1–3, pp. 195–201, Mar. 1998.

[107] A. Abdennabi and M. Koken, “Differential Electrolytic Potentiometry, a Detector in Flow Injection Analysis for Precipitation Reactions,” *Talanta*, vol. 46, no. 4, pp. 639–646, Aug. 1998.

[108] S. M. A. Fraihat and A. M. S. Abulkibash, “Differential Electrolytic Potentiometry a Detector in Flow Injection Analysis for Cyanide Determination,” *J. Mater. Sci. Eng. A*, vol. 1, pp. 248–252, 2011.

[109] T. a. Saleh and a. M. Abulkibash, “Application of dc and Mark-Space Bias Differential Electrolytic Potentiometry for Determination of Cyanide Using a Programmable Syringe Pump,” *Appl. Water Sci.*, vol. 1, pp. 67–72, 2011.

[110] A. Abulkibash, M. Koken, M. Khaled, and S. Sultan, “Differential Electrolytic Potentiometry, a Detector in Flow Injection Analysis for Oxidation-Reduction Reactions,” *Talanta*, vol. 52, no. 6, pp. 1139–1142, Sep. 2000.

[111] N. García-Villar, J. Saurina, and S. Hernández-Cassou, “Flow Injection Differential Potentiometric Determination of Lysine by Using a Lysine Biosensor,” *Anal. Chim. Acta*, vol. 477, no. 2, pp. 315–324, Feb. 2003.

[112] P. Dutta, R. Rasaily, M. R. Saha, U. Mitra, S. K. Bhattacharya, M. K. Bhattacharya, and M. Lahiri, "Ciprofloxacin for Treatment of Severe Typhoid Fever in Children.," *Antimicrob. Agents Chemother.*, vol. 37, no. 5, pp. 1197–1199, May 1993.

[113] M. J. Levenson, S. C. Parisier, J. Dolitsky, and G. Bindra, "Ciprofloxacin: Drug of Choice in the Treatment of Malignant External Otitis (MEO).," *Laryngoscope*, vol. 101, no. 8, pp. 821–824, Aug. 1991.

[114] R. van Furth, J. W. van't Wout, J. Zwartendijk, and P. A. Wertheimer, "Ciprofloxacin for Treatment of Malakoplakia," *Lancet*, vol. 339, no. 8786, pp. 148–149, Jan. 1992.

[115] F. Belal, A. A. Al-Majed, and A. M. Al-Obaid, "Methods of Analysis of 4-Quinolone Antibacterials," *Talanta*, vol. 50, no. 4, pp. 765–786, 1999.

[116] J. Vella, F. Busuttil, N. S. Bartolo, C. Sammut, V. Ferrito, A. Serracino-Inglott, L. M. Azzopardi, and G. LaFerla, "A simple HPLC-UV Method for the Determination of Ciprofloxacin in Human Plasma.," *J. Chromatogr. B. Analyt. Technol. Biomed. Life Sci.*, vol. 989, pp. 80–5, May 2015.

[117] O. Sagirli, S. Demirci, and A. Önal, "Determination of Ciprofloxacin in Human Serum by Online Heart-Cutting Liquid Chromatography," *Chromatographia*, vol. 79, no. 3–4, pp. 137–144, Jan. 2016.

[118] E. S. Zimmermann, B. G. S. Torres, and T. Dalla Costa, "Validation of a Sensitive HPLC/Fluorescence Method for Assessment of Ciprofloxacin Levels in Plasma and Prostate Microdialysate Samples from Rats.," *Biomed. Chromatogr.*, vol. 30, no. 3, pp. 330–336, Mar. 2016.

[119] L. Fratini and E. E. S. Schapoval, "Ciprofloxacin Determination by Visible Light Spectrophotometry Using Iron (III) Nitrate," *Int. J. Pharm.*, vol. 127, no. 2, pp. 279–282, 1996.

[120] P. Djurdjević, M. Todorović, M. J. Stankov, and J. Odović, "Spectrophotometry Determination of Ciprofloxacin in Serum Using Iron (III) Ion as Chromogenic Agent," *Anal. Lett.*, vol. 33, no. 4, pp. 657–665, 2000.

[121] V. Hoang and N. Yen, “Adsorptive Cathodic Stripping Voltammetric Determination of Ciprofloxacin in Bulk Powder, Pharmaceutical Dosage Forms and Urine,” *Trop. J. Pharm. Res.*, vol. 12, no. 5, pp. 783–790, Oct. 2013.

[122] A. N. Kawde, M. A. Aziz, N. Odewunmi, N. Hassan, and A. AlSharaa, “Electroanalytical Determination of Antibacterial Ciprofloxacin in Pure Form and in Drug Formulations,” *Arab. J. Sci. Eng.*, vol. 39, no. 1, pp. 131–138, 2014.

[123] M. Behpour, S. Masoum, and M. Meshki, “Application of Electrochemical Techniques at a Nanostructure Based Modified Sensor for Analyte Quantitation,” *Synth. React. Inorganic, Met. Nano-Metal Chem.*, vol. 46, no. 7, pp. 1026–1032, 2016.

[124] M. Liang, S. Y. Xi Xia1, and L. Jie, “Voltammetric Determination of Ciprofloxacin Hydrochloride on Multi-Wall Carbon Nanotube Modified Electrode,” *Chinese J. Antibiot.*, no. 12, 2009.

[125] A. A. Ensafi, A. R. Allafchain, and R. Mohammadzadeh, “Characterization of MgFe2O4 Nanoparticles as a Novel Electrochemical Sensor: Application for the Voltammetric Determination of Ciprofloxacin,” *Anal. Sci.*, vol. 28, pp. 705–710, 2012.

[126] P. Gayen and B. P. Chaplin, “Selective Electrochemical Detection of Ciprofloxacin with a Porous Nafion/Multi-Walled Carbon Nanotube Composite Film Electrode,” *ACS Appl. Mater. Interfaces*, p. acsami.5b07337, 2015.

[127] M. P. Kingsley, P. K. Kalambate, and A. K. Srivastava, “Simultaneous Determination of Ciprofloxacin and Paracetamol by Adsorptive Stripping Voltammetry Using Copper Zinc Ferrite Nanoparticles Modified Carbon Paste Electrode,” *RSC Adv.*, vol. 6, no. 18, pp. 15101–15111, 2016.

[128] A. M. Abulkibash, S. M. Sultan, A. M. Al-Olyan, and S. M. Al-Ghannam, “Differential Electrolytic Potentiometric Titration Method for the Determination of Ciprofloxacin in Drug Formulations,” *Talanta*, vol. 61, no. 2, pp. 239–244, 2003.

[129] F. E. O. Suliman and S. M. Sultan, “Sequential Injection Technique Employed for Stoichiometric Studies, Optimization and Quantitative Determination of

Some Fluoroquinolone Antibiotics Complexed with Iron (III) In Sulfuric Acid Media," *Talanta*, vol. 43, no. 4, pp. 559–568, 1996.

[130] V. Uivarosi, "Metal Complexes of Quinolone Antibiotics and their Applications: An Update.," *Molecules*, vol. 18, no. 9, pp. 11153–11197, Jan. 2013.

[131] S. M. Sultan and F.-E. O. Suliman, "Flow Injection Spectrophotometric Determination of the Antibiotic Ciprofloxacin in Drug Formulations," *Analyst*, vol. 117, no. 9, p. 1523, Jan. 1992.

[132] I. Turel, N. Bukovec, and E. Farkas, "Complex Formation Between Some Metals and a Quinolone Family Member (Ciprofloxacin)," *Polyhedron*, vol. 15, no. 2, pp. 269–275, 1996.

[133] C. C. Nweze, M. G. Abdulganiyu, and O. G. Erhabor, "Comparative Analysis of Vitamin C in Fresh Fruits Juice of Malus domestica , Citrus sinensi, Ananas comosus and Citrullus lanatus by Iodometric Titration," *Int. J. Sci. Environ. Technol.*, vol. 4, no. 1, pp. 17–22, 2015.

[134] M. K. Wilson, B. C. Baguley, C. Wall, M. B. Jameson, and M. P. Findlay, "Review of High-Dose Intravenous Vitamin C as an Anticancer Agent," *Asia. Pac. J. Clin. Oncol.*, vol. 10, no. 1, pp. 22–37, 2014.

[135] S. J. Padayatty, A. Katz, Y. Wang, P. Eck, O. Kwon, J.-H. Lee, S. Chen, C. Corpe, A. Dutta, S. K. Dutta, and M. Levine, "Vitamin C as an Antioxidant: Evaluation of its Role in Disease Prevention," *J. Am. Coll. Nutr.*, vol. 22, no. 1, pp. 18–35, 2003.

[136] C. S. Johnston, G. M. Barkyoumb, and S. S. Schumacher, "Vitamin C Supplementation Slightly Improves Physical Activity Levels and Reduces Cold Lncidence in Men with Marginal Vitamin C Status: A Randomized Controlled Trial.," *Nutrients*, vol. 6, no. 7, pp. 2572–2583, Jul. 2014.

[137] V. Edefonti, M. Hashibe, M. Parpinel, F. Turati, D. Serraino, K. Matsuo, A. F. Olshan, J. P. Zevallos, D. M. Winn, K. Moysich, Z.-F. Zhang, H. Morgenstern, F. Levi, K. Kelsey, M. McClean, C. Bosetti, C. Galeone, S. Schantz, G.-P. Yu, P. Boffetta, Y.-C. Amy Lee, S.-C. Chuang, C. La Vecchia, and A. Decarli, "Natural vitamin C Intake and the Risk of Head and Neck Cancer: A Pooled

Analysis in the International Head and Neck Cancer Epidemiology Consortium," *Int. J. Cancer*, vol. 137, pp. 448–462, 2015.

[138] F. Forastiere, R. Pistelli, P. Sestini, C. Fortes, E. Renzoni, F. Rusconi, V. Dell'Orco, G. Ciccone, and L. Bisanti, "Consumption of Fresh Fruit Rich in Vitamin C and Wheezing Symptoms in Children. SIDRIA Collaborative Group, Italy (Italian Studies on Respiratory Disorders in Children and the Environment).," *Thorax*, vol. 55, no. 4, pp. 283–288, 2000.

[139] "USP-NF25," 2007.

[140] L. Suntornsuk, W. Gritsanapun, S. Nilkamhank, and A. Paochom, "Quantitation of Vitamin C content in Herbal Juice Using Direct Titration," *J. Pharm. Biomed. Anal.*, vol. 28, no. 5, pp. 849–855, 2002.

[141] C. Routoir and D. C. Analytique, "High-Performance Liquid Chromatographic Determination Vitamin C in Fresh Fruits from West Africa," *J. Food Compos. Drug Anal.*, vol. 269, no. 1, pp. 265–269, 1988.

[142] V. Bansal, A. Sharma, C. Ghanshyam, and M. L. Singla, "Rapid HPLC Method for Determination of Vitamin C, Phenolic Acids, Hydroxycinnamic Acid, and Flavonoids in Seasonal Samples of Emblica officinalis Juice," *J. Liq. Chromatogr. Relat. Technol.*, vol. 38, no. 5, pp. 619–624, 2015.

[143] I. Klimczak and A. Gliszczyńska-Świgło, "Comparison of UPLC and HPLC Methods for Determination of Vitamin C," *Food Chem.*, vol. 175, pp. 100–5, 2015.

[144] A. Baghizadeh, H. Karimi-Maleh, Z. Khoshnama, A. Hassankhani, and M. Abbasghorbani, "A Voltammetric Sensor for Simultaneous Determination of Vitamin C and Vitamin B6 in Food Samples Using ZrO2 Nanoparticle/Ionic Liquids Carbon Paste Electrode," *Food Anal. Methods*, pp. 549–557, 2014.

[145] S. Gheibi, H. Karimi-Maleh, M. A. Khalilzadeh, and H. Bagheri, "A New Voltammetric Sensor for Electrocatalytic Determination of Vitamin C in Fruit Juices and Fresh Vegetable Juice Using Modified Multi-Wall Carbon Nanotubes Paste Electrode," *J. Food Sci. Technol.*, vol. 52, no. 1, pp. 276–284, 2015.

[146] S. M. Al-Ghannam and A. M. Al-Olyan, “Differential Electrolytic Potentiometric Titration of Vitamin C in Pharmaceutical Preparations,” *J. Food Drug Anal.*, vol. 13, no. 4, pp. 295–300, 2005.

[147] G. P. P. Kamatou, I. Vermaak, and A. M. Viljoen, “An updated Review of Adansonia Digitata: a Commercially Important African Tree,” *South African J. Bot.*, vol. 77, no. 4, pp. 908–919, 2011.

[148] J. Rahul, M. K. Jain, S. P. Singh, R. K. Kamal, Anuradha, A. Naz, A. K. Gupta, and S. K. Mrityunjay, “Adansonia Digitata L. (baobab): a Review of Traditional Information and Taxonomic Description,” *Asian Pac. J. Trop. Biomed.*, vol. 5, no. 1, pp. 79–84, 2015.

[149] J. Gebauer, K. El-Siddig, and G. Ebert, “Baobab (Adansonia digitata L .): a Review on a Multipurpose Tree with Promising Future in the Sudan,” *Gartenbauwissenschaft*, vol. 67, no. 4, pp. 155–160, 2002.

[150] R. Zhang, V. L. Wilson, A. Hou, and G. Meng, “Source of Lead Pollution, its Influence on Public Health and the Countermeasures,” *Int. J. Heal. Anim. Sci. Food Saf.*, vol. 2, no. 1, pp. 18–31, 2015.

[151] P. B. Tchounwou, C. G. Yedjou, A. K. Patlolla, and D. J. Sutton, “Heavy Metal Toxicity and the Environment,” in *Molecular, Clinical and Environmental Toxicology*, vol. 3, A. Luch, Ed. Springer, 2012, pp. 133–164.

[152] G. Flora, D. Gupta, and A. Tiwari, “Toxicity of Lead: A Review with Recent Updates,” *Interdiscip. Toxicol.*, vol. 5, no. 2, pp. 47–58, Jun. 2012.

[153] M. Pal, M. Sachdeva, N. Gupta, P. Mishra, M. Yadav, and A. Tiwari, “Lead Exposure in Different Organs of Mammals and Prevention by Curcumin-Nanocurcumin: A Review,” *Biol. Trace Elem. Res.*, vol. 168, no. 2, pp. 380–91, Dec. 2015.

[154] J. García-Lestón, J. Méndez, E. Pásaro, and B. Laffon, “Genotoxic Effects of Lead: An Updated Review,” *Environ. Int.*, vol. 36, no. 6, pp. 623–36, Aug. 2010.

[155] H. Yang, X. Huo, T. A. Yekeen, Q. Zheng, M. Zheng, and X. Xu, “Effects of Lead and Cadmium Exposure from Electronic Waste on Child Physical

Growth," *Environ. Sci. Pollut. Res. Int.*, vol. 20, no. 7, pp. 4441–7, Jul. 2013.

[156] J. M. Besser, C. G. Ingersoll, W. G. Brumbaugh, N. E. Kemble, T. W. May, N. Wang, D. D. MacDonald, and A. D. Roberts, "Toxicity of Sediments from Lead-Zinc Mining Areas to Juvenile Freshwater Mussels (Lampsilis Siliquoidea) Compared to Standard Test Organisms," *Environ. Toxicol. Chem.*, vol. 34, no. 3, pp. 626–639, 2015.

[157] T. A. Jarvis, T. R. Capo, and G. K. Bielmyer-Fraser, "Dietary Metal Toxicity to the Marine Sea Hare, Aplysia Californica," *Comp. Biochem. Physiol. C. Toxicol. Pharmacol.*, vol. 174–175, pp. 54–64, Jan. 2015.

[158] B. Pourrut, M. Shahid, C. Dumat, P. Winterton, and E. Pinelli, "Lead Uptake, Toxicity, and Detoxification in Plants," *Rev. Environ. Contam. Toxicol.*, vol. 213, pp. 113–36, Jan. 2011.

[159] A. Romero-Freire, F. J. Martin Peinado, and C. A. M. van Gestel, "Effect of Soil Properties on the Toxicity of Pb: Assessment of the Appropriateness of Guideline Values," *J. Hazard. Mater.*, vol. 289, pp. 46–53, May 2015.

[160] J. S. Fritz and B. G. Barbara, "Potentiometric Titration of Metal Ions Using a Silver Electrode," *Anal. Chem.*, vol. 36, no. 4, pp. 737–741, 1964.

[161] M. Shamsipur, M. R. Ganjali, and A. Rouhollahi, "Lead-Selective Membrane Potentiometric Sensor Based on an 18-Membered Thiacrown Derivative," *Anal. Sci. Int. J. Japan Soc. Anal. Chem.*, vol. 17, no. 8, pp. 935–8, 2001.

[162] M.-R. Huang, Y.-B. Ding, and X.-G. Li, "Lead-Ion Potentiometric Sensor Based on Electrically Conducting Microparticles of Sulfonic Phenylenediamine Copolymer.," *Analyst*, vol. 138, no. 13, pp. 3820–9, 2013.

[163] A. Jasi, M. Guzi, G. Lisak, J. Bobacka, and M. Boche, "Solid-Contact Lead (II) Ion-Selective Electrodes for Potentiometric Determination of Lead (II) in Presence of High Concentrations of Na (I), Cu (II), Cd (II), Zn (II), Ca (II) and Mg (II)," *Sensors Actuators B Chem.*, vol. 218, pp. 25–30, 2015.

[164] A. Kamal, R. Tejpal, V. Bhalla, and R. K. Kumar, M. & Mahajan, "Selective and Sensitive Lead (II) Solid-Contact Potentiometric Sensor Based on Naphthalene-

Sulfonamide Derivative," *Int. J. Environ. Sci. Technol.*, vol. 12, no. 8, pp. 2567–2578, 2015.

[165] M. Rashid, F. Khan, and R. Wahab, "Zirconium (IV) Phosphosulphosalicylate-Based Ion Selective Membrane Electrode for Potentiometric Determination of Pb (II) Ions," *Arab. J. Chem.*, 2015.

[166] Y. Hoon, W. Sik, H. Joo, S. Min, and T. Kee, "Lead (II) Ion Selective Poly (aniline) Solid Contact Electrode Based on 1, 2 bis (N ' Benzoylthioureido) Ethane, -Propane and -Butane Ionophores," *J. Anal. Chem.*, vol. 70, no. 5, pp. 621–626, 2015.

[167] H. Bagheri, A. Afkhami, A. Shirzadmehr, H. Khoshsafar, H. Khoshsafar, and H. Ghaedi, "Novel Potentiometric Sensor for the Determination of Cd2+ Based on a New Nano-Composite," *Int. J. Environ. Anal. Chem.*, vol. 93, no. 5, pp. 578–591, 2013.

[168] M. Shariyati, H. A. Zamani, A. Dehnavi, and M. R. Abedi, "Construction of a Fe3+ Carbon Paste Electrode Based on Multi- Walled Carbon Nanotubes (MWCNTs)/Nanosilica," *Int. J. Electrochem. Sci.*, vol. 9, pp. 8320–8329, 2014.

[169] F. Faridbod, H. A. Zamani, M. Hosseini, and M. Pirali-hamedani, "Praseodymium Selective Carbon Paste Electrode Based on Carbon Nanotubes and Ionic Liquids," *Int. J. Electrochem. Sci.*, vol. 6, pp. 3694–3703, 2011.

[170] A. A. Abraham, M. Rezayi, N. S. A. Manan, L. Narimani, A. N. Bin Rosli, and Y. Alias, "A Novel Potentiometric Sensor Based on 1,2-Bis (N'-benzoylthioureido)benzene and Reduced Graphene Oxide for Determination of Lead (II) Cation in Raw Milk," *Electrochim. Acta*, vol. 165, pp. 221–231, 2015.

[171] J. O. Egekeze and F. W. Oehme, "Cyanides and their Toxicity: A Literature Review.," *Tijdschr. Diergeneeskd.*, vol. 105, no. 8, 1980.

[172] C. A. Johnson, "The Fate of Cyanide in Leach Wastes at Gold Mines: An Environmental Perspective," *Appl. Geochemistry*, vol. 57, pp. 194–205, 2015.

[173] J. Marsden and I. House, *The Chemistry of Gold Extraction*, 2nd ed. SME, 2006.

[174] J. Ma and P. K. Dasgupta, "Recent Developments in Cyanide Detection: A

review," *Anal. Chim. Acta*, vol. 673, no. 2, pp. 117–125, 2010.

[175] E. O. Otu, J. J. Byerley, and C. W. Robinson, "Ion Chromatography of Cyanide and Metal Cyanide Complexes: A Review," *Int. J. Environ. Anal. Chem.*, vol. 63, no. 1, pp. 81–90, Apr. 1996.

[176] M. F. Cengiz, M. Z. Durak, S. Nilufer, and K. Bilgin, "Ion Chromatographic Determination of Free Cyanide in Different Classes of Bottled Natural Mineral Water Consumed in Turkey," *Int. J. Food Prop.*, vol. 2912, no. August 2014, p. 140506210349007, 2014.

[177] H. Sulistyarti, T. J. Cardwell, and S. D. Kolev, "Determination of Cyanide as Tetracyanonickelate (II) by Flow Injection and Spectrophotometric Detection," *Anal. Chim. Acta*, vol. 357, no. 1–2, pp. 103–109, 1997.

[178] T. Saleh and A. Abulkibash, "Application of Dc And Mark-Space Bias Differential Electrolytic Potentiometry for Determination of Cyanide Using a Programmable Syringe Pump," *Appl. Water Sci.*, 2011.

[179] M. Keusgen, J. P. Kloock, D. T. Knobbe, M. Jünger, I. Krest, M. Goldbach, W. Klein, and M. J. Schöning, "Direct Determination of Cyanides by Potentiometric Biosensors," *Sensors Actuators, B Chem.*, vol. 103, no. 1–2, pp. 380–385, 2004.

[180] P. C. do Nascimento and G. Schwedt, "Comparative Studies of the Determination of Cyanide at Low Concentration Levels in Waste Waters," *Anal. Chim. Acta*, vol. 283, no. 2, pp. 755–761, 1993.

[181] J. M. J. Bassett, R.C. Denney, G.H. Jeffery, *Vogel's Textbook of Quantitative Inorganic Analysis*, Fourth edi. UK: Longman Group Limited, 1978.

[182] S. E. Iyuke, A. S. Abdulkareem, and A. S. Afolabi, "Optimizing Carbon Nanotube Continuous Production in a Swirled Ferrocene Vaporizer," in *SACEC*, 2005, pp. 1–8.

[183] J. Kong, A. M. Cassell, and H. Dai, "Chemical vapor deposition of methane for single-walled carbon nanotubes," *Chem. Phys. Lett.*, vol. 292, no. 4–6, pp. 567–574, Aug. 1998.

[184] A. R. Harutyunyan, T. Tokune, and E. Mora, "Liquid as a required catalyst phase

for carbon single-walled nanotube growth," *Appl. Phys. Lett.*, vol. 87, no. 5, p. 051919, 2005.

[185] R. Brukh and S. Mitra, "Mechanism of Carbon Nanotube Growth by CVD," *Chem. Phys. Lett.*, vol. 424, no. 1–3, pp. 126–132, Jun. 2006.

[186] a. C. Dillon, T. Gennett, K. M. Jones, J. L. Alleman, P. a. Parilla, and M. J. Heben, "A Simple and Complete Purification of Single-Walled Carbon Nanotube Materials," *Adv. Mater.*, vol. 11, no. 16, pp. 1354–1358, 1999.

[187] D. C. Harris, *Quantitative Chemical Analysis*, 8th ed. New York: Clancy Marshall, 2010.

[188] P. L. Breuer, C. A. Sutcliffe, and R. L. Meakin, "Cyanide Measurement by Silver Nitrate Titration: Comparison of Rhodanine and Potentiometric End-Points," *Hydrometallurgy*, vol. 106, no. 3–4, pp. 135–140, 2011.

[189] "www.flowinjectiontutorial." .

Vitae

Name	**:**	Abdalghaffar Mohammad Abdalghaffar Osman
Nationality	**:**	Sudanese
Date of Birth	**:**	May 17, 1976
Email	**:**	amaokf@kfupm.edu.sa , abdalghaffar@hotmail.co.uk
Address	**:**	Chemistry Department, College of Science, King Fahd University of Petroleum and Minerals, Dhahran, KSA

Academic Background	**:**	**PhD** in Chemistry, King Fahd University of Petroleum and Minerals, Dhahran, KSA (May 2016).
		MSc in Chemistry, Sudan University of Science and Technology, Khartoum, Sudan (2007).
		BSc (Honor, First Class) in Chemistry, Faculty of Science, Sudan University of Science and Technology, Khartoum, Sudan (2000).

Professional Experience

2011 – 2016	**:**	Lecturer B, Department of Chemistry, King Fahd University of Petroleum & Minerals, Dhahran, KSA.
2009 – 2011	**:**	Lecturer, Department of Pharmaceutical Chemistry, Faculty of Pharmacy, Prince Sattam Bin Abdul-Aziz University, Al-Kharj, KSA.
2002 – 2009	**:**	Teaching Assistant/Lecturer, Department of Chemistry, faculty of Science, Sudan University of Science & Technology, Sudan.